

# Tetrahydroquinoline-Capped Histone Deacetylase 6 Inhibitor SW-101 Ameliorates Pathological Phenotypes in a Charcot–Marie–Tooth Type 2A Mouse Model

Sida Shen,<sup>¶</sup> Cristina Picci,<sup>¶</sup> Kseniya Ustinova, Veronick Benoy, Zsófia Kutil, Guiping Zhang, Maurício T. Tavares, Jiří Pavlíček, Chad A. Zimprich, Matthew B. Robers, Ludo Van Den Bosch, Cyril Bařinka,\* Brett Langley,\* and Alan P. Kozikowski\*



Cite This: *J. Med. Chem.* 2021, 64, 4810–4840



Read Online

ACCESS |



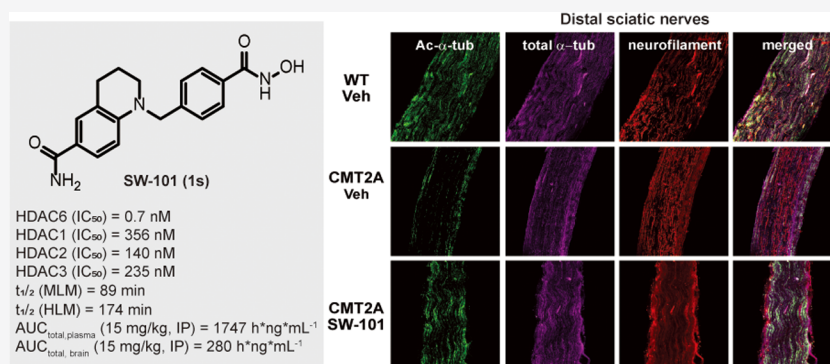
Metrics & More



Article Recommendations



Supporting Information



**ABSTRACT:** Histone deacetylase 6 (HDAC6) is a promising therapeutic target for the treatment of neurodegenerative disorders. SW-100 (**1a**), a phenylhydroxamate-based HDAC6 inhibitor (HDAC6i) bearing a tetrahydroquinoline (THQ) capping group, is a highly potent and selective HDAC6i that was shown to be effective in mouse models of Fragile X syndrome and Charcot–Marie–Tooth disease type 2A (CMT2A). In this study, we report the discovery of a new THQ-capped HDAC6i, termed SW-101 (**1s**), that possesses excellent HDAC6 potency and selectivity, together with markedly improved metabolic stability and druglike properties compared to SW-100 (**1a**). X-ray crystallography data reveal the molecular basis of HDAC6 inhibition by SW-101 (**1s**). Importantly, we demonstrate that SW-101 (**1s**) treatment elevates the impaired level of acetylated  $\alpha$ -tubulin in the distal sciatic nerve, counteracts progressive motor dysfunction, and ameliorates neuropathic symptoms in a CMT2A mouse model bearing mutant *MFN2*. Taken together, these results bode well for the further development of SW-101 (**1s**) as a disease-modifying HDAC6i.

## INTRODUCTION

The histone deacetylases (HDACs) are a class of proteins responsible for the hydrolytic removal of acetyl groups from acetylated lysine  $\epsilon$ -amino groups on the histone tails. The inhibition of HDACs has served as a practical therapeutic approach for cancer therapy based on the successful launch of five pan-HDAC inhibitors on the global market.<sup>1</sup> However, broad-spectrum HDAC inhibitory activities may be associated with various adverse effects and toxicities that could limit the application in indications where long-term drug treatment is required, such as neurodegenerative disorders and auto-immune diseases.<sup>1</sup> To date, 18 known mammalian HDACs have been identified that can be divided into Zn<sup>2+</sup>-dependent (classes I, IIa, IIb, IV) and NAD<sup>+</sup>-dependent (class III) families. It has been found that several HDAC isoforms are capable of modulating the acetylation status of nonhistone proteins, thereby affecting a variety of cellular functions without influencing the acetylation status of chromatin.<sup>2,3</sup>

Among them, the cytoplasmic class IIb HDAC6 exhibits unique characteristics.<sup>4</sup> It contains tandem catalytic domains (CD1 and CD2), a C-terminal zinc finger ubiquitin-binding domain (ZnF-UBP), and an N-terminal microtubule-binding domain (MBD).<sup>5</sup> Moreover, its CD1 has been shown to have negligible deacetylase activity on substrates with internal lysine residues,<sup>6,7</sup> while CD2 is primarily responsible for the deacetylation of a host of HDAC6 nonhistone substrates, including  $\alpha$ -tubulin, heat shock protein 90, peroxiredoxin, cortactin, survivin, and  $\beta$ -catenin.<sup>8</sup> In addition, the zinc finger

Received: December 21, 2020

Published: April 8, 2021



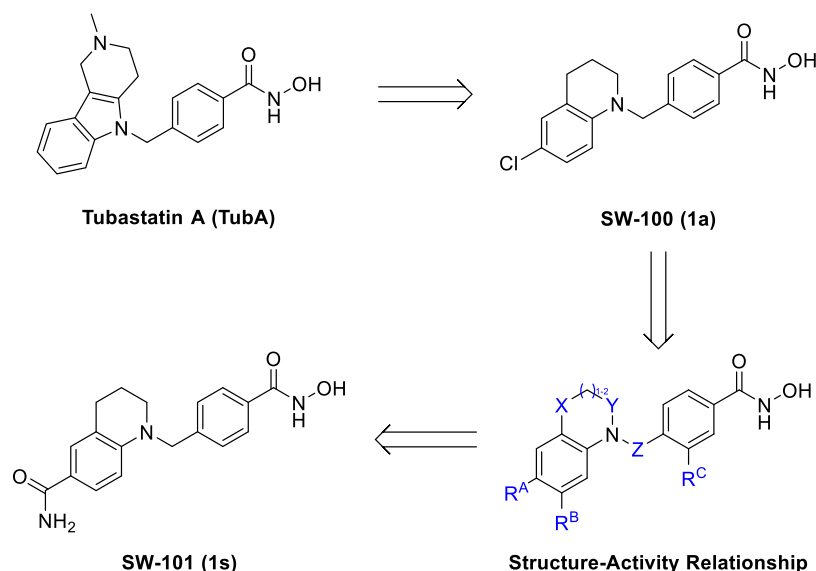


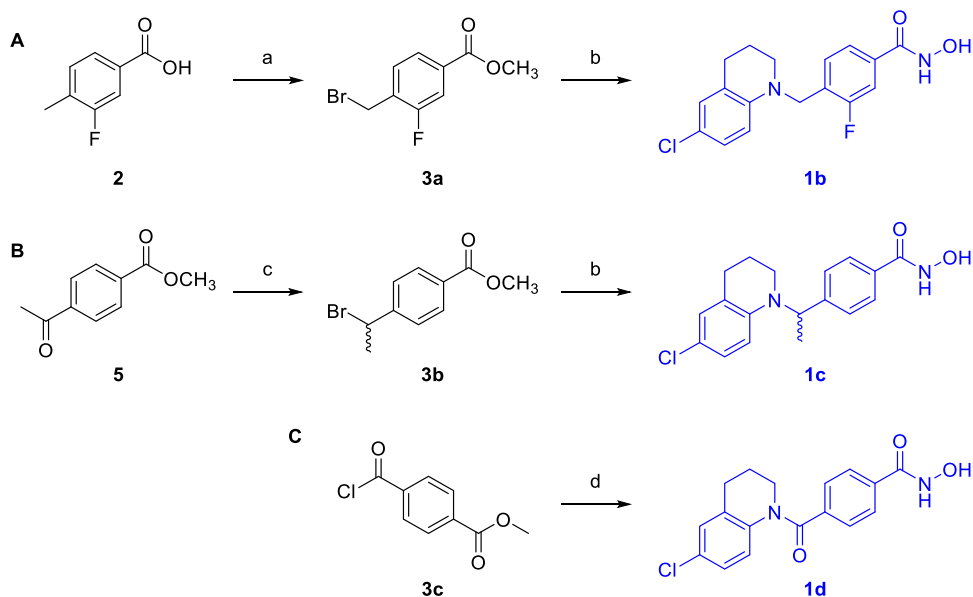
**Figure 1.** Structures of selective HDAC6is Tubastatin A (TubA), SW-100 (1a), and SW-101 (1s).

domain binds ubiquitin with high affinity, which participates in protein clearance and degradation via the aggresomal pathway.<sup>9</sup>  $\alpha$ -Tubulin was one of the first substrates of cytoplasmic HDAC6 to be identified. It has been extensively demonstrated that the pharmacological inhibition of HDAC6 enhances the level of acetylated  $\alpha$ -tubulin (Ac- $\alpha$ -tub) at lysine 40 and thereby restores the impaired mitochondrial axonal transport observed in models of neurodegenerative disorders.<sup>10</sup> As defective  $\alpha$ -tubulin acetylation has been observed in various neurodegenerative conditions, including Alzheimer's disease (AD),<sup>11,12</sup> Charcot–Marie–Tooth disease (CMT),<sup>13–15</sup> amyotrophic lateral sclerosis,<sup>16</sup> Rett syndrome,<sup>17</sup> and Fragile X syndrome (FXS),<sup>18</sup> selective inhibition of HDAC6 may provide a potential therapeutic intervention for these diseases. Although the discovery of novel HDAC6 inhibitors (HDAC6is) has become an attractive area of research in the past decade, only a limited number of druglike candidates have been investigated and shown to possess efficacy in animal models of neurodegenerative disorders.<sup>19</sup>

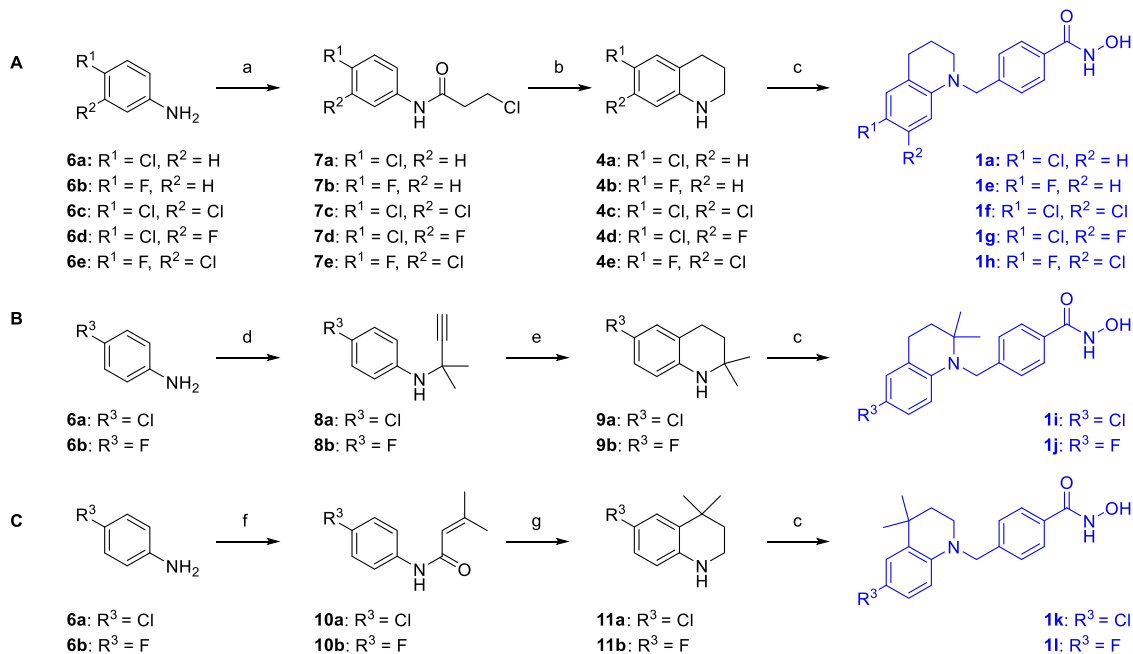
CMT disease is classified as a group of hereditary motor and sensory neuropathies<sup>20</sup> and is the most common inherited peripheral neuropathy. It affects about 17–40 per 100 000 individuals, who usually experience progressive loss of sensation and muscle atrophy due to the damage of the peripheral nerves over time.<sup>21</sup> No effective disease-modifying therapies are currently available on the market for CMT. Different electrophysiological characteristics divide CMT into two major subgroups: demyelinating-type CMT1 and axonal-type CMT2. It has been demonstrated recently that various genetic forms of CMT2 might originate through similar pathogenic mechanisms consisting of impaired  $\alpha$ -tubulin acetylation and defective axonal transport.<sup>22</sup> The intraperitoneal (IP) injection of the selective HDAC6i Tubastatin A (TubA, Figure 1, 25–50 mg/kg) was shown to have some positive effects in various animal models of neurodegenerative diseases.<sup>19,23,24</sup> Significantly, in mutant heat shock protein  $\beta$ -1-induced CMT type 2F (CMT2F) models<sup>13</sup> and mutant glycyl-tRNA synthetase-induced CMT type 2D (CMT2D) models,<sup>14,15</sup> TubA treatment restored the impaired levels of Ac- $\alpha$ -tub in sciatic nerves, rescued defective axonal transport, and ameliorated the CMT phenotypes. Moreover, other recent

studies have shown that the clinical-stage selective HDAC6i, CKD-504, improved myelination both in Schwann cells from CMT1A patients and in the sciatic nerves of C22 mice. Additionally, this HDACi reversed both the behavioral and electrophysiological phenotypes in the C22 mouse model of CMT1A.<sup>25</sup> These results thus support the potential of selective HDAC6is as therapeutic interventions for different types of CMT.

SW-100 (1a, Figure 1) is a phenylhydroxamate-based HDAC6i bearing a 6-chloro-1,2,3,4-tetrahydroquinoline moiety as its capping group,<sup>18</sup> which was designed by simplification of the tricyclic-capped HDAC6i, TubA. In our previous work,<sup>18</sup> it was found that SW-100 (1a) exhibited low nanomolar potency for the inhibition of HDAC6 with at least a thousand-fold selectivity over all other Class I, II, and IV HDAC isoforms. This compound also demonstrated significantly improved brain penetrance relative to TubA. Like TubA, SW-100 (1a) has shown robust ameliorative actions in CMT. CMT type 2A (CMT2A) is the most common axonal form of CMT2, accounting for 20% of CMT2, caused by mutations in the mitofusin 2 (*MFN2*) gene on chromosome 1p36.<sup>26</sup> In the *MFN2*<sup>R94Q</sup>-induced mouse model of CMT2A, SW-100 (20 mg/kg, twice a day, IP) was found to reverse  $\alpha$ -tubulin acetylation defects in distal parts of nerves and to ameliorate motor and sensory dysfunction.<sup>27</sup> In addition to CMT, therapeutic efficacy of SW-100 (1a) has been examined in a mouse model of Fragile X syndrome (FXS). FXS is a genetic condition caused by a full mutation of the fragile X mental retardation 1 (*FMR1*) gene, with a prevalence of 1 per 3000–4000 individuals in males. Symptoms of FXS include learning difficulty, cognitive impairment, and specific physical features.<sup>28</sup> In an *Fmr1*<sup>-/-</sup> mouse model of the intellectual deficiencies associated with FXS, SW-100 (20 mg/kg, twice a day, IP) selectively restored the impaired Ac- $\alpha$ -tub levels in the hippocampus and improved memory and learning impairments in mice.<sup>18</sup> In further support of the advancement of this particular HDAC6i, SW-100 (1a) exhibited negative results (1.5–1000  $\mu$ g/well) in the Ames test consisting of four strains of *Salmonella typhimurium* (TA98, TA100, TA1535, and TA1537) and one strain of *Escherichia coli* (WP2 uvrA) under the conditions with/without S9 liver fraction,<sup>18</sup>

Scheme 1. Synthesis Routes to 1b–d<sup>a</sup>

<sup>a</sup>Reagents and conditions. (a) (i)  $\text{CH}_3\text{I}$ ,  $\text{K}_2\text{CO}_3$ , *N,N*-dimethylformamide (DMF), rt; (ii) NBS, AIBN,  $\text{CCl}_4$ , 80 °C; (b) (i) 6-chloro-1,2,3,4-tetrahydroquinoline (**4a**),  $\text{K}_2\text{CO}_3$ , DMF, 100 °C; (ii) NaOH, 50 wt % aq.  $\text{NH}_2\text{OH}$ , THF/MeOH (1:1, v/v), 0 °C to rt; (c) (i)  $\text{NaBH}_4$ , EtOH, 0 °C; (ii)  $\text{CBr}_4$ ,  $\text{PPh}_3$ , dichloromethane (DCM), 0 °C to rt; (d) (i) **4a**, triethylamine (TEA), DCM, 0 °C; (ii) NaOH, 50 wt % aq.  $\text{NH}_2\text{OH}$ , THF/MeOH (1:1, v/v), 0 °C to rt.

Scheme 2. Synthetic Routes to SW-100 (**1a**) and 1e–l<sup>a</sup>

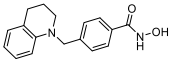
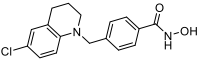
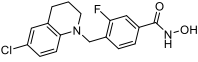
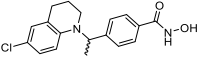
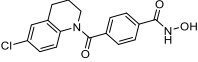
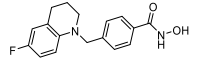
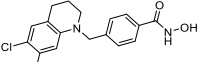
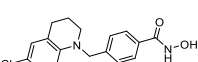
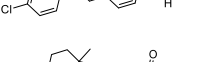
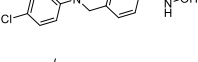
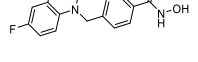
<sup>a</sup>Reagents and conditions. (a) 3-Chloropropanoyl chloride, acetone, reflux; (b) (i)  $\text{AlCl}_3$ , 140 °C (neat); (ii)  $\text{LiAlH}_4$ , THF, 0 °C to reflux; (c) (i) **3d**,  $\text{K}_2\text{CO}_3$ , DMF, 100 °C; (ii) NaOH, 50 wt % aq.  $\text{NH}_2\text{OH}$ , THF/MeOH (1:1, v/v), 0 °C to rt; (d) 3-chloro-3-methyl-1-butene, Cu/CuI, TEA, THF, rt; (e) (i)  $\text{CuCl}$ , THF, 120 °C (MW); (ii)  $\text{H}_2$ , Pd/C (10 wt %), EtOAc, rt; (f) 3,3-dimethylacryloyl chloride,  $\text{CHCl}_3$ , reflux; (g) (i)  $\text{AlCl}_3$ , toluene, 80 °C; (ii)  $\text{LiAlH}_4$ , THF, 0 °C to reflux.

suggesting that SW-100 (**1a**) has the potential to be a nonmutagenic hydroxamate-based HDAC6i, which would be beneficial for its application in neurodegenerative disorders.<sup>1</sup> However, SW-100 (**1a**) was found to be metabolically unstable in liver microsomes and hepatocytes ( $t_{1/2} < 30$  min), a property that would be responsible for limited drug concentrations and accordingly high clearance rates in the

brain and plasma.<sup>18</sup> SW-100 (**1a**) was thus dosed twice a day to achieve adequate drug exposure in the above-mentioned animal studies.<sup>18,27</sup>

Encouraged by the *in vivo* efficacy of SW-100 (**1a**), we designed and synthesized new HDAC6is derived from the scaffold of SW-100 (**1a**) and performed structure–activity relationship (SAR) studies (Figure 1). One of these analogues,

Table 1. HDAC1/6 Inhibition by THQ-Based HDAC6is 1a–l<sup>ad</sup>

Compound	Structure	Enzyme Inhibition (IC <sub>50</sub> , nM)		Selectivity Index <sup>b</sup>
		HDAC6	HDAC1	HDAC1/6
1 <sup>b</sup>		15	11,000	733
1a (SW-100)		2.9 ± 0.0	5230 ± 40	1803
1b		12.4 ± 5.5	21,200 ± 1150	1710
1c		383 ± 21	8430 ± 30	22
1d		961 ± 15	10,500 ± 6,710	11
1e		5.1 ± 0.2	5240 ± 45	1027
1f		3.6 ± 0.1	2620 ± 115	728
1g		4.8 ± 0.8	3220 ± 85	670
1h		3.4 ± 0.3	1870 ± 5	550
1i		328 ± 4.8	19,550 ± 700	60
1j		161 ± 3	14,100 ± 1,900	88
1k		37.8 ± 16	19,600 ± 2,450	519
1l		45.1 ± 0.1	21,100 ± 800	468
NexA <sup>c</sup>		5.1 ± 0.6	2186	572
TSA <sup>d</sup>	-	1.5 ± 0.2	16.8 ± 1.5	11

<sup>a</sup>IC<sub>50</sub> values are the mean of two experiments ± standard errors (SEM) obtained from curve-fitting of a 10-point enzymatic assay starting from 30 μM with 3-fold serial dilution against HDAC1 and HDAC6 (Reaction Biology Corp, Malvern, PA). An acetylated, fluorogenic peptide derived from residues 379–382 of p53 (RHKKAc, 50 μM) was used as a substrate in these assays. <sup>b</sup>Compound 1 was reported as compound 5 in ref 29. <sup>c</sup>The enzymatic data for selective HDAC6i Nexturastat A (NexA) determined under the same conditions were extracted from ref 18. <sup>d</sup>Pan-HDACi Trichostatin A (TSA) was used as a positive control.

termed SW-101 (1s), overcomes the metabolic stability issue while retaining excellent HDAC6 potency and selectivity in both enzymatic and cellular assessments. Structural character-

ization of SW-101 (1s) in a complex with the catalytic domain 2 of *Danio rerio* HDAC6 (zHDAC6-CD2) reveals the basis for its HDAC6 inhibition. Absorption, distribution, metabolism,

Table 2. Tubulin/Histone Acetylation State Evaluation of Selected THQ-Based HDAC6is<sup>a</sup>

compd	ratio Ac- $\alpha$ -tub/ $\alpha$ -tub (1 $\mu$ M inhibitor)				ratio Ac- $\alpha$ -tub/ $\alpha$ -tub (0.01 $\mu$ M inhibitor)				ratio Ac-H3/H4 (1 $\mu$ M inhibitor)			
	n	mean	SEM	Dunnett	n	mean	SEM	Dunnett	n	mean	SEM	Dunnett
vehicle	6	0.20	0.01	*	6	0.81	0.10	ns	8	1.00	0.00	
SW-100	3	1.00	0.00		3	1.00	0.00		4	1.21	0.19	ns
1b	3	1.38	0.16	ns	3	1.21	0.07	ns	4	1.10	0.15	ns
1e	3	1.37	0.22	ns	3	1.36	0.13	ns	4	1.18	0.12	ns
1f	3	1.54	0.27	ns	3	1.38	0.15	ns	4	1.32	0.17	ns
1g	3	1.50	0.26	ns	3	1.16	0.12	ns	4	1.22	0.14	ns
1h	3	1.53	0.28	ns	3	1.14	0.15	ns	4	1.31	0.13	ns
TubA	3	1.30	0.18	ns	3	0.91	0.27	ns	4	1.01	0.09	ns
TSA	3	1.88	0.37	*	n/d <sup>b</sup>	n/d	n/d	n/a <sup>c</sup>	4	7.99	2.83	****

<sup>a</sup>All compounds were tested at 1 and 0.01  $\mu$ M. The acetylation state of  $\alpha$ -tubulin and histone was quantified by Western blot. Ratios of acetylated  $\alpha$ -tubulin (Ac- $\alpha$ -tub) and  $\alpha$ -tubulin ( $\alpha$ -tub) were normalized to the SW-100 group. Ratios of acetylated histone H3 (Ac-H3) and histone H4 (H4) were normalized to the vehicle group. TSA and TubA were tested as positive controls. Dunnett's multiple comparison test. \* $p$  < 0.05, \*\*\*\* $p$  < 0.0001. <sup>b</sup>n/d, not determined. <sup>c</sup>n/a, not applied.

excretion, and toxicity (ADMET) evaluation shows significantly improved druglike properties relative to the parent compound SW-100 (1a). We demonstrate that SW-101 (20 mg/kg, once a day, IP), whether administered before or after the onset of symptoms, elevates the level of Ac- $\alpha$ -tub in the distal sciatic nerve, counteracts progressive motor dysfunction, and ameliorates neuropathic symptoms in mutant *MFN2*-induced CMT2A mice.

## RESULTS AND DISCUSSION

**Synthesis and Biological Evaluation of Analogues 1b–l.** The SAR studies started from the exploration of different substituents (e.g., halogen and methyl groups) on the tetrahydroquinoline (THQ) capping group and the benzyl linker of SW-100 (1a) to examine their influence on HDAC6 activity and selectivity,  $\alpha$ -tubulin/histone acetylation, and metabolic stability of the inhibitor.

To synthesize 1b, which contains a fluorine atom on the linker's phenyl ring (Scheme 1A), the bromomethyl benzoate 3a was initially obtained via a two-step procedure according to the methods developed previously,<sup>29</sup> consisting of esterification of commercially available 3-fluoro-4-methylbenzoic acid (2) with iodomethane and free-radical bromination with *N*-bromosuccinimide (NBS) catalyzed by azobisisobutyronitrile (AIBN). These steps were then followed by an efficient alkylation reaction with 6-chloro-1,2,3,4-tetrahydroquinoline (4a, Scheme 2A).<sup>18</sup> The resulting ester intermediate was converted in turn to the desired hydroxamate analogue 1b upon treatment with aqueous  $\text{NH}_2\text{OH}/\text{NaOH}$  solution. To synthesize 1c containing an additional methyl group in the benzylic position (Scheme 1B), commercially available methyl 4-acetylbenzoate (5) was subjected to reduction using  $\text{NaBH}_4$  and then bromination under  $\text{CBr}_4/\text{PPh}_3$  conditions to afford 3b. This intermediate was then reacted with 4a and transformed to the hydroxamate using the same procedure as above to afford 1c. To prepare 1d bearing a carbonyl group on the benzylic position (Scheme 1C), commercially available methyl 4-(chlorocarbonyl)benzoate (3c) was reacted with 4a to form the corresponding ester intermediate, which upon treatment with aqueous hydroxylamine afforded 1d.

To prepare 1e–1h bearing different halogens on the capping group (Scheme 2A), the synthetic route to SW-100 (1a) published previously was followed.<sup>18</sup> Several commercially available anilines 6a–e were first converted to the phenylpropanamides 7a–e by reaction with 3-chloropropanoyl

chloride. In turn, these were converted to their lactams via an intramolecular Friedel–Crafts acylation reaction followed by reduction using  $\text{LiAlH}_4$  to provide the desired THQ building blocks 4a–e. These intermediates were then alkylated with commercially available methyl 4-(bromomethyl)benzoate (3d) to give the corresponding ester precursors, which afforded the desired hydroxamates 1e–h as well as SW-100 (1a) using similar methods to those described above. To synthesize 1i and 1j bearing two methyl groups at the C-2 position of the THQ moiety (Scheme 2B), anilines 6a and 6b were first converted to the alkyne intermediates 8a and 8b by reaction with 3-chloro-3-methyl-1-butyne catalyzed by  $\text{Cu}/\text{CuI}$  under basic conditions. 8a and 8b then underwent cyclization under microwave conditions followed by hydrogenation to form the THQ compounds 9a and 9b. Further transformation of 9a and 9b to the hydroxamates 1i and 1j was performed as above. To synthesize 1k and 1l bearing two methyl groups at the C-4 position of their THQ moiety (Scheme 2C), anilines 6a and 6b were reacted with 3,3-dimethylacryloyl chloride under reflux to afford the amide intermediates 10a and 10b, respectively. 10a and 10b then underwent cyclization catalyzed by  $\text{AlCl}_3$  and reduction with  $\text{LiAlH}_4$  to afford THQ compounds 11a and 11b, whose transformation to the hydroxamates 1k and 1l was carried out in the same way.

The new analogues 1b–f were evaluated for their ability to inhibit HDAC1 and HDAC6 along with the parent compound SW-100 (1a) (Table 1; performed by reaction biology). The initial SAR data revealed the following. (a) In comparison with compound 1 ( $\text{IC}_{50}$  = 15 nM; SI = 733-fold) that does not have any substituent on the THQ cap, analogues bearing a single chloro or fluoro group at the C6 position of the THQ moiety (1a and 1e) exhibited low nanomolar potency against HDAC6 and more than a thousand-fold selectivity over HDAC1 (SI = 1803- and 1027-fold). (b) An additional halogen substituent at the C7 position of the THQ moiety (1f, 1g, and 1h) maintained low nanomolar potency against HDAC6, while selectivity over HDAC1 was reduced to factors ranging in hundreds. (c) The incorporation of a fluorine atom on the benzyl linker (1b;  $\text{IC}_{50}$  = 12.4 nM; SI = 1710-fold) resulted in a 5.4-fold decrease in HDAC6 potency relative to SW-100 ( $\text{IC}_{50}$  = 2.9 nM; SI = 1803-fold) while retaining thousand-fold selectivity over HDAC1. (d) The presence of two methyl groups at either the C-2 or C-4 position of the cap group (1i–1l) caused a significant decrease in potency and selectivity. (e) The presence of a methyl or carbonyl group at the benzylic

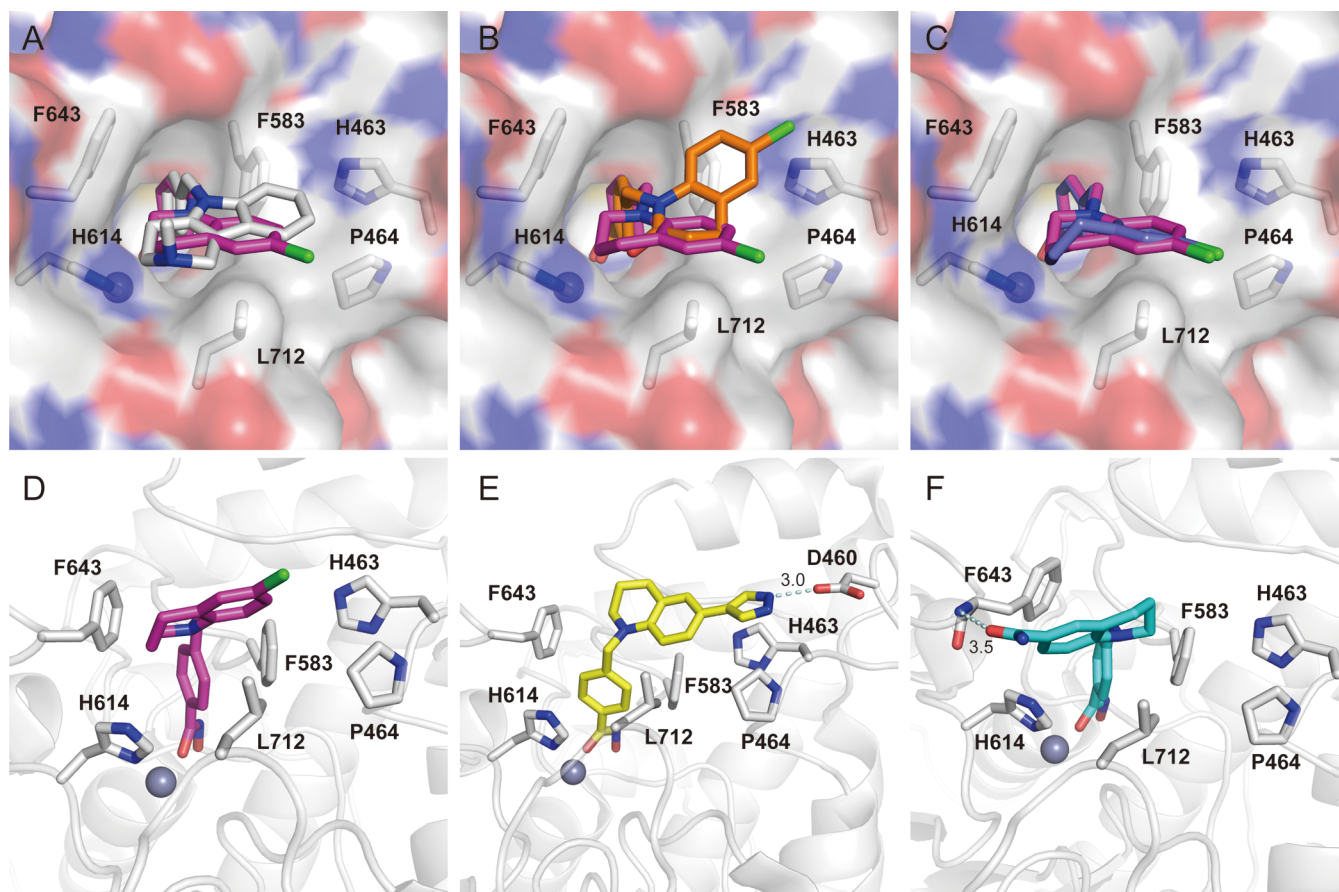


**Figure 2.** Molecular docking study results for the SW-100 derivatives based on the zHDAC6 crystal complex (PDB entry 6THV). (A–C) Superimposed docking poses of TubA (A), **1m** (B), and **18c** (C) with SW-100 (**1a**). (D–E) Docking poses of SW-100 (**1a**,+.00 D), **1q** (E), and **1s** (F).

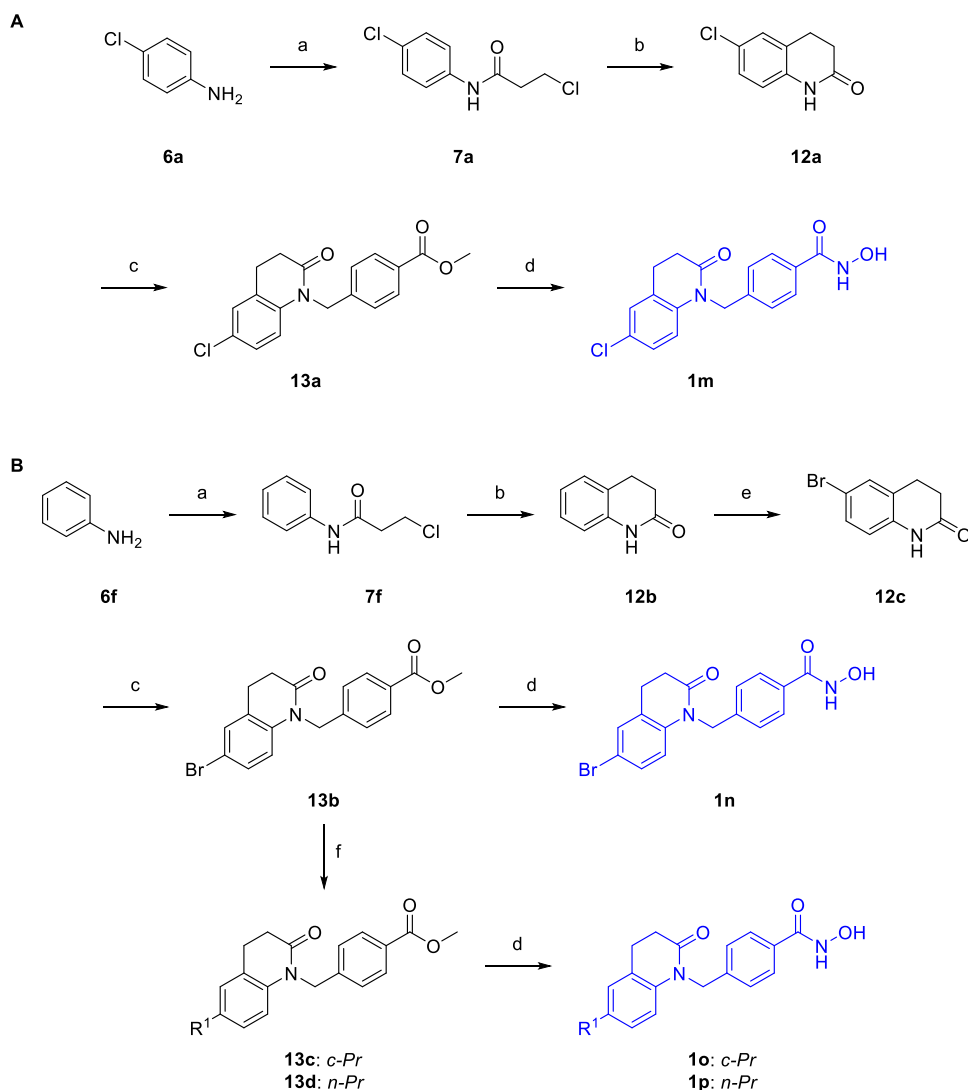
position (**1c** and **1d**) resulted in submicromolar activity against HDAC6. Overall, based on these SAR results, we established that the C6 position of THQ is a favorable position for modification, as the corresponding compounds retain both low nanomolar HDAC6 potency and a thousand-fold selectivity over HDAC1. However, it should be noted that among these newly developed THQ-capped HDAC6is, the parent compound SW-100 (**1a**) still exhibited the best HDAC6 potency and the highest selectivity over HDAC1.

Based on the *in vitro* inhibitory data (Table 1), THQ-capped HDAC6is bearing different halogens (**1b**, **1e**, **1f**, **1g**, and **1h**) that maintained low nanomolar HDAC6 potency ( $IC_{50} < 20$  nM) and over 500-fold selectivity ( $SI > 500$ -fold) were evaluated along with SW-100 (**1a**) in N2a cells (Table 2 and Figure S1). TubA and trichostatin A (TSA) were included as positive controls. Levels of Ac- $\alpha$ -tub and acetylated histone 3 (Ac-H3) were quantified to investigate the selectivity of the newly developed analogues for HDAC6 and class I HDACs, respectively, and these data were normalized to SW-100 and vehicle groups, respectively. In comparison with SW-100 (**1a**), all of the selected HDAC6is exhibited slightly enhanced abilities to promote  $\alpha$ -tubulin acetylation, ranging from 1.14-fold to 1.53-fold at both high ( $1 \mu M$ ) and low ( $0.01 \mu M$ ) test concentrations. As is known for the HDAC6i TubA, all of these THQ-based analogues did not significantly increase the level of Ac-H3 ( $< 1.5$ -fold) relative to the vehicle group at the concentration of  $1 \mu M$ . As histones are deacetylated predominantly by class I HDAC isoforms, these cellular results

demonstrate that the functional selectivity of these newly developed HDAC6is along with SW-100 (**1a**) is consistent with their excellent selectivity over HDAC1 in the enzymatic assays.

Previously, we found that SW-100 (**1a**) possesses a short half-life ( $t_{1/2} < 30$  min) in both liver microsomes and hepatocytes.<sup>18</sup> For this reason, compounds **1**, **1b**, **1e**, **1g**, **1i**, and **1k** were assessed for their metabolic stability in mouse and human liver microsomes (Table 5). Unfortunately, only compound **1** lacking any substituent showed an acceptable half-life in both mouse ( $t_{1/2} = 40$  min) and human ( $t_{1/2} = 182$  min) liver microsomes (Table 5). In contrast, the half-lives of **1b**, **1e**, **1g**, **1i**, and **1k** were even shorter than those of SW-100. Therefore, these results indicate that a halogen substituent at the C6 position is not favorable for optimizing metabolic stability.

**Synthesis and Biological Evaluation of Analogues 1m–s and 18a–g.** It has been reported that the THQ moiety can be metabolized to a quinolinium species in human liver microsomes, a reaction that is catalyzed primarily by CYP3A4.<sup>30</sup> Moreover, a recent metabolite analysis revealed that <sup>18</sup>F-labeled THQ-based hydroxamate **1e** was rapidly metabolized to the corresponding carboxylate in mouse plasma within 15 min, while about 80% of the intact compound remained in the mouse brain after 30 min.<sup>31</sup> In addition, it has been reported that different capping groups and liners may influence the hydrolysis rate of the hydroxamate in plasma.<sup>32</sup> Therefore, to increase the metabolic stability of the series while

Scheme 3. Synthetic Routes to 1m–p<sup>a</sup>

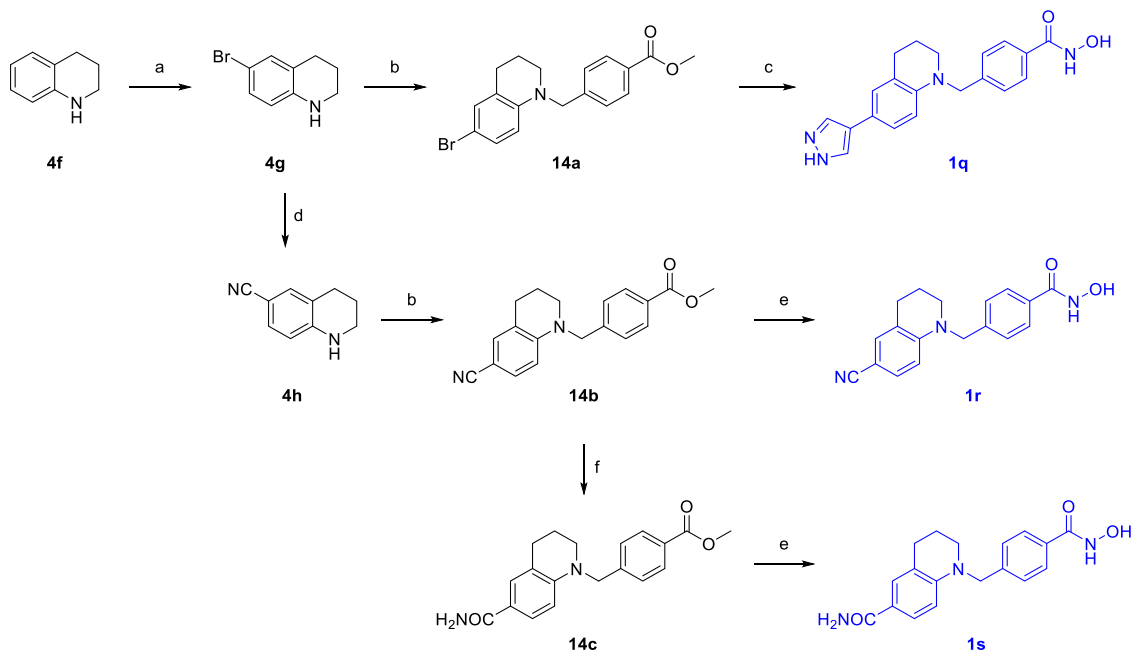
<sup>a</sup>Reagents and conditions. (a) 3-Chloropropanoyl chloride, acetone, reflux; (b)  $\text{AlCl}_3$ , 140 °C (neat); (c) 3d, NaH (60% dispersion in oil), DMF, 0 °C to rt; (d) NaOH, 50 wt % aq.  $\text{NH}_2\text{OH}$ , THF/MeOH (1:1, v/v), 0 °C to rt; (e) NBS, DMF, 0 °C; (f) cyclopropylboronic acid or *n*-propylboronic acid,  $\text{Pd}(\text{PPh}_3)_4$ ,  $\text{Cs}_2\text{CO}_3$ , toluene/ $\text{H}_2\text{O}$  (10:1, v/v), 140 °C (MW).

retaining HDAC6 potency and selectivity, we further investigated 3,4-dihydroquinolin-2-one analogues **1m–p**, a carbonyl group at the C-2 position, additional THQ analogues **1q–s** containing a nonhalogen substituent at the C6 position, and tetrahydro-1-benzazepine (THB)-capped analogues **18a–g** containing a 7-membered ring system.

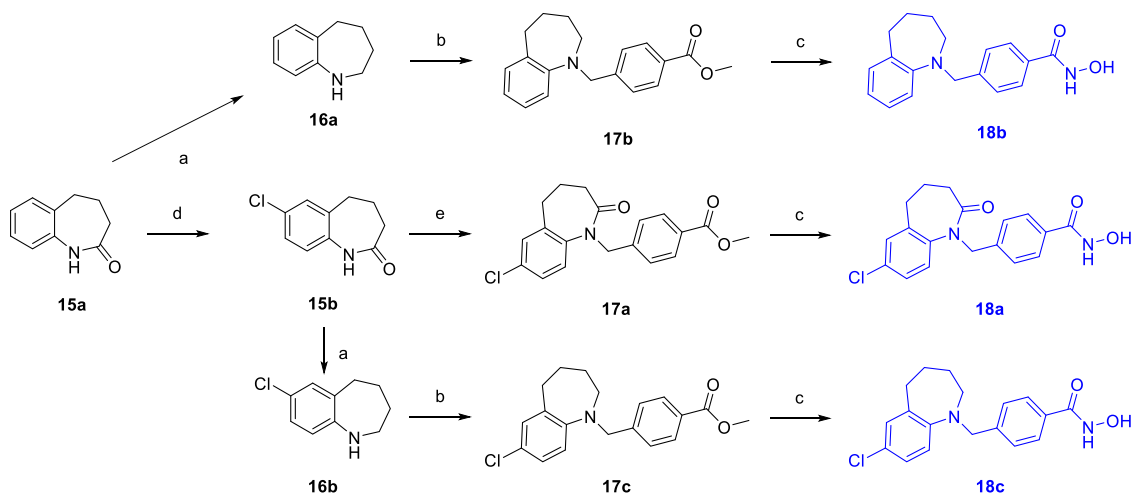
Molecular docking studies were carried out to investigate their docking poses in the active site of HDAC6 using the zHDAC6-CD2/TubA crystal complex (PDB entry 6THV)<sup>24</sup> as a template. The results indicate that the capping group of SW-100 (**1a**) exhibits comparable hydrophobic interactions with the pocket rim relative to TubA (Figure 2A), while the presence of the C-2 carbonyl group (**1m**) pushes the bicyclic ring toward the L1-loop pocket<sup>33,34</sup> defined by H463, P464, F583, and L712 (Figure 2B). Moreover, the enlarged THB ring system (**18c**) shows a similar docking pose to SW-100 (**1a**), while the extra methylene group may provide more flexibility (Figure 2C). It has been recently demonstrated that the additional hydrogen-binding interactions between the ligand and the key residues may improve HDAC6 potency;<sup>35</sup>

we thus designed THQ analogues **1q** and **1s** bearing pyrazole and carboxamide, respectively, at their C6 positions. The docking results suggest that, compared to SW-100 (**1a**, Figure 2D), **1q** forms an additional hydrogen bond with D460 (Figure 2E), while **1s** shows an extra interaction with the main chain of F643 (Figure 2F).

To prepare lactam analogues **1m–p** (Scheme 3), 3,4-dihydroquinolin-2(1H)-ones **12a** and **12b** were prepared following the procedure used in the synthesis of **4a** with the omission of the reduction step. **12b** was further converted to **12c** through bromination with NBS in DMF. Lactam intermediates **12a** and **12c** bearing different halogens were subject to a two-step procedure consisting of efficient alkylation with commercial methyl 4-(bromomethyl)benzoate (**3d**) under NaH/DMF conditions to provide the corresponding esters and transformation to hydroxamates **1m** and **1n** under the same basic conditions as above. Moreover, the ester intermediate **13b** reacted with cyclopropyl or *n*-propyl boronic acid catalyzed by  $\text{Pd}_2(\text{dba})_3/\text{Cs}_2\text{CO}_3$  under microwave heating to generate intermediates **13c** and **13d** (Scheme 3B), which

Scheme 4. Synthetic Routes to 1q–s<sup>a</sup>

<sup>a</sup>Reagents and conditions. (a) NBS, DMF, 0 °C; (b) **3d**, K<sub>2</sub>CO<sub>3</sub>, DMF, 100 °C; (c) (i) 4-pyrazoleboronic acid pinacol ester, Pd(PPh<sub>3</sub>)<sub>4</sub>, K<sub>2</sub>CO<sub>3</sub>, dioxane/H<sub>2</sub>O (10:1, v/v), reflux; (ii) NaOH, 50 wt % aq. NH<sub>2</sub>OH, THF/MeOH (1:1, v/v), 0 °C to rt; (d) Zn(CN)<sub>2</sub>, Pd<sub>2</sub>(dba)<sub>3</sub>, S-Phos, DMF/H<sub>2</sub>O (99:1), 170 °C (MW); (e) NaOH, 50 wt % aq. NH<sub>2</sub>OH, THF/MeOH (1:1, v/v), 0 °C to rt; (f) K<sub>2</sub>CO<sub>3</sub>, H<sub>2</sub>O<sub>2</sub>, dimethyl sulfoxide (DMSO), 0 °C to rt.

Scheme 5. Synthetic Routes to 18a–c<sup>a</sup>

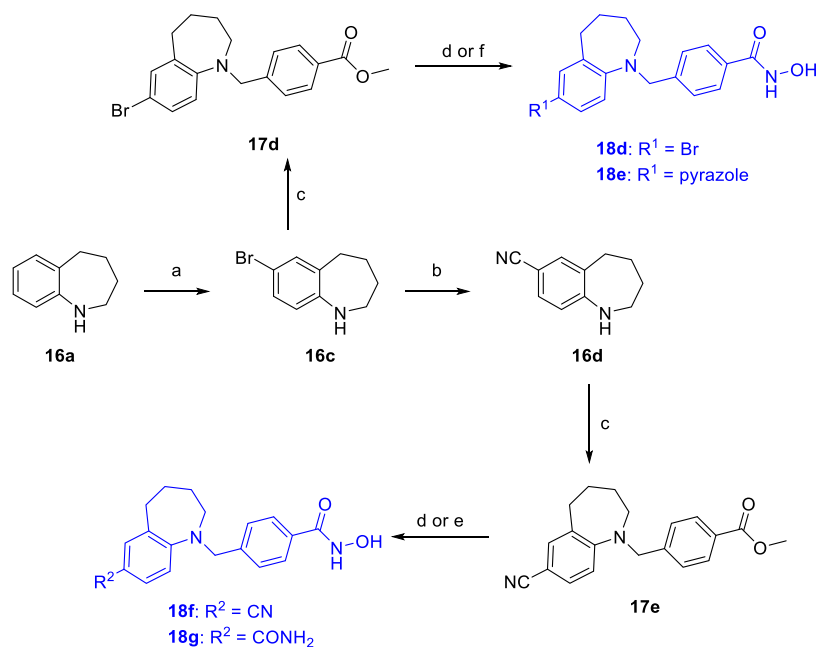
<sup>a</sup>Reagents and conditions. (a) LiAlH<sub>4</sub>, THF, 0 °C to reflux; (b) **3d**, K<sub>2</sub>CO<sub>3</sub>, DMF, 80 °C; (c) NaOH, 50 wt % aq. NH<sub>2</sub>OH, THF/MeOH (1:1, v/v), 0 °C to rt; (d) SO<sub>2</sub>Cl<sub>2</sub> (1.0 M in DCM), toluene, 0 °C to rt; (e) **3d**, NaH (60% dispersion in oil), DMF, 0 °C to rt.

upon the same formation of hydroxamate afforded analogues **1o** and **1p** containing cyclopropyl and *n*-propyl group at the C6 position, respectively.

To prepare the additional THQ-based HDAC6is **1q–s** (Scheme 4), 1,2,3,4-tetrahydroquinoline (**4f**) was first converted to 6-bromo-1,2,3,4-tetrahydroquinoline (**4g**) with NBS in DMF. Compound **4g** was coupled with methyl 4-(bromomethyl)benzoate (**3d**) to provide the ester intermediate **14a**, followed by the Suzuki coupling reaction with 4-pyrazoleboronic acid pinacol ester catalyzed by Pd(PPh<sub>3</sub>)<sub>4</sub>/K<sub>2</sub>CO<sub>3</sub> to afford an intermediate containing a 1*H*-pyrazol-4-yl group at the C6 position of the THQ moiety. Finally, the

desired hydroxamate **1q** was obtained employing the same conditions as mentioned above. On the other hand, compound **4g** was reacted with Zn(CN)<sub>2</sub> catalyzed by Pd<sub>2</sub>(dba)<sub>3</sub>/S-Phos under microwave heating to generate 1,2,3,4-tetrahydroquinoline-6-carbonitrile (**4h**). This intermediate was alkylated with **3d** to obtain the 6-cyano ester **14b**, part of which was hydrated to afford the 6-carbamylated ester **14c**. The subsequent transformation to the hydroxamates **1r** and **1s** was efficiently performed as above, starting from **14b** and **14c**, respectively.

The preparation of THB-based analogues **18a–c** (Scheme 5) was initiated by conversion of commercially available 4,5-dihydro-1*H*-benz[*b*]azepin-2(3*H*)-one (**15a**) to 2,3,4,5-tetra-

Scheme 6. Synthetic Routes to 18d–g<sup>a</sup>

<sup>a</sup>Reagents and conditions. (a) NBS, DMF, 0 °C; (b) Zn(CN)<sub>2</sub>, Pd<sub>2</sub>(dba)<sub>3</sub>, S-Phos, DMF/H<sub>2</sub>O (99:1, v/v), 170 °C (MW); (c) **3d**, K<sub>2</sub>CO<sub>3</sub>, DMF, 100 °C; (d) NaOH, 50 wt % aq. NH<sub>2</sub>OH, THF/MeOH (1:1, v/v), 0 °C to rt; (e) (i) K<sub>2</sub>CO<sub>3</sub>, H<sub>2</sub>O<sub>2</sub>, DMSO, 0 °C to rt; (ii) NaOH, 50 wt % aq. NH<sub>2</sub>OH, THF/MeOH (1:1, v/v), 0 °C to rt; (f) (i) 4-pyrazoleboronic acid pinacol ester, Pd(PPh<sub>3</sub>)<sub>4</sub>, K<sub>2</sub>CO<sub>3</sub>, dioxane/H<sub>2</sub>O (10:1, v/v), reflux; (ii) NaOH, 50 wt % aq. NH<sub>2</sub>OH, THF/MeOH (1:1, v/v), 0 °C to rt.

hydro-1*H*-benz[*b*]azepine (**16a**) with LiAlH<sub>4</sub> and to 7-chloro-4,5-dihydro-1*H*-benz[*b*]azepin-2(3*H*)-one **15b** with SO<sub>2</sub>Cl<sub>2</sub>. The chlorinated lactam **15b** was coupled with methyl 4-(bromomethyl)benzoate (**3d**) under NaH/DMF conditions followed by hydroxamate formation to provide **18a**. On the other hand, lactam **15b** was reduced with LiAlH<sub>4</sub> to afford the corresponding amine **16b**. Finally, the hydroxamates **18a–c** were prepared in the usual manner from the ester precursors **16a–c**.

To prepare additional THB-based HDAC6is **18d–g** (Scheme 6), 2,3,4,5-tetrahydro-1*H*-benz[*b*]azepine (**16a**) was first converted to the 7-bromo-2,3,4,5-tetrahydro-1*H*-benz[*b*]azepine (**16c**) with NBS in DMF. Compound **16c** was coupled with methyl 4-(bromomethyl)benzoate (**3d**) to provide ester intermediate **17d**, which underwent Suzuki coupling reaction with 4-pyrazoleboronic acid pinacol ester to afford an ester intermediate containing a 1*H*-pyrazol-4-yl substituent at the C7 position of the tetrahydrobenz[*b*]azepine ring system. These precursors were carried on efficiently to hydroxamates **18d** and **18e** as above. On the other hand, compound **16c** was reacted with Zn(CN)<sub>2</sub> to generate 2,3,4,5-tetrahydro-1*H*-benz[*b*]azepine-7-carbonitrile (**16d**), which was coupled with **3d** to provide the 7-cyano ester **17e**. Part of this material was hydrated to afford the 7-carbamyl ester. Both ester precursors upon treatment with aqueous hydroxylamine eventually afforded hydroxamates **18f** and **18g**.

The newly prepared analogues **1m–s** and **18a–g** were assessed for their inhibitory activity against HDAC1, HDAC6, and HDAC8 in-house along with SW-100 (IC<sub>50</sub> = 0.5 nM; HDAC1/6 = 1538-fold; HDAC8/6 = 6120-fold) under optimized experimental conditions<sup>36</sup> (Table 3). Lactam analogues **1m** and **1n** containing chlorine and bromine at the C6-position, respectively, retained comparable low nanomolar HDAC6 potency (IC<sub>50</sub> = 2.9 and 0.9 nM), while their

selectivities over HDAC1 (SI = 95- and 119-fold) and HDAC8 (SI = 718- and 826-fold) were noticeably reduced. On the other hand, the replacement of halogen with a cyclopropyl or *n*-propyl group, forming **1o** and **1p**, respectively, led to weakened HDAC6 inhibition (IC<sub>50</sub> = 2.7 and 12 nM) and dramatically reduced selectivity over HDAC1 (SI = 43- and 26-fold). The additional THQ-capped analogues **1q–s** bearing pyrazole, nitrile, or amide functionality exhibited comparable HDAC6 inhibition (IC<sub>50</sub> = 0.3–1.3 nM) relative to SW-100 (**1a**), while their selectivity over HDAC1 and HDAC8 was reduced. In analogy to our SAR studies in the THQ series, several functional groups were placed on the 7-membered THB ring system, forming compounds **18a–g**. The HDAC enzymatic results shown in Table 3 indicate that all THB-capped compounds retained nanomolar HDAC6 potency (IC<sub>50</sub> = 0.8–17 nM). However, their selectivity over HDAC1 and HDAC8 varied from 54- to 8644-fold. The potencies of **18d** and **18e** at HDAC6 were 18- and 34-fold lower compared to SW-100, respectively, indicating that their affinity for HDAC6 might be negatively impacted by the bulkier bromo or pyrazolyl substituents along with that of their 7-membered rings. Moreover, substituents other than halogens (e.g., pyrazolyl, cyano, and carbamyl) at the C7 position of THB (**18e–g**) resulted in significantly reduced selectivity over HDAC1 (SI = 54- to 64-fold). Notably, **18c**, the THB version of SW-100, showed 2-fold reduced HDAC6 potency (IC<sub>50</sub> = 1.0 nM) but was found to be the most selective HDAC6i (HDAC1/6 = 1900-fold and HDAC1/8 = 8644-fold) among all of these THQ and THB analogues. Overall, only two THQ analogues bearing a pyrazole (**1q**) and carboxamide (**1s**) functional group, respectively, and one THB analogue bearing chlorine (**18c**) demonstrated similar HDAC6 potency (IC<sub>50</sub> ≤ 1 nM) compared with the parent compound, SW-100, and maintained at least a 500-fold selectivity for HDAC6.

Table 3. HDAC1/6/8 Inhibition by 1m–s and 18a–g<sup>ab</sup>

Compound	Structure	Enzymatic activity (IC <sub>50</sub> , nM)			Selectivity Index	
		HDAC6	HDAC1	HDAC8	HDAC1/6	HDAC8/6
SW-100		0.5 ± 0.1	769 ± 1108	3060 ± 402	1538	6120
1m		2.9 ± 0.6	276 ± 133	2080 ± 193	95	718
1n		0.9 ± 0.1	107 ± 51	743 ± 76	119	826
1o		2.7 ± 0.7	117 ± 65	1500 ± 514	43	556
1p		12.0 ± 0.1	306 ± 57	2680 ± 1040	26	223
1q		0.3 ± 0.1	184 ± 33	792 ± 100	613	2640
1r		1.3 ± 0.6	141 ± 3	1490 ± 531	108	1146
1s		0.7 ± 0.3	356 ± 59	651 ± 134	509	930
18a		0.8 ± 0.1	126 ± 44	1170 ± 217	156	1463
18b		5.0 ± 3.5	1320 ± 414	5610 ± 2130	264	1122
18c		1.0 ± 0.5	1900 ± 906	8640 ± 780	1900	8640
18d		9 ± 12	1590 ± 596	4360 ± 2820	177	484
18e		17 ± 13	1080 ± 211	2820 ± 30	64	166
18f		4.6 ± 0.5	248 ± 44	2220 ± 463	54	482
18g		2.4 ± 1.5	150 ± 39	1060 ± 28	63	442
NexA <sup>b</sup>		1.6 ± 0.4	151 ± 20	988 ± 264	94	618
SAHA	-	6.7 ± 1.0	31 ± 12	1030	5	154

<sup>a</sup>IC<sub>50</sub> values are the mean of two experiments ± SEM calculated by nonlinear regression analysis from experimental  $v_i/v_0$  values for each HDAC isoform. Ac-GAK(Ac)-AMC (10 μM, HDAC1 and HDAC6) and Boc-Lys(TFA)-AMC (10 μM, HDAC8) were used as substrates in a fluorescence-based assay for IC<sub>50</sub> determination. Fourteen-point IC<sub>50</sub> curves were generated using a 3-fold inhibitor dilution series; inhibitor concentration ranges used: 100 μM to 0.063 pM for HDAC1 and HDAC8; and 3 μM to 1.88 pM for HDAC6. Pan-HDACi SAHA was used as a positive control. <sup>b</sup>The enzymatic data for selective HDAC6i Nexturstat A (NexA) determined under the same conditions were extracted from ref 35.

Table 4. Tubulin/Histone Acetylation State Evaluation of Selected THQ-Based and THB-Based HDAC6is<sup>a</sup>

compd	ratio Ac- $\alpha$ -tub/ $\alpha$ -tub (1 $\mu$ M inhibitor)				ratio Ac- $\alpha$ -tub/ $\alpha$ -tub (10 nM inhibitor)				ratio Ac-H3/H4 (1 $\mu$ M inhibitor)			
	<i>n</i>	mean	SEM	Dunnett	<i>n</i>	mean	SEM	Dunnett	<i>n</i>	mean	SEM	Dunnett
Veh	13	0.19	0.04	**	18	0.70	0.07	ns	14	1.00	0.00	n/a
TSA	10	1.76	0.27	*	n/d	n/d	n/d	n/a	10	37.23	14.35	***
TubA	10	1.11	0.13	ns	11	1.08	0.14	ns	10	0.93	0.21	ns
SW-100	10	1.00	0.00	n/a	11	1.00	0.00	n/a	10	0.97	0.18	ns
1m	3	1.51	0.10	ns	3	0.93	0.08	ns	3	5.56	1.09	ns
1q	3	2.14	0.18	**	3	2.65	0.46	***	3	3.96	1.31	ns
1s	6	1.82	0.22	*	6	1.45	0.19	ns	7	1.81	0.33	ns
18a	3	1.73	0.61	ns	4	2.81	0.22	****	2	2.52	1.29	ns
18b	3	0.78	0.20	ns	4	0.98	0.24	ns	2	0.62	0.17	ns
18c	3	0.55	0.19	ns	4	0.89	0.23	ns	2	0.71	0.30	ns
18e	3	1.78	0.20	ns	3	0.95	0.03	ns	3	2.52	1.08	ns
18f	3	0.98	0.26	ns	4	1.38	0.24	ns	2	0.70	0.36	ns
18g	3	1.19	0.37	ns	4	2.40	0.32	***	2	1.01	0.65	ns

<sup>a</sup>All compounds were tested at 1  $\mu$ M and 10 nM, and the acetylation of  $\alpha$ -tubulin and histone was quantified by Western blot. Ratios of Ac- $\alpha$ -tub to  $\alpha$ -tub were normalized to SW-100. Ratios of Ac-H3 and H4 were normalized to the vehicle. TSA and TubA were tested as positive controls. Dunnett's multiple comparison test. \* $p$  < 0.05, \*\* $p$  < 0.01, \*\*\* $p$  < 0.001, \*\*\*\* $p$  < 0.0001.

The ability of selected HDAC6is to influence the levels of Ac- $\alpha$ -tub and Ac-H3 were further evaluated in N2a cells (Table 4 and Figures S2–S4). Lactam analogues **1m** and **18a** exhibited improved ability to increase the level of Ac- $\alpha$ -tub at the concentration of 1  $\mu$ M relative to SW-100. Notably, a 2.81-fold improvement (normalized to SW-100) in the level of Ac- $\alpha$ -tub was observed after treatment with 0.01  $\mu$ M of **18a**. However, **1m** and **18a** also induced histone acetylation, resulting in a 5.56- and 2.52-fold increase in the level of Ac-H3 relative to the vehicle, respectively. A similar behavior was observed in the pair of pyrazole substituted HDAC6is **1q** and **18e**. Both compounds significantly increased the level of Ac- $\alpha$ -tub using test concentrations of 1 and 0.01  $\mu$ M while also strongly elevating the level of Ac-H3 (3.96- and 2.52-fold) normalized to the vehicle. The carboxamide-substituted HDAC6is **1s** and **18g** displayed an enhanced ability to improve the level of Ac- $\alpha$ -tub at both concentrations in comparison with SW-100. On the other hand, the levels of Ac-H3 relative to the vehicle group were also increased by 1.81- and 2.52-fold, respectively. In addition, the selected THB analogues **18b**, **18c**, and **18f** showed comparable effects on the levels of Ac- $\alpha$ -tub and Ac-H3 relative to SW-100 (**1a**). **18c** was found to be the most selective HDAC6i with low nanomolar HDAC6 activity in this study, while it exhibited relatively weaker effects on the levels of Ac- $\alpha$ -tub at both high (0.55-fold) and low (0.89-fold) concentrations normalized to SW-100 (**1a**).

Liver microsomal stability assays were conducted to determine the metabolic stability properties of the new HDAC6is (Table 5). As expected, lactam analogues **1m** and **18a** exhibited favorable half-lives ( $t_{1/2}$  > 110 min) although they did not display good functional selectivity in the above-mentioned cellular assay. Carboxamide analogues **1s** and **18f** also overcame the metabolic issues and exhibited acceptable half-lives ( $t_{1/2}$  > 89 min) in both mouse and human microsomes. THB analogue **18b** without any substituent on the cap showed similar half-lives (mouse:  $t_{1/2}$  = 40 min; human:  $t_{1/2}$  = 242 min) as its corresponding THQ analogue **1** (mouse:  $t_{1/2}$  = 40 min; human:  $t_{1/2}$  = 181 min). Interestingly,

THB analogue **18c** containing chlorine (mouse:  $t_{1/2}$  = 61 min; human:  $t_{1/2}$  = 213 min) was much more stable than its corresponding THQ analogue SW-100 (mouse:  $t_{1/2}$  = 32 min; human:  $t_{1/2}$  = 48 min). In addition, THB analogue **18e** bearing a carbonitrile group displayed short half-lives in mouse ( $t_{1/2}$  = 18 min) and human ( $t_{1/2}$  = 22 min) microsomes.

**Biochemical Characterization of SW-101 (1s)**. In the enzymatic assays, **1s** exhibited subnanomolar HDAC6 potency ( $IC_{50}$  = 0.7 nM) and at least 500-fold selectivity over HDAC1 (SI = 509-fold) and HDAC8 (SI = 930-fold). In the cell-based assays, **1s** displayed an improved ability to significantly increase the level of Ac- $\alpha$ -tub at two test concentrations (1.0 and 0.01  $\mu$ M) relative to SW-100 while increasing the levels of Ac-H3 less than 2-fold when normalized to the vehicle group at a concentration of 1.0  $\mu$ M. These results validate its acceptable HDAC6 activity and selectivity in cells. Moreover, the liver microsomal stability assay revealed that **1s** possesses half-lives of 89 min and 174 min in mouse and human microsomes, respectively, which at least in part addresses the metabolic instability of the parent compound SW-100. Although the THB-based analogue **18c** was found to be the most selective HDAC6i among these analogues, compared to **1s**, it exhibited an apparently weaker ability to enhance the levels of Ac- $\alpha$ -tub at high and low concentrations and a slightly shorter half-life in mouse microsomes (**1s**:  $t_{1/2}$  = 174 min vs **18c**:  $t_{1/2}$  = 60 min). Therefore, we selected the THQ-based HDAC6i **1s**, termed SW-101, to further perform full-panel HDAC profiling, HDAC1/6 target engagement assays in cells, and the determination of its  $EC_{50}$  for tubulin acetylation, thus providing a better understanding of its pharmacological properties in comparison with SW-100 (**1a**) and other known HDAC inhibitors.

To investigate the selectivity against other HDAC isozymes, SW-100 (**1a**) and SW-101 (**1s**) were selected for further HDAC isoform profiling (Table 6). Both SW-100 (**1a**) and SW-101 (**1s**) exhibited subnanomolar potency against HDAC6 ( $IC_{50}$  = 0.5 vs 0.7 nM), while SW-100 (**1a**) is more selective over all of the tested HDAC isoforms. SW-100 (**1a**) showed 1000-fold selectivity over classes I, IIa, and IV isoforms except

Table 5. Metabolic Stability Assessment of Selected HDAC6 Inhibitors in Pooled Human and Male Mouse Liver Microsomes<sup>a</sup>

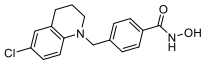
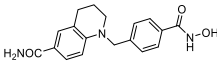
Compound	Structure	Mouse liver microsomes		Human liver microsomes	
		%remaining at 60 min	<i>t</i> <sub>1/2</sub> (min)	%remaining at 60 min	<i>t</i> <sub>1/2</sub> (min)
Verapamil	-	6.5	16.1	16.6	22.2
<b>1</b>		34.1	40.4	73.0	181.5
<b>1a (SW-100)</b>		27.3	31.9	42.6	48.3
<b>1b</b>		17.2	24.8	n/d	n/d
<b>1e</b>		47.3	49.7	11.4	18.9
<b>1g</b>		19.1	25.7	n/d	n/d
<b>1i</b>		20.3	25.4	n/d	n/d
<b>1k</b>		6.8	15.9	n/d	n/d
<b>1m</b>		77.7	174.3	92.6	577
<b>1s (SW-101)</b>		56.0	89.1	76.3	173.6
<b>18a</b>		68.1	110.1	95.3	721.9
<b>18b</b>		34.7	39.6	83.9	241.6
<b>18c</b>		34.7	60.6	83.9	213.3
<b>18e</b>		10.1	18.3	15.0	22.2
<b>18f</b>		80.8	195.6	84.9	252.8

<sup>a</sup>All tests were performed in duplicate with nicotinamide adenine dinucleotide phosphate (NADPH).

for HDAC2 (SI = 564-fold). On the other hand, SW-101 (**1s**) displayed submicromolar potency against different class I (HDAC1, 2, 3, and 8) and class IIa (HDAC4, 5, 7, and 9) isozymes while retaining at least 156-fold isoform selectivity. Molecular docking studies using the hHDAC1 crystal complex (PDB entry5ICN)<sup>37</sup> shown in Figure S5A–C suggest that the long and flexible alkyl chains of pan-HDACis (e.g., SAHA, Panobinostat, and Givinostat) allow the ligands to more readily occupy the pocket rim. On the other hand, HDAC6is containing short and bulky capping groups (e.g., TubA, SW-100, and SW-101) can only occupy the entrance of the HDAC1 active site (Figure S5D–F), which may result in significantly weaker binding affinity. In contrast, it has been well-demonstrated that the short aromatic linkers and bulky hydrophobic capping groups of selective HDAC6is are favorable functional groups to engage with the aromatic crevice and the key L1-loop pocket of HDAC6,<sup>33,34,38</sup> leading to high HDAC6 inhibitory activity.

The potency and selectivity of SW-100 (**1a**) and SW-101 (**1s**) were further evaluated in living cells using the NanoBRET target engagement assay (Figures 3A,B),<sup>18,36</sup> in which the IC<sub>50</sub> values are determined based on a competitive displacement of a cell-permeable SAHA-based fluorescent tracer.<sup>39</sup> The results showed that SW-100 (**1a**) and SW-101 (**1s**) exhibited micromolar potency against HDAC1 (IC<sub>50</sub> = 4.83 and 1.37 μM), while SAHA (positive control) displayed an IC<sub>50</sub> of 0.24 μM against HDAC1 (Figure 3A). At the same time, the cellular potencies of SW-100 (**1a**) and SW-101 (**1s**) against the CD2 deacetylase domain of HDAC6 (Figure 3B) were determined to be 0.09 and 0.06 μM, respectively, representing a 54-fold and 23-fold selectivity over HDAC1. This intracellular engagement assay can reflect a more native cellular context in the presence of various proteins and cofactors relative to *in vitro* enzymatic assays. While our data rely on overexpressed HDACs, in future studies it will be valuable to characterize target occupancy under native expression systems, for example,

Table 6. Full HDAC Isoform Profiling of SW-100 (1a) and SW-101 (1s)<sup>ab</sup>

Compound		SW-100 (1a)		SW-101 (1s)	
Structure					
Isoform		IC <sub>50</sub> (nM)	SI <sup>b</sup>	IC <sub>50</sub> (nM)	SI
Class IIb	HDAC6	0.5 ± 0.1	1	0.7 ± 0.3	1
	HDAC1	769 ± 108	1538	356 ± 59	509
Class I	HDAC2	282 ± 16	564	140 ± 11	200
	HDAC3	1270 ± 155	2540	235 ± 25	335
	HDAC8	3060 ± 402	6120	651 ± 134	930
	HDAC4	2140 ± 666	4280	454 ± 76	649
Class IIa	HDAC5	1480 ± 285	2960	276 ± 67	394
	HDAC7	511 ± 264	1022	109 ± 23	156
	HDAC9	3400 ± 736	6800	650 ± 329	929
Class IV	HDAC11	5720 ± 2670	11,400	5310 ± 834	7586

<sup>a</sup>IC<sub>50</sub> values are the mean of two experiments ± SEM calculated by nonlinear regression analysis from experimental  $v_i/v_0$  values for each HDAC isoform. <sup>b</sup>SI, HDAC6 selectivity index over other HDAC isoforms.

using the CRISPR-Cas system to introduce the NanoLuc reporter into native genomic loci.

In another set of cell-based experiments, using tubulin acetylation as a functional readout for HDAC6 in RPMI8226 cells, we determined the EC<sub>50</sub> values of SW-100 (1a) and SW-101 (1s) against HDAC6 to be 0.14 and 0.16 μM, respectively (Figure 3C). These values are 7.8- and 6.8-fold lower compared to the EC<sub>50</sub> of 1.09 μM for a well-characterized HDAC6i, TubA,<sup>24</sup> thereby confirming efficient inhibitory effects of these new THQ-based HDAC6is on the α-tubulin deacetylation function of HDAC6.

**Structural Characterization of the zHDAC6/SW-101 Complex.** We solved a crystal structure of zHDAC6-CD2 in complex with SW-101 (1s) to an ultrahigh-resolution limit of 1.13 Å (PDB entry 6ZW1; Figure 4 and Table S1). The inhibitor was modeled into well-resolved  $F_o - F_c$  positive electron density peaks in the final stages of the refinement (Figure S6). The structure of the complex does not reveal any major rearrangement of the protein relative to unliganded zHDAC6<sup>40</sup> (PDB entry 5EEM) with the root-mean-square deviation (rmsd) of 0.14 Å for 284 corresponding Cα atoms between the two structures. The hydroxamate functional group of SW-101 (1s) coordinates the active-site Zn<sup>2+</sup> ion in a bidentate fashion, with interatomic distances of 2.3 and 1.9 Å between the Zn<sup>2+</sup> ion and the hydroxamate C=O and N–O groups, respectively. Furthermore, the hydroxamate C=O group accepts a hydrogen bond from the hydroxyl group of Y745 (2.5 Å), and the N–O group forms hydrogen bonds with the side chains of H573 (2.7 Å) and H574 (2.7 Å; Figure 4A). The THQ cap is positioned within van der Waals distances from the side chains of H463, F583, P464, and L712 of the L1-loop pocket, with the side chain of L712 (modeled in two conformations) contributing the most prominently to the interface. Additionally, unlike the molecular docking study of SW-101 (1s) shown in Figure 2F, the piperidine ring of the cap comes into contact with the side chain of F643 (4.1 Å), and the amide function of the THQ cap is engaged in water-mediated interactions with side chains of D460 and H463

(Figure 4B,C). We note, however, that the C6-position of the THQ cap is solvent-exposed. Consequently, its derivatization with small functional moieties should not have a critical impact on affinity for HDAC6 as such added functions are unlikely to sterically block and/or significantly enhance HDAC6/inhibitor interactions. This observation is in line with our SAR data, as all compounds inhibit HDAC6 in the low nanomolar range, and limited differences in measured IC<sub>50</sub> values cannot be easily explained by the structural data only and likely result from a combination of various additional factors, such as desolvation energy and deformation energy of a ligand upon target binding.

Inhibitor selectivity for HDAC6 is predominantly dictated by a combination of the physicochemical characteristics of the cap and linker groups. Generally, HDAC6-specific compounds comprise a bulky aromatic functionality in the linker region, such as phenyl, pyridyl, and isoxazolyl groups,<sup>41</sup> as the active site tunnel of HDAC6 is wider compared to other isoforms and can thus easily accommodate large moieties.<sup>23</sup> The cap group is also critical for both HDAC isoform selectivity as well as inhibitor potency. In the vast majority of structures of HDAC6 complexes reported to date, the cap group interacts with residues of the so-called L1-loop pocket delineated by the side chains of H463, F583, P464, and L712.<sup>41</sup> It is also assumed that characteristics of inhibitor capping groups modulate the coordination mode of the active site Zn<sup>2+</sup> ion by the hydroxamate function of an inhibitor, but any causative structural features are yet to be defined.<sup>33</sup> We compared the binding mode of SW-101 (1s) with those of TubA (PDB entry 6THV)<sup>24</sup> and phenothiazine-based KV70 (PDB entry SW5K)<sup>38</sup> inhibitors, both of which feature a rigid polycyclic cap directly linked to the phenylhydroxamate function via a methylene group (Figure 5A). The capping groups of the three compounds spatially overlap and follow the shallow surface contour of the L1 loop (Figure 5B). Moreover, a slight displacement of the TubA methylene linker of approximately 1.0 Å is observed compared to KV70/SW-101 structures (Figure 5C). In addition, while bidentate zinc coordination is

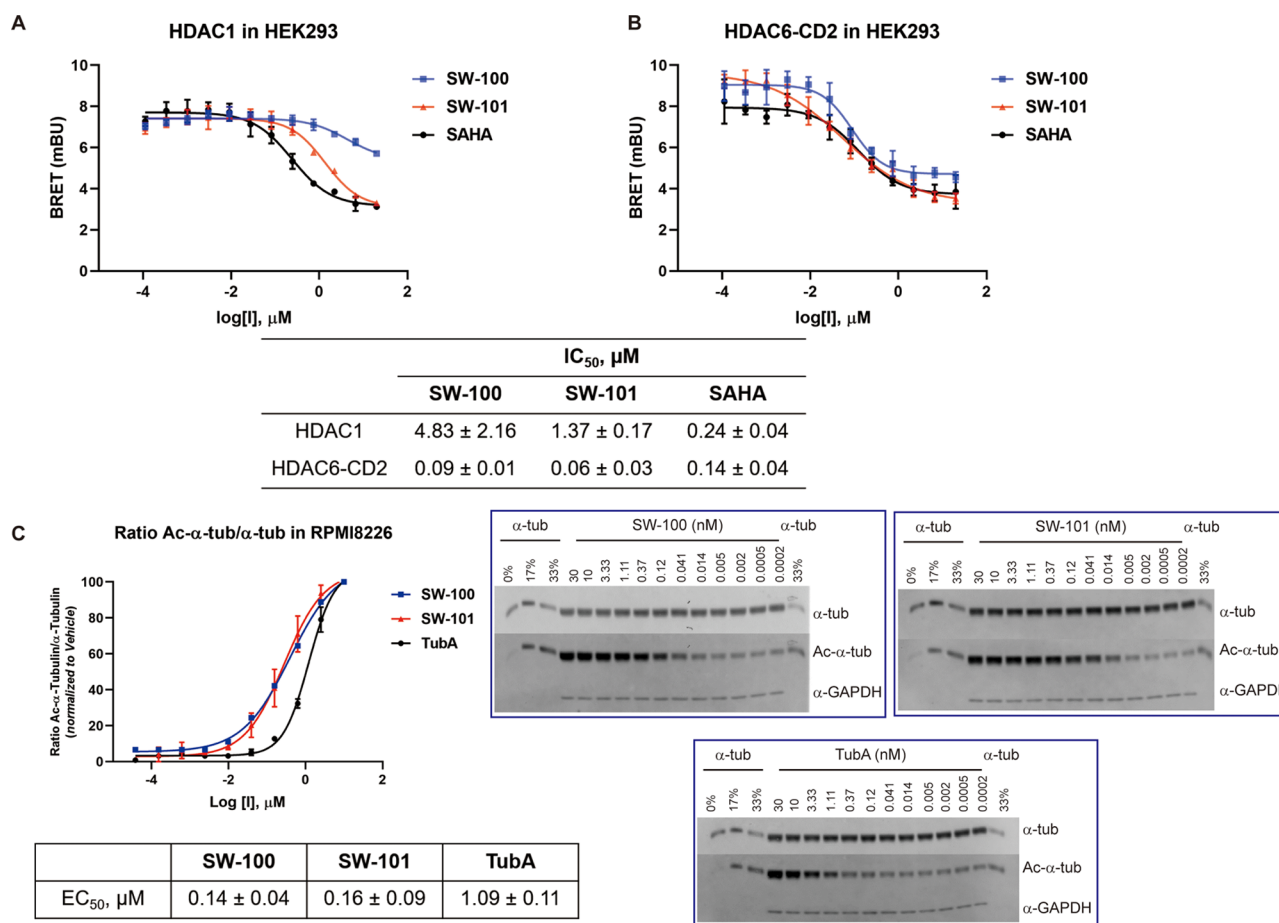


**Figure 3.** Target engagement and functional effect characterization of selective HDAC6is SW-100 (**1a**) and SW-101 (**1s**) in cells. (A and B) HDAC1 and HDAC6-CD2 NanoBRET target engagement assay for compounds SW-100 (**1a**) and SW-101 (**1s**) in HEK293 cells. IC<sub>50</sub> values are the mean of four replicates ± SD obtained from curve-fitting of a 12-point engagement assay starting from a concentration of 20 μM with 3-fold serial dilution. SAHA was used as a positive control. (C) Cellular EC<sub>50</sub> values of inhibitors against HDAC6 were determined in RPMI8226 cells using quantification of tubulin acetylation levels by Western blotting as a functional readout. EC<sub>50</sub> values are presented as means of three replicates ± SEM obtained from curve-fitting of a 10-point assay starting from a concentration of 10 μM with 4-fold/3-fold serial dilution. The levels of Ac- $\alpha$ -tub were normalized to  $\alpha$ -tubulin.

observed for SW-101, both TubA and KV70 engage with the active-site Zn<sup>2+</sup> ion in an energetically less favorable monodentate coordination mode (Figure 5D), which is, however, more frequently observed in HDAC6 complexes with inhibitors featuring rigid capping groups. Overall, the reported structure adds yet another piece of information on how (rigid) capping groups modulate the positioning of the aryl-hydroxamate zinc-binding moieties, yet the definite mechanistic explanations of this phenomenon will require more detailed studies.

**In Vitro ADMET Evaluation and In Vivo Brain/Plasma Pharmacokinetic Profiling of SW-101.** To further investigate the druglike properties of SW-101 (**1s**), we performed several essential ADMET assessments *in vitro* and profiled brain and plasma pharmacokinetic (PK) parameters (Table 7). SW-101 exhibited excellent metabolic stability in mouse/human plasma and liver S9 fraction, with half-lives ranging from 127 to 1000 min. Furthermore, SW-101 did not show inhibitory effects on a series of cytochrome P450 enzymes (CYPs) up to 100 μM, including 1A2, 2C9, 2D6, and 3A4-M, while only displaying modest inhibition against 2C19 (IC<sub>50</sub> = 47 μM). Additionally, SW-101 was evaluated for inhibition of hERG potassium channel activity in an automated patch-clamp

electrophysiology assay. SW-101 (**1s**) did not block hERG activity in Chinese hamster ovary (CHO) cells stably expressing the hERG potassium channel at concentrations up to 10 μM (30% inhibition at 10 μM, Figure S7). These data represent an improvement over the parent compound, SW-100 (**1a**).<sup>18</sup> Notably, the Ames test using four strains of *S. typhimurium* (TA98, TA100, TA1535, and TA1537) with or without the liver S9 fraction gave negative results up to 100 μM (Tables 7 and S2), indicating a lack of mutagenicity as observed previously with SW-100 (**1a**).<sup>18</sup> SW-101 (**1s**) displayed reduced plasma protein binding in mouse (75.9%) and human (85.8%) relative to SW-100 (mouse: 98.3%; human: 99.5%; performed by Pharmaron, Irvine, CA), in line with its decreased lipophilicity (SW-101, cLog P = 1.53; SW-100, cLog P = 3.03, calculated by SwissADME<sup>42</sup>), which is beneficial for improving the free drug exposure *in vivo*. The metabolic stability of SW-101 (**1s**) led to noticeably improved plasma PK profiles (15 mg/kg, IP; AUC<sub>total, plasma</sub> = 1747 h × ng/mL; Table 7) compared to SW-100 (20 mg/kg, IP; AUC<sub>total, plasma</sub> = 120 h × ng/mL; performed by Pharmaron, Irvine, CA). Moreover, the free drug exposure of SW-101 (**1s**) in plasma was determined to be 421 h × ng/mL, which is significantly greater than the modest unbound SW-100 (**1a**) in

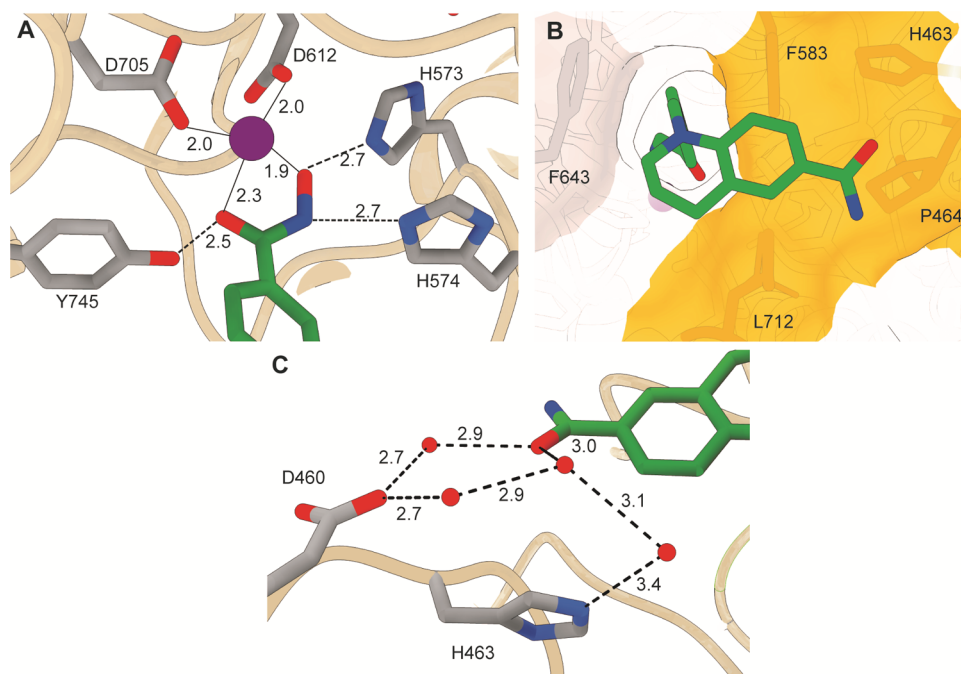


**Figure 4.** Crystal structure of the zHDAC6-CD2/SW-101 complex (PDB entry 6ZW1). (A) Details of bidentate active-site zinc ion coordination by SW-101 (**1s**). HDAC6 residues and the inhibitor are in stick representation with carbon atoms colored gray and green, respectively, and the  $\text{Zn}^{2+}$  ion is shown as a purple sphere. H-Bonding and covalent coordination distances between atoms in Ångstroms are shown as black dashed and solid lines, respectively. (B) Interactions between the THQ cap and the L1-loop pocket formed by residues H463, P464, H463, and L712 (semitransparent yellow surface representation). F463 interacting with the piperidine ring is colored gray. (C) Indirect hydrogen bonds between the THQ cap and D460 and H463 of the enzyme.

plasma (protein binding in mouse plasma = 98.32%;  $\text{AUC}_{\text{unbound, plasma}} = 2.0 \text{ h} \times \text{ng/mL}$ ; performed by Pharmaron, Irvine, CA). On the other hand, although SW-101 (**1s**) exhibited a low brain/plasma ratio ( $\text{AUC}_{\text{total, brain}}/\text{AUC}_{\text{total, plasma}} = 0.16$ ), the compound still maintained comparable drug exposure in the brain (15 mg/kg, IP,  $\text{AUC}_{\text{total, brain}} = 280 \text{ h} \times \text{ng/mL}$ ) relative to SW-100 (20 mg/kg, IP;  $\text{AUC}_{\text{total, brain}} = 300 \text{ h} \times \text{ng/mL}$ ; performed by Pharmaron, Irvine, CA), which can be attributed to the better druglike properties of SW-101 (**1s**).

**Pharmacological Inhibition of HDAC6 by SW-101 Ameliorates Sensory and Motor Neuropathy in a CMT2A Mouse Model.** Previous studies have revealed that a mutant MFN2-induced CMT2A (CMT2A<sup>R94Q</sup>) mouse model recapitulates many of the clinical symptoms seen in patients, including motor dysfunction, mechanical allodynia, and thermal hyperalgesia.<sup>27,43</sup> Corresponding to this neuropathy, CMT2A<sup>R94Q</sup> mice display progressive  $\alpha$ -tubulin acetylation loss in axonal microtubules within the distal portion of sciatic nerves.<sup>27,43</sup> Therefore, we further examined whether SW-101 treatment could prevent or restore the  $\alpha$ -tubulin acetylation deficit and the symptoms of neuropathy in the CMT2A<sup>R94Q</sup> mouse model.

To reveal the dose-dependent effects of SW-101 (**1s**) on  $\alpha$ -tubulin acetylation, wild-type (WT) mice were treated with 10, 15, or 20 mg/kg per 12 h of SW-101 (**1s**) or vehicle solution by IP injection for three days. No obvious adverse effects were observed. Immunoblot analysis for Ac- $\alpha$ -tub/total  $\alpha$ -tub in sciatic nerve tissues showed that the level of Ac- $\alpha$ -tub was significantly increased in the 20 mg/kg treatment group (175% OD Ac- $\alpha$ -tub) compared to the vehicle-treated control (Figure 6A). To further evaluate the time-dependent effects of SW-101 (**1s**) on  $\alpha$ -tubulin acetylation, WT mice were treated with 20

mg/kg of SW-101 (**1s**) or vehicle solution and euthanized after 6, 12, 24, and 48 h. The analysis demonstrated that the level of Ac- $\alpha$ -tub was the highest at the 6 h time point (150% OD Ac- $\alpha$ -tub relative to the vehicle) and slowly declined to baseline levels over 48 h (Figure 6B). The levels of Ac- $\alpha$ -tub were still slightly greater than the vehicle after 24 h. On the other hand, the parent compound SW-100 (5–30 mg/kg, IP) was previously evaluated in WT mice,<sup>27</sup> which also showed maximum  $\alpha$ -tubulin acetylation in the 20 mg/kg group (175% OD Ac- $\alpha$ -tub relative to the vehicle). In the time-dependent assessment, SW-100 (**1a**) exhibited about 125% OD Ac- $\alpha$ -tub after 6 h relative to the control, with the effect diminishing after 24 h. In total, 20 mg/kg of SW-100 (**1a**) was thus given twice a day in our prior work.<sup>27</sup> The comparison demonstrates that SW-101 shows a better ability to induce  $\alpha$ -tubulin acetylation in sciatic nerves of WT mice due to its improved PK profiles. Therefore, based on these data, we chose to administrate 20 mg/kg SW-101 (**1s**) once a day by IP injection in our animal efficacy studies.

Next, we employed a randomized longitudinal crossover treatment study using CMT2A mice and WT littermates to determine if SW-101 (**1s**) could exert any therapeutic efficacy when given before or after the onset of neuropathic symptoms. To achieve this goal, WT and CMT2A littermates were treated with vehicle solution or SW-101 (20 mg/kg per day, IP) from 4 to 26 weeks of age. Unlike the design of the efficacy studies used in our studies of SW-100 (**1a**),<sup>27</sup> in this work, vehicle-treated arms were switched to an SW-101-treated group, and the SW-101-treated arms were shifted to a vehicle group at 26 weeks of age (crossover time point) for 12 weeks until the end of the study (38 weeks of age), which provided an opportunity to evaluate the ability of SW-101 (**1s**) to ameliorate before/after the onset of sensory and neuropathy in the same CMT2A

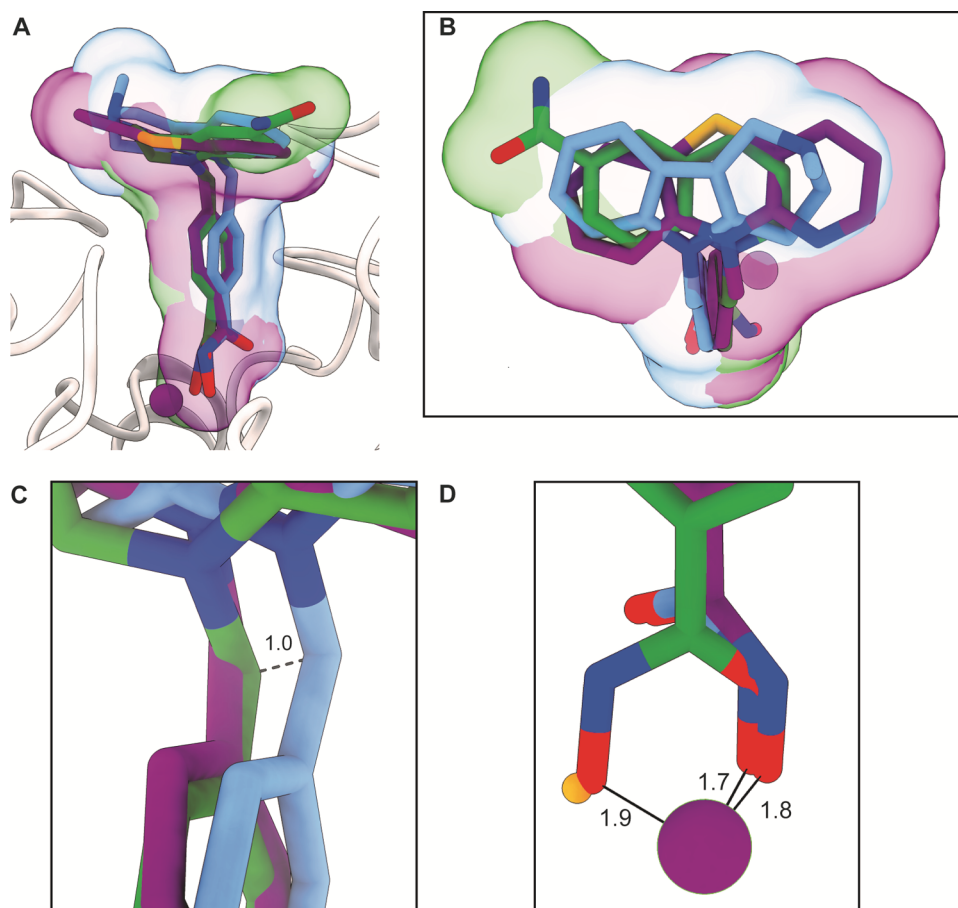


**Figure 5.** Superposition of SW-101 (PDB entry 6ZW1), phenothiazine-based inhibitor KV70 (PDB entry SWSK), and Tuba (PDB entry 6THV) in the substrate tunnel of HDAC6. (A) Overall view; (B) top view; and (C) zoomed view of the methylene linker connecting the phenylhydroxamate zinc-binding group and the cap moiety. (D) Details of zinc coordination by hydroxamate functions. The van der Waals surface areas (volumes) of SW-101, KV70, and Tuba are shown in green, purple, and blue colors, respectively. Distances between atoms in Ångstroms are shown as black lines—solid lines for coordination bonds and dashed lines for hydrogen bonds. The water molecule is shown as an orange sphere.

mouse study. Mice were evaluated for motor performance, mechanical allodynia, and thermal hyperalgesia prior to the treatment and throughout the 34 weeks of the treatment.

To determine SW-101 (**1s**) therapeutic efficacy on motor performance, mice were analyzed by the Rotarod performance test starting at 18 weeks of age. As can be seen in Figure 7A and as observed in prior works,<sup>27,43</sup> vehicle-treated CMT2A mice at 26 weeks of age display motor performances that are significantly lower than their age-matched, vehicle-treated WT littermates. Treatment of CMT2A mice with SW-101 (**1s**), by contrast, resulted in improved motor performance that was similar to WT controls. At 26 weeks of age (crossover time point), CMT2A vehicle and SW-101 treatment groups were switched for 12 weeks until the end of the study (Figure 5A, yellow background). SW-101 treatment of CMT2A mice that had received the vehicle for the first 26 weeks resulted in significant improvement in motor function. By contrast, vehicle treatment of CMT2A mice that had received SW-101 (**1s**) for the first 26 weeks resulted in significantly lower motor performance.

To determine the therapeutic efficacy of SW-101 (**1s**) on mechanical allodynia and thermal hyperalgesia, mice were analyzed by von Frey and Hargreaves assays. As previously observed,<sup>27</sup> vehicle-treated CMT2A mice exhibited significantly lower paw withdrawal thresholds (PWTs) and paw withdrawal latency (PWLs) than their vehicle-treated WT

littermates by 7 weeks of age, which remained substantially lower through to the crossover time point at 26 weeks of age (Figure 7B,C). By contrast, CMT2A mice treated with SW-101 (**1s**) resulted in paw withdrawal values for von Frey and Hargreaves assays that were similar to WT controls. In the fully established sensory and motor neuropathy in CMT2A mice (>26 weeks), SW-100 (**1a**) treatment showed significant improvement in von Frey thresholds relative to vehicle-treated CMT2A mice after 10 weeks, while the results remained apparently lower than the levels in WT mice.<sup>27</sup> The results suggest that SW-101 (**1s**) has better effects on CMT2A mice after the onset of sensory and motor neuropathy at a lower daily dose compared to the parent compound SW-100 (**1a**).

After the crossover time point, the switch to vehicle treatment in CMT2A mice (previously received SW-101) resulted in significantly lower PWTs and PWLs. By contrast, switching CMT2A vehicle treatment to SW-101 resulted in PWTs and PWLs that were not different from their treatment-matched WT controls within 4 weeks of treatment (Figure 7B,C, yellow background).

Sciatic nerves from the same mice were harvested, and distal nerve segments were analyzed for Ac- $\alpha$ -tub, total  $\alpha$ -tubulin, and neurofilament levels by immunofluorescence confocal microscopy. The 26-week-old vehicle-treated CMT2A mice had a significantly lower Ac- $\alpha$ -tub level compared to their age-matched WT littermates (Figure 8B). By contrast, the

Table 7. ADMET/PK Evaluation of SW-101<sup>a</sup>

In vitro ADMET profiles		
plasma stability ( $t_{1/2}$ , min)	mouse	127
	human	>400
liver S9 fraction ( $t_{1/2}$ , min)	mouse	213
	human	>1000
CYP inhibition ( $IC_{50}$ , $\mu$ M)	1A2	>100
	2C9	>100
	2C19	47
	2D6	>100
	3A4-M	>100
hERG inhibition @ 10 $\mu$ M	hERG-CHO, automated patch-clamp	30%
Ames test (+/- S9)	T98, TA100, TA1535, TA1537	negative (5–100 $\mu$ M)
Plasma protein binding (%)	mouse	75.9
	human	85.8
In vivo mouse PK studies (15 mg/kg, IP) <sup>b</sup>		
plasma	$C_{max}$ (ng/mL)	3583
	$t_{max}$ (h)	0.08
	AUC <sub>total, 0-inf</sub> (h $\times$ ng/mL)	1747
	AUC <sub>unbound, 0-inf</sub> (h $\times$ ng/mL)	421
	$t_{1/2}$ (h)	0.44
brain	$C_{max}$ (ng/mL)	223
	$t_{max}$ (h)	0.25
	AUC <sub>total, 0-inf</sub> (h $\times$ ng/mL)	280
	$t_{1/2}$ (h)	2.9
AUC <sub>total, brain</sub> /AUC <sub>total, plasma</sub>		0.16

<sup>a</sup>ADMET evaluation and PK profiling were conducted by AMRI Global, Albany, NY. <sup>b</sup>SW-101 was tested in a formulation composed of 35% PEG400, 5% Tween80, 10% EtOH, and 50% PBS (1 $\times$ ). Data are presented as the mean from three male C57BL/6J mice.

treatment of CMT2A mice with SW-101 (**1s**) for 22 weeks resulted in a considerably higher Ac- $\alpha$ -tub level than vehicle-treated CMT2A mice, which was not statistically different from WT littermates. After the crossover time point, 12 weeks of vehicle treatment in CMT2A mice (previously received SW-101) resulted in significantly lower distal sciatic nerve  $\alpha$ -tubulin acetylation compared to the SW-101-treated CMT2A cohort at the time of the switch. By contrast, CMT2A mice treated with SW-101 (**1s**) for 12 weeks after the switch resulted in significantly higher distal sciatic nerve  $\alpha$ -tubulin

acetylation compared to the vehicle-treated CMT2A cohort at the time of the switch (Figure 8B). In contrast to the changes seen in the Ac- $\alpha$ -tub level, total  $\alpha$ -tubulin levels were not statistically different among genotypes or treatment groups (Figure 8), ruling out the possibility that the decreased  $\alpha$ -tubulin acetylation seen in vehicle-treated CMT2A distal sciatic nerves was a result of the  $\alpha$ -tubulin loss.

Overall, these data suggest that the HDAC6 inhibitor SW-101 (**1s**), given before or after the onset of symptoms, improves  $\alpha$ -tubulin acetylation of the distal sciatic nerve, counteracts progressive motor dysfunction, and ameliorates neuropathic symptoms in MFN2 mutant-induced CMT2A mice.

## CONCLUSIONS

CMT2A, caused by mutations in the MFN2 gene, is the most common inherited motor and sensory neuropathy. In the last decade, several HDAC6is (e.g., TubA, ACY-738, and ACY-775) have been tested *in vivo* and proved to be potential therapeutic interventions for different types of CMT2, including CMT2D and CMT2F.<sup>13–15,44</sup> SW-100 is the first HDAC6i investigated in the CMT2A model, and this inhibitor was able to rescue defective  $\alpha$ -tubulin acetylation and to enhance motor performance at both the presymptomatic and postsymptomatic stages of CMT2A mice. However, in previous studies, we found that the half-life of SW-100 (**1a**) was relatively short in liver microsomes and hepatocytes, resulting in its low drug concentrations in the brain and plasma, thereby requiring a repeated daily dose for the animal efficacy studies, thus limiting its further preclinical development.

In this study, we investigated the SAR of THQ-based HDAC6is and overcame the metabolic stability issue of the parent compound SW-100 (**1a**) while maintaining excellent HDAC6 potency and selectivity at both the enzymatic and cellular levels. SAR studies led to the identification of a new THQ-based HDAC6i, named SW-101 (**1s**). Further, *in vitro* ADMET assessments revealed that SW-101 (**1s**) did not show noticeable CYP or hERG inhibition while proving negative in the Ames test. Additionally, *in vivo* PK profiling showed that the improvement in metabolic stability led to a significantly enhanced drug exposure in plasma and the brain in comparison with SW-100 (**1a**). Finally, in the MFN2 mutant-induced

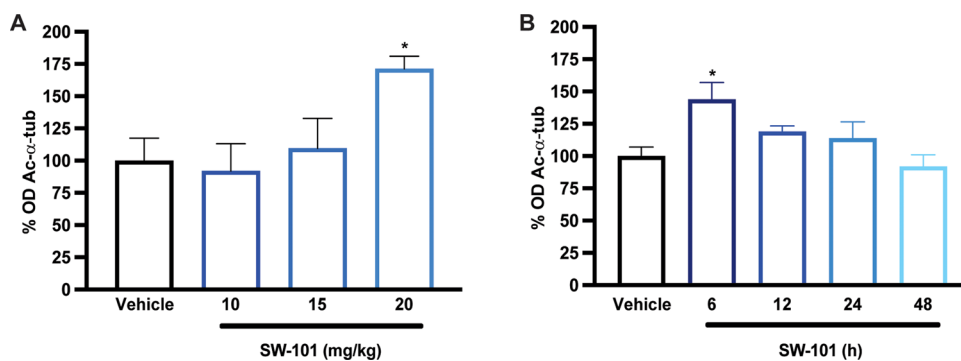


**Figure 6.** HDAC6 inhibition by SW-101 (**1s**) increases the Ac- $\alpha$ -tub in sciatic nerves of WT mice. (A) Western blot analysis of Ac- $\alpha$ -tub in sciatic nerves of WT mice at different concentrations of SW-101 (mg/kg/12 h for 3 days;  $n = 3$  mice per drug concentration). The amount of Ac- $\alpha$ -tub compared to the total  $\alpha$ -tubulin levels was quantified by densitometry, and the values were normalized to the vehicle.  $*P < 0.05$ ; SW-101 vs vehicle; unpaired  $t$ -test. Error bars are presented as SEM. (B) Western blot analysis of Ac- $\alpha$ -tub in sciatic nerves of WT mice 6, 12, 24, and 48 h after SW-101 injection (20 mg/kg,  $n = 3$  mice per treatment group). The amount of Ac- $\alpha$ -tub compared to the total  $\alpha$ -tubulin levels was quantified by densitometry, and the values were normalized to the vehicle.  $*P < 0.05$ ; SW-101 vs vehicle; unpaired  $t$ -test. Error bars are presented as SEM.

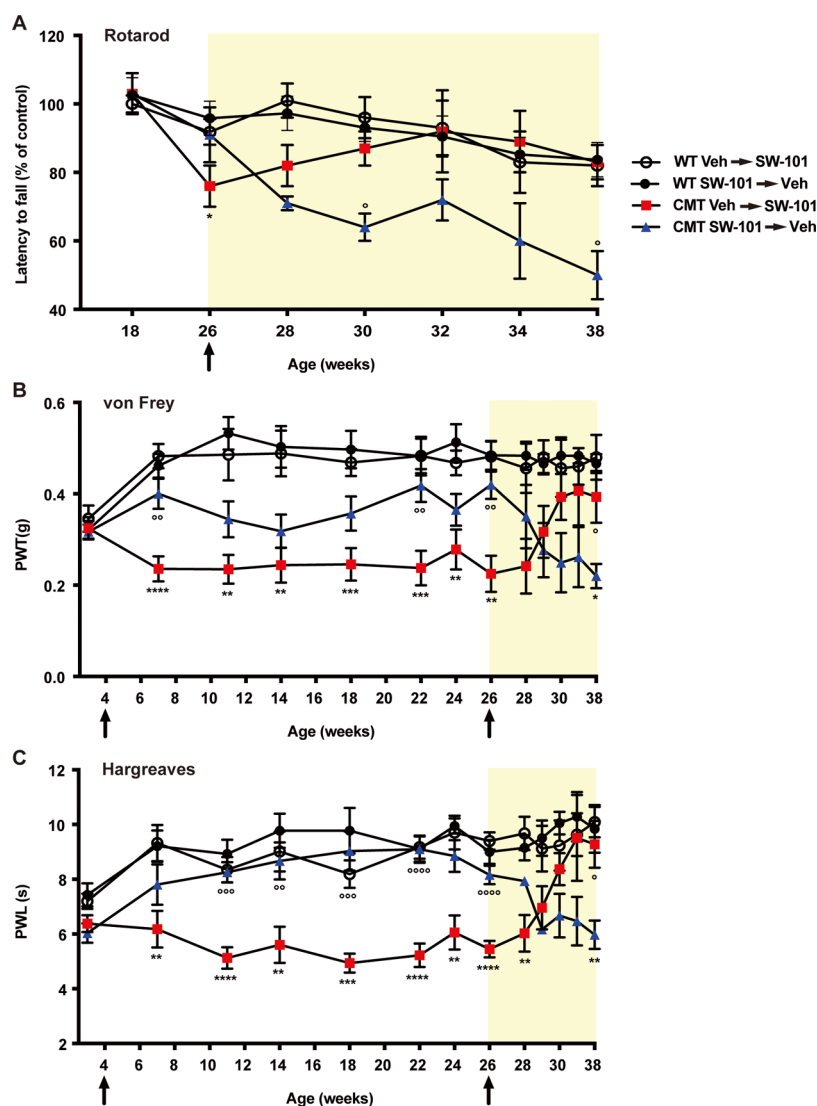


**Figure 7.** Pharmacological inhibition of HDAC6 by SW-101 (**1s**) reverses motor deficits and neuropathic pain in CMT2A mice. (A) Latency to fall from an accelerating rod in vehicle-treated WT (WT Veh;  $n = 14$ ) and CMT2A (CMT2A Veh;  $n = 13$ ) or SW-101-treated WT (WT SW-101;  $n = 14$ ) and CMT2A (CMT2A SW-101;  $n = 13$ ) mice. Latencies to fall are expressed as percentages of WT Veh at 18 weeks of age. Vehicle and SW-101 treatment were switched from 26 to 38 weeks of age so that previously vehicle-treated mice received SW-101, while SW-101-treated mice received the vehicle (yellow background).  $*P < 0.05$ , WT vs CMT2A Veh;  $^{\circ}P < 0.05$ , CMT2A Veh vs CMT2A SW-101; two-way analysis of variance (ANOVA) repeated measures and Dunnett's multiple comparisons. Error bars are presented as SEM. (B) PWTs to varying forces of von Frey filaments and (C) PWLs to a standard radiant heat source applied to the hind paws. Vehicle and SW-101 treatments were switched from 26 to 38 weeks of age so that previously vehicle-treated CMT2A mice received SW-101 and SW-101-treated CMT2A mice received the vehicle (yellow background).  $**P < 0.01$ ,  $***P < 0.001$ ,  $****P < 0.0001$ , WT Veh vs CMT Veh;  $^{\circ}P < 0.05$ ,  $^{\circ\circ}P < 0.01$ ,  $^{\circ\circ\circ}P < 0.001$ ,  $^{\circ\circ\circ\circ}P < 0.0001$ , CMT2A Veh vs CMT2A SW-101; two-way ANOVA repeated measures and Dunnett's multiple comparisons. Error bars are presented as SEM.

CMT2A mouse model, a single daily dose treatment of SW-101 elevated the impaired level of Ac- $\alpha$ -tub in the distal sciatic nerve, counteracted progressive motor dysfunction, and ameliorated neuropathic symptoms. More importantly, SW-101 (**1s**) shows a better ability to rescue the fully established sensory and motor neuropathy in CMT2A mice with a lower daily dose relative to the parent compound SW-100 (**1a**), thereby providing strong support for the further advancement of SW-101 (**1s**) as a promising preclinical drug candidate for the treatment of CMT2A and related neurodegenerative disorders.

## EXPERIMENTAL SECTION

**Chemistry.** *General Information.*  $^1\text{H}$  and  $^{13}\text{C}$  NMR spectra were obtained on a 400/101 MHz Bruker spectrometer, except where

noted otherwise, using the solvent residual peak as the internal reference (chemical shifts:  $\text{CDCl}_3$ ,  $\delta$  7.26/77.0;  $\text{CD}_3\text{OD}$ , 3.31/49.15;  $\text{DMSO-}d_6$ , 2.50/39.52;  $\text{acetone-}d_6$ , 2.05/29.84 and 206.26). The following abbreviations for multiplicities were used: s, singlet; d, doublet; t, triplet; q, quartet; q, quintet; m, multiplet; dd, double doublet; dt, double triplet; ddd, double double doublet; and br s, broad singlet. Thin-layer chromatography (TLC) plates (Merck silica gel 60  $F_{254}$ , 250  $\mu\text{m}$  thickness) were used to monitor reaction progress, and spots were visualized under UV light (254 nm). High-resolution mass spectrometry (HRMS) was carried out on a Shimadzu IT-TOF instrument under the following conditions: column, ACE 3AQ (50 mm  $\times$  2.1 mm, id); mobile phase, 8–100%  $\text{CH}_3\text{CN}/\text{H}_2\text{O}$  containing 0.1% formic acid at a flow rate of 0.5 mL/min for 4 min. Flash chromatography was performed on a Combi-Flash Rf system (Teledyne ISCO) with silica gel cartridges. Preparative high-performance liquid chromatography (HPLC) was

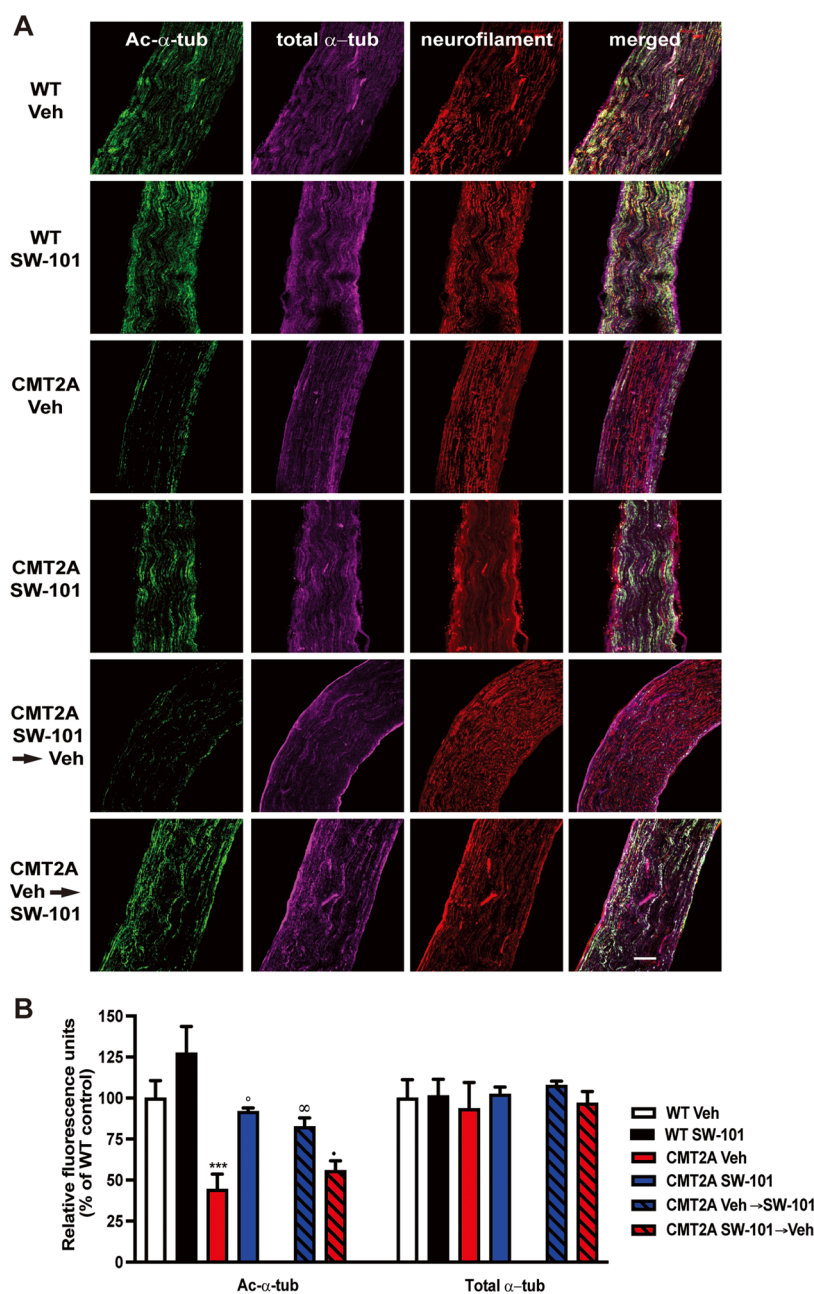


**Figure 8.** (A) Representative confocal images of distal sciatic nerves, immunostained for Ac- $\alpha$ -tub (green), total  $\alpha$ -tubulin (red), and neurofilaments (magenta) from vehicle-treated WT (WT Veh), SW-101-treated WT (WT SW-101), vehicle-treated CMT2A (CMT2A Veh), and SW-101-treated CMT2A (CMT2A SW-101) at 26 weeks of age, as well as vehicle-treated CMT2A switched to SW-101 (CMT2A Veh  $\rightarrow$  SW-101) and SW-101-treated CMT2A switched to the vehicle (CMT2A SW-101  $\rightarrow$  Veh) at 38 weeks of age. Scale bar is 40  $\mu$ m. (B) Quantification of Ac- $\alpha$ -tub levels in distal sciatic nerves. Values were quantified by pixel intensity using Fiji, and Ac- $\alpha$ -tub or total  $\alpha$ -tubulin was normalized to the neurofilament. \*\*\* $P$  < 0.0005 CMT2A Veh vs WT Veh;  $^{\circ}$  $P$  < 0.05 CMT2A Veh vs CMT2A SW-101;  $^{\infty}$  $P$  < 0.05 CMT2A Veh vs CMT2A Veh switched to SW-101 at 26 weeks;  $^{\bullet}$  $P$  < 0.05 CMT2A SW-101 vs CMT2A SW-101 switched to the vehicle at 26 weeks; one-way ANOVA followed by Tukey's multiple comparison test. Error bars are presented as SEM.  $n$  = 3 mice per treatment group.

used in the purification of all final compounds using a Shimadzu preparative LC under the following conditions: column, ACE 5AQ (150 mm  $\times$  21.2 mm, id); mobile phase: 8–100% MeOH (CH<sub>3</sub>CN)/H<sub>2</sub>O containing 0.05% TFA at a flow rate of 17 mL/min for 30 mins; UV detection at 254 and 280 nm. Analytical HPLC was carried out on an Agilent 1260 series instrument under the following conditions: column, ACE 3 (150 mm  $\times$  4.6 mm, id); mobile phase, 8–100% MeOH (CH<sub>3</sub>CN)/H<sub>2</sub>O containing 0.05% TFA at a flow rate of 1.0 mL/min for 25 min; UV detection at 254 nm. The purities of all tested compounds were >95%, as determined by analytical HPLC.

4-((6-Chloro-3,4-dihydroquinolin-1(2H)-yl)methyl)-N-hydroxybenzamide (**1a**, SW-100). **General Procedure A Step (i):** To a round-bottom flask charged with 6-chloro-1,2,3,4-tetrahydroquinoline (**4a**, 2.43 g, 14.6 mmol) and methyl 4-(bromomethyl)benzoate (**3d**, 4.99 g, 21.9 mmol) in DMF (30 mL) was added K<sub>2</sub>CO<sub>3</sub> (4.03 g, 29.2 mmol). The resulting mixture was stirred at 100  $^{\circ}$ C for 2 h. After completion of the reaction, the solution was cooled to room temperature, quenched with H<sub>2</sub>O (30 mL), and extracted with EtOAc (20 mL  $\times$  3). The combined organic extracts were washed with brine (20 mL), dried over Na<sub>2</sub>SO<sub>4</sub>, and concentrated under vacuum. The crude product was purified by flash chromatography

(0–20% EtOAc/hexane) to afford the ester intermediate as a white solid (3.6 g, 78%). **Step (ii)**: In a round-bottom flask, NaOH (1.8 g, 45.6 mmol) was dissolved in 50% aqueous NH<sub>2</sub>OH (36 mL, approx. 50 equiv) at 0 °C. A solution of the ester intermediate (3.6 g, 11.4 mmol) in THF/MeOH (1:1, 20/20 mL) was added dropwise, and stirring was continued for 30 min while warming to room temperature. The solution was neutralized with 2 N HCl to pH ~7 and then extracted with EtOAc (30 mL × 3). The organic layers were separated, washed with brine, dried over Na<sub>2</sub>SO<sub>4</sub>, and concentrated under vacuum. The crude product was purified by preparative HPLC (8–100% CH<sub>3</sub>CN/H<sub>2</sub>O containing 0.05% TFA) and lyophilized to afford the desired product **1a** as a white powder (1.8 g, 50%). <sup>1</sup>H NMR (DMSO-*d*<sub>6</sub>) δ 11.16 (s, 1H), 8.94 (br s, 1H), 7.70 (d, *J* = 8.2 Hz, 2H), 7.28 (d, *J* = 8.1 Hz, 2H), 6.94 (d, *J* = 2.4 Hz, 1H), 6.87 (dd, *J* = 8.8, 2.5 Hz, 1H), 6.36 (d, *J* = 8.8 Hz, 1H), 4.51 (s, 2H), 3.39–3.35 (m, 3H), 2.73 (t, *J* = 6.1 Hz, 2H), 1.96–1.82 (m, 2H). <sup>13</sup>C NMR (DMSO-*d*<sub>6</sub>) δ 164.2, 143.7, 142.0, 131.4, 128.2, 127.2 (2C), 126.5 (2C), 126.4, 123.9, 118.7, 111.9, 53.9, 27.4, 21.4. ESI HRMS calcd for C<sub>17</sub>H<sub>16</sub>ClN<sub>2</sub>O<sub>2</sub>: [M – H]<sup>–</sup>, *m/z* 316.0906; found: 316.0899.

**4-((6-Chloro-3,4-dihydroquinolin-1(2H)-yl)methyl)-3-fluoro-N-hydroxybenzamide (1b)**. **1b** was synthesized from **4a** (55 mg, 0.32 mmol) and **3a** (120 mg, 0.5 mmol) following *General Procedure A* and was obtained as a pink powder (30 mg, 18% over two steps). <sup>1</sup>H NMR (DMSO-*d*<sub>6</sub>) δ 11.26 (s, 1H), 9.11 (s, 1H), 7.53 (t, *J* = 9.3 Hz, 2H), 7.22 (t, *J* = 7.8 Hz, 1H), 6.96 (d, *J* = 2.3 Hz, 1H), 6.90 (dd, *J* = 8.8, 2.5 Hz, 1H), 6.38 (d, *J* = 8.7 Hz, 1H), 4.55 (s, 2H), 3.40–3.35 (m, 2H, overlapping with water peak), 2.74 (t, *J* = 6.3 Hz, 2H), 1.97–1.87 (m, 2H). <sup>13</sup>C NMR (DMSO-*d*<sub>6</sub>) δ 162.7, 160.0 (d, *J* = 243 Hz), 143.5, 133.5 (d, *J* = 6.7 Hz), 128.3 (d, *J* = 4.8 Hz), 128.2 (d, *J* = 5.9 Hz), 128.1, 126.4, 124.1, 122.9 (d, *J* = 1.1 Hz), 119.0, 113.9 (d, *J* = 23.1 Hz), 111.8, 49.3, 48.3 (d, *J* = 3.4 Hz), 27.3, 21.4. ESI HRMS calcd for C<sub>17</sub>H<sub>17</sub>ClFN<sub>2</sub>O<sub>2</sub>: [M + H]<sup>+</sup>, *m/z* 335.0957; found: 335.0965.

**4-(1-(6-Chloro-3,4-dihydroquinolin-1(2H)-yl)ethyl)-N-hydroxybenzamide (1c)**. **1c** was synthesized from **4a** (121 mg, 0.71 mmol) and **3b** (260 mg, 1.07 mmol) following *General Procedure A* and was obtained as a pink powder (30 mg, 11% over two steps). <sup>1</sup>H NMR (DMSO-*d*<sub>6</sub>) δ 11.15 (s, 1H), 8.99 (s, 1H), 7.71 (d, *J* = 8.2 Hz, 2H), 7.35 (d, *J* = 8.3 Hz, 2H), 6.94 (d, *J* = 2.4 Hz, 1H), 6.90 (dd, *J* = 8.8, 2.5 Hz, 1H), 6.59 (d, *J* = 8.9 Hz, 1H), 5.09 (q, *J* = 6.9 Hz, 1H), 3.32–3.18 (m, 1H), 3.10–3.00 (m, 1H), 2.69 (t, *J* = 6.2 Hz, 2H), 1.90–1.71 (m, 2H), 1.52 (d, *J* = 6.9 Hz, 3H). <sup>13</sup>C NMR (DMSO-*d*<sub>6</sub>) δ 164.1, 145.9, 143.9, 131.3, 128.2 (2C), 127.1, 126.6 (2C), 126.3, 124.5, 118.5, 112.2, 54.7, 42.5, 27.7, 21.4, 16.9. ESI HRMS calcd for C<sub>18</sub>H<sub>20</sub>ClN<sub>2</sub>O<sub>2</sub>: [M + H]<sup>+</sup>, *m/z* 331.1208; found: 331.1189.

**4-(6-Chloro-1,2,3,4-tetrahydroquinoline-1-carbonyl)-N-hydroxybenzamide (1d)**. (i) To a stirred solution of **4a** (180 mg, 1.08 mmol) in DCM (10 mL) were added TEA (0.225 mg, 1.62 mmol) and methyl 4-(chlorocarbonyl)benzoate (**3d**, 256 mg, 1.29 mmol) at 0 °C. The resulting mixture was stirred for an additional 40 min at 0 °C. The reaction mixture was concentrated under vacuum. The crude product was purified by flash chromatography (0–60% EtOAc/hexane) to afford a colorless oil (300 mg, 84.4%). (ii) **1d** was synthesized from the ester intermediate (300 mg, 0.92 mmol) following *General Procedure A, Step (ii)* and was obtained as a white powder (180 mg, 60%). <sup>1</sup>H NMR (DMSO-*d*<sub>6</sub>) δ 11.28 (br s, 1H), 9.09 (br s, 1H), 7.72 (d, *J* = 8.2 Hz, 2H), 7.43 (d, *J* = 8.2 Hz, 2H), 7.30 (d, *J* = 2.2 Hz, 1H), 6.98 (dd, *J* = 8.6, 2.1 Hz, 1H), 6.87 (br s, 1H), 3.73 (t, *J* = 6.3 Hz, 2H), 2.83 (t, *J* = 6.6 Hz, 2H), 1.93 (q, *J* = 6.5 Hz, 2H). <sup>13</sup>C NMR (DMSO-*d*<sub>6</sub>) δ 168.7, 163.4, 138.7, 137.5, 134.0, 133.7, 128.3, 128.2, 128.0 (2C), 126.8 (2C), 126.5, 125.3, 44.6, 26.1, 23.1. ESI HRMS calcd for C<sub>17</sub>H<sub>15</sub>ClN<sub>2</sub>O<sub>3</sub>: [M + H]<sup>+</sup>, *m/z* 331.0844; found: 331.0842.

**4-((6-Fluoro-3,4-dihydroquinolin-1(2H)-yl)methyl)-N-hydroxybenzamide (1e)**. **1e** was synthesized from **4b** (400 mg, 2.70 mmol) and **3d** (924 mg, 4.05 mmol) following *General Procedure A* and was obtained as a light-pink powder (390 mg, 48% over two steps). <sup>1</sup>H NMR (DMSO-*d*<sub>6</sub>) δ 11.16 (s, 1H), 9.00 (s, 1H), 7.70 (d, *J* = 8.1 Hz, 2H), 7.30 (d, *J* = 8.1 Hz, 2H), 6.77 (dd, *J* = 9.3, 2.9 Hz, 1H), 6.69 (td, *J* = 8.7, 3.0 Hz, 1H), 6.35 (dd, *J* = 9.0, 4.7 Hz, 1H), 4.48 (s, 2H), 3.33

(t, *J* = 5.5 Hz, 2H), 2.74 (t, *J* = 6.2 Hz, 2H), 1.95–1.85 (m, 2H). <sup>13</sup>C NMR (DMSO-*d*<sub>6</sub>) δ 164.2, 153.9 (d, *J* = 233.5 Hz), 142.4, 141.6 (d, *J* = 1.2 Hz), 131.3, 127.2 (2C), 126.6 (2C), 123.5 (d, *J* = 6.6 Hz), 115.2 (d, *J* = 21.5 Hz), 112.8 (d, *J* = 21.4 Hz), 111.3 (d, *J* = 7.4 Hz), 54.4, 49.6, 27.6, 21.7. ESI HRMS calcd for C<sub>17</sub>H<sub>17</sub>FN<sub>2</sub>O<sub>2</sub>: [M + H]<sup>+</sup>, *m/z* 301.1347; found: 301.1335.

**4-((6,7-Dichloro-3,4-dihydroquinolin-1(2H)-yl)methyl)-N-hydroxybenzamide (1f)**. **1f** was synthesized from **4c** (90 mg, 0.45 mmol) and **3d** (154 mg, 0.68 mmol) following *General Procedure A* and was obtained as a pink powder (20 mg, 6% over two steps). <sup>1</sup>H NMR (DMSO-*d*<sub>6</sub>) δ 11.14 (br s, 1H), 8.99 (br s, 1H), 7.71 (d, *J* = 8.2 Hz, 2H), 7.28 (d, *J* = 8.1 Hz, 2H), 7.12 (s, 1H), 6.52 (s, 1H), 4.56 (s, 2H), 3.42–3.36 (m, 2H), 2.72 (t, *J* = 6.0 Hz, 2H), 1.95–1.85 (m, 2H). <sup>13</sup>C NMR (CDCl<sub>3</sub>) δ 170.1, 158.8, 138.5, 128.6, 128.2, 128.0, 127.8, 127.7 (2C), 127.2, 116.8, 114.2 (2C), 55.3, 45.5, 31.6, 25.4. ESI HRMS calcd for C<sub>17</sub>H<sub>17</sub>Cl<sub>2</sub>N<sub>2</sub>O<sub>2</sub>: [M + H]<sup>+</sup>, *m/z* 351.0662; found: 351.0657.

**4-((6-Chloro-7-fluoro-3,4-dihydroquinolin-1(2H)-yl)methyl)-N-hydroxybenzamide (1g)**. **1g** was synthesized from **4d** (110 mg, 0.59 mmol) and **3d** (203 mg, 0.89 mmol) following *General Procedure A* and was obtained as an off-white powder (75 mg, 38% over two steps). <sup>1</sup>H NMR (DMSO-*d*<sub>6</sub>) δ 11.14 (br s, 1H), 7.70 (d, *J* = 8.2 Hz, 2H), 7.29 (d, *J* = 8.2 Hz, 2H), 7.04 (d, *J* = 8.7 Hz, 1H), 6.37 (d, *J* = 13.2 Hz, 1H), 4.54 (s, 2H), 3.39–3.35 (m, 2H, overlapping with water peak), 2.70 (t, *J* = 6.1 Hz, 2H), 1.99–1.81 (m, 2H). <sup>13</sup>C NMR (DMSO-*d*<sub>6</sub>) δ 164.1, 156.5 (d, *J* = 238 Hz), 145.1 (d, *J* = 9.9 Hz), 141.4, 131.5, 129.4, 127.2 (2C), 126.5 (2C), 119.4 (d, *J* = 2.7 Hz), 103.6 (d, *J* = 17.9 Hz), 98.5 (d, *J* = 25.4 Hz), 53.8, 49.1, 26.6, 21.2. ESI HRMS calcd for C<sub>17</sub>H<sub>17</sub>ClFN<sub>2</sub>O<sub>2</sub>: [M + H]<sup>+</sup>, *m/z* 335.0957; found: 335.0952.

**4-((7-Chloro-6-fluoro-3,4-dihydroquinolin-1(2H)-yl)methyl)-N-hydroxybenzamide (1h)**. **1h** was synthesized from **4e** (160 mg, 0.86 mmol) and **3d** (296 mg, 1.30 mmol) following *General Procedure A* and was obtained as an off-white powder (150 mg, 21% over two steps). <sup>1</sup>H NMR (DMSO-*d*<sub>6</sub>) δ 11.15 (s, 1H), 8.99 (s, 1H), 7.71 (d, *J* = 8.1 Hz, 2H), 7.29 (d, *J* = 8.2 Hz, 2H), 6.99 (d, *J* = 9.7 Hz, 1H), 6.43 (d, *J* = 6.4 Hz, 1H), 4.52 (s, 2H), 3.36 (t, *J* = 5.6 Hz, 2H, overlapping with water peak), 2.73 (t, *J* = 6.1 Hz, 2H), 1.95–1.82 (m, 2H). <sup>13</sup>C NMR (DMSO-*d*<sub>6</sub>) δ 164.1, 148.5 (d, *J* = 233 Hz), 142.3 (d, *J* = 1.5 Hz), 141.7, 131.5, 127.2 (2C), 126.5 (2C), 122.6 (d, *J* = 5.7 Hz), 116.7 (d, *J* = 8.2 Hz), 116.4 (d, *J* = 5.0 Hz), 110.7, 54.1, 49.2, 27.1, 21.3. ESI HRMS calcd for C<sub>17</sub>H<sub>17</sub>ClFN<sub>2</sub>O<sub>2</sub>: [M + H]<sup>+</sup>, *m/z* 335.0957; found: 335.0955.

**4-((6-Chloro-2,2-dimethyl-3,4-dihydroquinolin-1(2H)-yl)methyl)-N-hydroxybenzamide (1i)**. **1i** was synthesized from **9a** (360 mg, 1.85 mmol) and **3d** (624 mg, 2.77 mmol) following *General Procedure A* and was obtained as an off-white powder (20 mg, 3% over two steps). <sup>1</sup>H NMR (DMSO-*d*<sub>6</sub>) δ 11.12 (s, 1H), 7.68 (d, *J* = 8.3 Hz, 2H), 7.31 (d, *J* = 8.5 Hz, 2H), 6.98 (d, *J* = 2.4 Hz, 1H), 6.83 (dd, *J* = 8.7, 2.6 Hz, 1H), 6.09 (d, *J* = 9.0 Hz, 1H), 4.50 (s, 2H), 2.78 (t, *J* = 6.5 Hz, 2H), 1.86 (t, *J* = 6.5 Hz, 2H), 1.21 (s, 6H). <sup>13</sup>C NMR (DMSO-*d*<sub>6</sub>) δ 164.3, 143.9, 143.7, 131.1, 127.8, 127.1 (2C), 126.2, 125.9 (2C), 124.1, 119.0, 113.4, 54.1, 48.4, 35.9, 26.1 (2C), 23.9. ESI HRMS calcd for C<sub>19</sub>H<sub>21</sub>ClN<sub>2</sub>O<sub>2</sub>: [M – H]<sup>+</sup>, *m/z* 343.1219; found: 343.1220.

**4-((6-Fluoro-2,2-dimethyl-3,4-dihydroquinolin-1(2H)-yl)methyl)-N-hydroxybenzamide (1j)**. **1j** was synthesized from **9b** (650 mg, 3.63 mmol) and **3d** (1241 mg, 5.45 mmol) following *General Procedure A* and was obtained as an off-white powder (310 mg, 63% over two steps). <sup>1</sup>H NMR (DMSO-*d*<sub>6</sub>) δ 11.12 (s, 1H), 8.98 (s, 1H), 7.68 (d, *J* = 8.2 Hz, 2H), 7.33 (d, *J* = 8.2 Hz, 2H), 6.80 (dd, *J* = 9.2, 3.0 Hz, 1H), 6.65 (td, *J* = 8.7, 3.0 Hz, 1H), 6.05 (dd, *J* = 9.0, 4.7 Hz, 1H), 4.46 (s, 2H), 2.77 (t, *J* = 6.4 Hz, 2H), 1.86 (t, *J* = 6.5 Hz, 2H), 1.20 (s, 6H). <sup>13</sup>C NMR (DMSO-*d*<sub>6</sub>) δ 164.3, 153.9 (d, *J* = 231 Hz), 144.2, 141.7, 131.1, 127.1 (2C), 125.9 (2C), 123.6 (d, *J* = 6.8 Hz), 114.8 (d, *J* = 21.4 Hz), 112.8 (d, *J* = 15.7 Hz), 112.6 (d, *J* = 1.0 Hz), 53.9, 48.8, 36.1, 26.0 (2C), 24.2. ESI HRMS calcd for C<sub>19</sub>H<sub>22</sub>FN<sub>2</sub>O<sub>2</sub>: [M + H]<sup>+</sup>, *m/z* 329.1660; found: 329.1658.

**4-((6-Chloro-4,4-dimethyl-3,4-dihydroquinolin-1(2H)-yl)methyl)-N-hydroxybenzamide (1k)**. **1k** was synthesized from **11a** (370 mg, 1.90 mmol) and **3d** (650 mg, 2.85 mmol) following *General Procedure*

A and was obtained as an off-white powder (30 mg, 45% over two steps). <sup>1</sup>H NMR (DMSO-*d*<sub>6</sub>) δ 11.11 (br s, 1H), 8.98 (br s, 1H), 7.69 (d, *J* = 8.3 Hz, 2H), 7.27 (d, *J* = 8.2 Hz, 2H), 7.13 (d, *J* = 2.6 Hz, 1H), 6.87 (dd, *J* = 8.8, 2.6 Hz, 1H), 6.37 (d, *J* = 8.9 Hz, 1H), 4.54 (s, 2H), 3.41–3.37 (m, 2H, overlapping with water peak), 1.78–1.71 (m, 2H), 1.25 (s, 6H). <sup>13</sup>C NMR (DMSO-*d*<sub>6</sub>) δ 164.1, 142.4, 141.9, 132.5, 131.4, 127.2 (2C), 126.4 (2C), 126.2, 125.2, 119.0, 112.2, 54.1, 45.8, 36.0, 32.0, 30.0 (2C). ESI HRMS calcd for C<sub>19</sub>H<sub>22</sub>ClN<sub>2</sub>O<sub>2</sub>: [M + H]<sup>+</sup>, *m/z* 345.1346; found: 345.1353.

4-((6-Fluoro-4,4-dimethyl-3,4-dihydroquinolin-1(2H)-yl)methyl)-*N*-hydroxybenzamide (**1l**). **1l** was synthesized from **11b** (310 mg, 1.73 mmol) and **3d** (592 mg, 2.60 mmol) following *General Procedure A* and was obtained as an orange powder (210 mg, 37% over two steps). <sup>1</sup>H NMR (DMSO-*d*<sub>6</sub>) δ 11.14 (s, 1H), 8.99 (s, 1H), 7.70 (d, *J* = 8.2 Hz, 2H), 7.29 (d, *J* = 8.2 Hz, 2H), 7.00 (dd, *J* = 10.4, 3.1 Hz, 1H), 6.69 (td, *J* = 8.6, 3.1 Hz, 1H), 6.34 (dd, *J* = 9.0, 4.9 Hz, 1H), 4.51 (s, 2H), 3.37 (m, 2H, overlapping with water peak), 1.78–1.71 (m, 2H), 1.25 (s, 6H). <sup>13</sup>C NMR (DMSO-*d*<sub>6</sub>) δ 164.2, 154.2 (d, *J* = 22.9 Hz), 142.4, 140.3, 132.2 (d, *J* = 5.6 Hz), 131.4, 127.2 (2C), 126.5 (2C), 112.7 (d, *J* = 21.6 Hz), 112.4 (d, *J* = 22.0 Hz), 111.5 (d, *J* = 7.4 Hz), 54.6, 45.9, 36.3, 32.1, 30.3 (2C). ESI HRMS calcd for C<sub>19</sub>H<sub>22</sub>FN<sub>2</sub>O<sub>2</sub>: [M + H]<sup>+</sup>, *m/z* 329.1660; found: 329.1659.

4-((6-Chloro-2-oxo-3,4-dihydroquinolin-1(2H)-yl)methyl)-*N*-hydroxybenzamide (**1m**). (i) To a stirred solution of **12a** (200 mg, 1.1 mmol) in DMF (20 mL) were added NaH (80 mg, 1.65 mmol) and **3d** (300 mg, 1.33 mmol) at 0 °C. Then, the resulting mixture was stirred at room temperature for 1 h. The reaction was quenched with H<sub>2</sub>O (15 mL), and the mixture was extracted with EtOAc (15 mL × 3). The combined organic layers were washed with brine (20 mL), dried over Na<sub>2</sub>SO<sub>4</sub>, and concentrated under vacuum. The crude product was purified by flash chromatography (0–80% EtOAc/hexane) to afford the ester intermediate **13a** as a colorless oil (50 mg, 14%). (ii) Compound **1m** was obtained from **13a** (50 mg, 0.15 mmol) following *General Procedure A, Step (ii)* as a white powder (29 mg, 58%). <sup>1</sup>H NMR (DMSO-*d*<sub>6</sub>) δ 11.13 (s, 1H), 8.99 (s, 1H), 7.67 (d, *J* = 8.2 Hz, 2H), 7.33 (d, *J* = 2.4 Hz, 1H), 7.27 (d, *J* = 8.1 Hz, 2H), 7.17 (dd, *J* = 8.7, 2.4 Hz, 1H), 6.87 (d, *J* = 8.7 Hz, 1H), 5.17 (s, 2H), 2.97 (t, *J* = 7.0 Hz, 2H), 2.71 (dd, *J* = 8.5, 6.2 Hz, 2H). <sup>13</sup>C NMR (DMSO-*d*<sub>6</sub>) δ 169.6, 164.0, 140.2, 138.2, 131.6, 128.8, 127.6, 127.2 (2C), 126.8, 126.5, 126.3 (2C), 116.9, 44.4, 30.7, 24.3. ESI HRMS calcd for C<sub>17</sub>H<sub>16</sub>ClN<sub>2</sub>O<sub>3</sub>: [M + H]<sup>+</sup>, *m/z* 331.0844; found: 331.0845.

4-((6-Bromo-2-oxo-3,4-dihydroquinolin-1(2H)-yl)methyl)-*N*-hydroxybenzamide (**1n**). **1n** was synthesized from **13b** (180 mg, 0.48 mmol) following *General Procedure A, Step (ii)* and was obtained as a white powder (90 mg, 50%). <sup>1</sup>H NMR (DMSO-*d*<sub>6</sub>) δ 11.14 (br s, 1H), 8.99 (br s, 1H), 7.67 (d, *J* = 8.2 Hz, 2H), 7.46 (d, *J* = 2.1 Hz, 1H), 7.29 (dd, *J* = 13.0, 5.2 Hz, 3H), 6.81 (d, *J* = 8.7 Hz, 1H), 5.16 (s, 2H), 2.97 (t, *J* = 7.3 Hz, 2H), 2.71 (dd, *J* = 8.3, 6.3 Hz, 2H). <sup>13</sup>C NMR (DMSO-*d*<sub>6</sub>) δ 169.6, 164.0, 140.2, 138.6, 131.6, 130.4, 129.7, 129.2, 127.2, 126.3, 117.3, 114.5, 44.3, 30.71, 24.25. ESI HRMS calcd for C<sub>17</sub>H<sub>16</sub>BrN<sub>2</sub>O<sub>3</sub>: [M + H]<sup>+</sup>, *m/z* 375.0339; found: 375.0334.

4-((6-Cyclopropyl-2-oxo-3,4-dihydroquinolin-1(2H)-yl)methyl)-*N*-hydroxybenzamide (**1o**). (i) In a microwave reaction tube, **13b** (200 mg, 0.54 mmol) was dissolved in toluene/H<sub>2</sub>O (5/0.5 mL). Cs<sub>2</sub>CO<sub>3</sub> (354 mg, 1.08 mmol), Pd(PPh<sub>3</sub>)<sub>4</sub> (6 mg, 0.054 mmol), and cyclopropylboronic acid (142 mg, 1.62 mmol) were added to the solution. The resulting mixture was heated at 140 °C for 45 min in a microwave reactor. After completion of the reaction, excess solid was filtered off, and the filtrate was concentrated under vacuum. The crude product was purified by flash chromatography (0–80% EtOAc/hexane) to afford intermediate **13c** as an off-white powder (130 mg, 48%). (ii) Compound **3o** was synthesized from **13c** (130 mg, 0.39 mmol) following *General Procedure A, Step (ii)* and was obtained as a white powder (35 mg, 27%). <sup>1</sup>H NMR (DMSO-*d*<sub>6</sub>) δ 11.13 (br s, 1H), 8.98 (br s, 1H), 7.66 (d, *J* = 8.3 Hz, 2H), 7.26 (d, *J* = 8.2 Hz, 2H), 6.93 (d, *J* = 1.5 Hz, 1H), 6.82 (dd, *J* = 8.3, 2.0 Hz, 1H), 6.74 (d, *J* = 8.4 Hz, 1H), 5.14 (s, 2H), 2.94–2.85 (m, 2H), 2.67 (dd, *J* = 8.5, 6.1 Hz, 2H), 1.86–1.75 (m, 1H), 0.90–0.80 (m, 2H), 0.60–0.52 (m, 2H). <sup>13</sup>C NMR (DMSO-*d*<sub>6</sub>) δ 169.6, 164.0, 140.7, 137.9, 136.7, 131.4, 127.1 (2C), 126.3 (3C), 124.9, 124.1, 115.1, 44.3, 31.2, 24.7,

14.3, 8.9 (2C). ESI HRMS calcd for C<sub>20</sub>H<sub>21</sub>N<sub>2</sub>O<sub>3</sub>: [M + H]<sup>+</sup>, *m/z* 337.1547; found: 337.1551.

*N*-Hydroxy-4-((2-oxo-6-propyl-3,4-dihydroquinolin-1(2H)-yl)-methyl)benzamide (**1p**). **1p** was synthesized from **13b** (200 mg, 0.54 mmol) and *n*-propylboronic acid (142 mg, 1.62 mmol) following the procedure for **1o** and was obtained as an off-white powder (70 mg, 29% over two steps). <sup>1</sup>H NMR (DMSO-*d*<sub>6</sub>) δ 11.13 (br s, 1H), 8.97 (br s, 1H), 7.67 (d, *J* = 8.1 Hz, 2H), 7.27 (d, *J* = 8.1 Hz, 2H), 7.05 (d, *J* = 1.1 Hz, 1H), 6.92 (dd, *J* = 8.1, 1.1 Hz, 1H), 6.77 (d, *J* = 8.2 Hz, 1H), 5.15 (s, 2H), 2.98–2.86 (m, 2H), 2.75–2.63 (m, 2H), 2.47–2.38 (m, 2H), 1.61–1.45 (m, 2H), 0.86 (t, *J* = 7.3 Hz, 3H). <sup>13</sup>C NMR (DMSO-*d*<sub>6</sub>) δ 169.6, 140.7, 137.0, 136.4, 131.4, 127.9, 127.1 (2C), 126.9, 126.3 (2C), 126.1, 115.0, 44.4, 36.4, 31.2, 24.7, 24.0, 13.7. ESI HRMS calcd for C<sub>20</sub>H<sub>23</sub>N<sub>2</sub>O<sub>3</sub>: [M + H]<sup>+</sup>, *m/z* 339.1703; found: 339.1704.

4-((6-(1*H*-Pyrazol-4-yl)-3,4-dihydroquinolin-1(2H)-yl)methyl)-*N*-hydroxybenzamide (**1q**). (i) Compound **14a** (50 mg, 0.14 mmol) was dissolved in dioxane/H<sub>2</sub>O (3/0.3 mL). K<sub>2</sub>CO<sub>3</sub> (39 mg, 0.28 mmol), Pd(PPh<sub>3</sub>)<sub>4</sub> (16 mg, 0.014 mmol), and 4-pyrazoleboronic acid pinacol ester (33 mg, 0.17 mmol) were added to the solution. The resulting mixture was refluxed overnight. After completion of the reaction, excess solid was filtered off, and the filtrate was concentrated under vacuum. The crude product was purified by flash chromatography (0–60% EtOAc/hexane) to afford the intermediate as a colorless oil. (ii) **1q** was synthesized from the intermediate (20 mg, 0.06 mmol) following *General Procedure A, Step (ii)* and was obtained as a gray powder (6.5 mg, 13% for two steps). <sup>1</sup>H NMR (DMSO-*d*<sub>6</sub>) δ 11.14 (s, 1H), 7.81 (s, 2H), 7.69 (d, *J* = 8.1 Hz, 2H), 7.31 (d, *J* = 8.1 Hz, 2H), 7.15 (s, 1H), 7.09 (dd, *J* = 8.4, 1.6 Hz, 1H), 6.39 (d, *J* = 8.4 Hz, 1H), 4.53 (s, 2H), 3.37–3.35 (m, 2H, overlapping with water peak), 2.77 (t, *J* = 6.0 Hz, 2H), 1.99–1.90 (m, 2H). <sup>13</sup>C NMR (126 MHz, DMSO-*d*<sub>6</sub>) δ 164.1, 143.2, 142.5, 131.3, 128.8, 128.7, 127.1 (2C), 126.6 (2C), 125.9, 123.9, 122.1, 121.7, 120.4, 111.0, 54.0, 49.6, 27.6, 21.9. ESI HRMS calcd for C<sub>20</sub>H<sub>19</sub>N<sub>4</sub>O<sub>2</sub>: [M – H]<sup>–</sup>, *m/z* 347.1513; found: 347.1507.

4-((6-Cyano-3,4-dihydroquinolin-1(2H)-yl)methyl)-*N*-hydroxybenzamide (**1r**). **1r** was synthesized from **14b** (100 mg, 0.33 mmol) following *General Procedure A, Step (ii)* and was obtained as a white powder (70 mg, 69%). <sup>1</sup>H NMR (500 MHz, DMSO-*d*<sub>6</sub>) δ 11.15 (br s, 1H), 8.99 (br s, 1H), 7.70 (d, *J* = 8.0 Hz, 2H), 7.31–7.24 (m, 4H), 6.47 (d, *J* = 8.6 Hz, 1H), 4.63 (s, 2H), 3.48 (t, *J* = 5.7 Hz, 2H), 2.76 (t, *J* = 6.2 Hz, 2H), 1.93 (p, *J* = 6.1 Hz, 2H). <sup>13</sup>C NMR (126 MHz, DMSO-*d*<sub>6</sub>) δ 164.0, 148.2, 141.0, 131.9, 131.5, 131.5, 127.3 (2C), 126.3 (2C), 122.5, 120.5, 110.4, 95.5, 53.5, 49.7, 27.0, 20.8. ESI HRMS calcd for C<sub>18</sub>H<sub>18</sub>N<sub>3</sub>O<sub>2</sub>: [M + H]<sup>+</sup>, *m/z* 308.1394; found: 308.1395.

1-(4-(Hydroxycarbonyl)benzyl)-1,2,3,4-tetrahydroquinoline-6-carboxamide (**1s**). **1s** was synthesized from **14c** (150 mg, 0.46 mmol) following *General Procedure A, Step (ii)* and was obtained as a white powder (70 mg, 50%). <sup>1</sup>H NMR (DMSO-*d*<sub>6</sub>) δ 11.13 (s, 1H), 7.69 (AA'XX' multiplet, *J*<sub>AX</sub> + *J*<sub>AX'</sub> = 8.2 Hz, 2H), 7.48 (s, 1H), 7.43 (br s, 1 H, CONH), 7.42 (dd, *J* = 8.6, 2.2 Hz, 1H), 7.29 (AA'XX' multiplet, *J*<sub>AX</sub> + *J*<sub>AX'</sub> = 8.1 Hz, 2H), 6.80 (br s, 1H, CONH), 6.39 (d, *J* = 8.6 Hz, 1H), 4.60 (s, 2H), 3.43–3.36 (m, 2H, overlapping with water peak), 2.77 (t, *J* = 6.2 Hz, 2H), 1.94 (p, *J* = 5.8 Hz, 2H). <sup>13</sup>C NMR (DMSO-*d*<sub>6</sub>) δ 167.9, 164.1, 147.2, 141.8, 131.4, 128.5, 127.2 (2C), 127.0, 126.4 (2C), 120.7 (2C), 109.4, 53.6, 49.6, 27.6, 21.5. ESI HRMS calcd for C<sub>18</sub>H<sub>18</sub>N<sub>3</sub>O<sub>3</sub>: [M – H]<sup>–</sup>, *m/z* 324.1354; found: 324.1357.

*Methyl 4-(Bromomethyl)-3-fluorobenzoate* (**3a**). (i) To a stirred solution of 3-fluoro-4-methylbenzoic acid (**2**, 308 mg, 2 mmol) in DMF (3 mL) were added K<sub>2</sub>CO<sub>3</sub> (552 mg, 4.0 mmol) and CH<sub>3</sub>I (0.2 mL, 3.0 mmol) at room temperature. The resulting mixture was stirred at the same temperature for 5 h. Then, the reaction was quenched with water (15 mL), and the mixture was extracted with EtOAc (15 mL × 3). The combined organic layers were washed with brine (20 mL), dried over Na<sub>2</sub>SO<sub>4</sub>, and concentrated under vacuum to give the methyl ester intermediate. The methyl ester intermediate (220 mg, 1.3 mmol) was dissolved in CCl<sub>4</sub> (5 mL). To the solution were added NBS (278 mg, 1.56 mmol) and AIBN (21 mg, 0.13

mmol). The resulting mixture was heated at 80 °C overnight. Then, the reaction was quenched with water (15 mL) and extracted with DCM (15 mL × 3). The combined organic layers were washed with brine (20 mL), dried over Na<sub>2</sub>SO<sub>4</sub>, and concentrated under vacuum. The crude product was purified by flash chromatography (0–50% EtOAc/hexane) to afford **3a** as a colorless solid (200 mg, 36% over two steps). <sup>1</sup>H NMR (CDCl<sub>3</sub>) δ 7.81 (dd, *J* = 8.0, 1.3 Hz, 1H), 7.72 (dd, *J* = 10.2, 1.3 Hz, 1H), 7.47 (t, *J* = 7.7 Hz, 1H), 4.52 (s, 2H), 3.92 (s, 3H). <sup>13</sup>C NMR (CDCl<sub>3</sub>) δ 165.5 (d, *J* = 2.7 Hz), 160.3 (d, *J* = 250 Hz), 132.4 (d, *J* = 7.7 Hz), 131.2 (d, *J* = 3.0 Hz), 130.1 (d, *J* = 14.7 Hz), 125.6 (d, *J* = 3.6 Hz), 116.9 (d, *J* = 23.2 Hz), 52.5, 24.6 (d, *J* = 4.2 Hz).

**Methyl 4-(1-Bromoethyl)benzoate (3b).** To a stirred solution of methyl 4-acetylbenzoate (**5**, 358 mg, 2.0 mmol) in EtOH (10 mL) was added NaBH<sub>4</sub> (152 mg, 4 mmol) at 0 °C. The resulting mixture was stirred at the same temperature for 1 h. The excess solvent was removed under vacuum, water was added, and the mixture was extracted with EtOAc (20 mL × 3). The combined organic extracts were washed with brine (40 mL), dried over Na<sub>2</sub>SO<sub>4</sub>, and concentrated under vacuum to obtain the intermediate as a colorless oil. The intermediate (310 mg, 1.72 mmol) was dissolved in DCM (20 mL). To the stirred solution were added CBr<sub>4</sub> (855 mg, 2.52 mmol) and PPh<sub>3</sub> (660 mg, 2.52 mmol) at 0 °C. Then, the resulting mixture was stirred at room temperature overnight. The reaction was quenched with water (10 mL), and the mixture was extracted with DCM (20 mL × 3). The combined organic extracts were washed with brine (30 mL), dried over Na<sub>2</sub>SO<sub>4</sub>, and concentrated under vacuum. The crude product was purified by flash chromatography (0–20% EtOAc/hexane) to obtain **3b** as a colorless oil (260 mg, 49% over two steps). <sup>1</sup>H NMR (CDCl<sub>3</sub>) δ 8.01 (d, *J* = 8.4 Hz, 2H), 7.50 (d, *J* = 8.2 Hz, 2H), 5.20 (q, *J* = 6.9 Hz, 1H), 3.92 (s, 3H), 2.05 (d, *J* = 6.9 Hz, 3H). <sup>13</sup>C NMR (CDCl<sub>3</sub>) δ 166.5, 148.0, 130.0 (3C), 126.9 (2C), 52.2, 48.0, 26.6.

**6-Chloro-1,2,3,4-tetrahydroquinoline (4a).** *General Procedure B Step (i):* To a three-necked flask charged with **7a** (4.6 g, 21.1 mmol) under an argon atmosphere was added AlCl<sub>3</sub> (5.47 g, 42.2 mmol) at 140 °C. The resulting mixture was stirred at the same temperature for 12 h. Then, the reaction was carefully quenched with 1 N HCl (20 mL) at 0 °C, and the mixture was extracted with EtOAc (30 mL × 3). The combined organic extracts were washed with brine (20 mL), dried over Na<sub>2</sub>SO<sub>4</sub>, and concentrated under vacuum. The crude product was purified by flash chromatography (0–80% EtOAc/hexane) to afford a white powder (3.1 g, 17.1 mmol). *(ii)* To a stirred solution of LiAlH<sub>4</sub> (1.95 g, 51.4 mmol) in THF (30 mL) was added a solution of the lactam intermediate (3.1 g, 17.1 mmol) dropwise in THF (20 mL) at 0 °C. The resulting mixture was stirred at the same temperature for 20 min and was then heated to reflux for an additional 1 h. The reaction was subsequently quenched with water (2.0 mL), 5 N NaOH (2.0 mL), and water (10 mL). The precipitate was filtered off and washed with EtOAc (20 mL × 3). The filtrate was washed with brine (20 mL), dried over Na<sub>2</sub>SO<sub>4</sub>, and concentrated under vacuum. Compound **4a** was obtained as a colorless oil (2.43 g, 69% over two steps) and used directly in the next step without further purification. <sup>1</sup>H NMR (CDCl<sub>3</sub>) δ 6.93–6.86 (m, 2H), 6.38 (d, *J* = 8.0 Hz, 1H), 3.77 (br s, 1H), 3.33–3.15 (m, 2H), 2.72 (t, *J* = 6.4 Hz, 2H), 1.94–1.88 (m, 2H). <sup>13</sup>C NMR (CDCl<sub>3</sub>) δ 143.2, 128.8, 126.3, 122.7, 120.9, 114.9, 41.7, 26.7, 21.6.

**6-Fluoro-1,2,3,4-tetrahydroquinoline (4b).** **4b** was synthesized from **7b** (1.0 g, 5.0 mmol) following *General Procedure B* and was obtained as a colorless solid (400 mg, 55% over two steps). <sup>1</sup>H NMR (CDCl<sub>3</sub>) δ 6.76–6.60 (m, 2H), 6.40 (dd, *J* = 9.5, 4.8 Hz, 1H), 3.53 (br s, 1H), 3.33–3.19 (m, 2H), 2.75 (t, *J* = 6.4 Hz, 2H), 2.02–1.83 (m, 2H). <sup>13</sup>C NMR (CDCl<sub>3</sub>) δ 156.4 (d, *J* = 233 Hz), 140.9 (d, *J* = 1.7 Hz), 122.7 (d, *J* = 6.6 Hz), 115.5 (d, *J* = 21.5 Hz), 114.8 (d, *J* = 7.6 Hz), 113.1 (d, *J* = 22.3 Hz), 42.0, 27.0, 21.9.

**6,7-Dichloro-1,2,3,4-tetrahydroquinoline (4c).** **4c** was synthesized from **7c** (510 mg, 2.0 mmol) following *General Procedure B* and was obtained as an off-white powder (90 mg, 23% over two steps). <sup>1</sup>H NMR (CDCl<sub>3</sub>) δ 6.97 (s, 1H), 6.52 (s, 1H), 3.89 (br s, 1H), 3.31–

3.22 (m, 2H), 2.68 (t, *J* = 6.4 Hz, 2H), 1.93–1.84 (m, 2H). <sup>13</sup>C NMR (CDCl<sub>3</sub>) δ 144.1, 130.3, 129.5, 121.3, 118.5, 114.6, 41.5, 26.4, 21.4.

**6-Chloro-7-fluoro-1,2,3,4-tetrahydroquinoline (4d).** **4d** was synthesized from **7d** (1.20 g, 5.26 mmol) following *General Procedure B* and was obtained as a white powder (110 mg, 11% over two steps). <sup>1</sup>H NMR (CDCl<sub>3</sub>) δ 6.90 (d, *J* = 8.1 Hz, 1H), 6.22 (d, *J* = 10.9 Hz, 1H), 3.91 (br s, 1H), 3.35–3.14 (m, 2H), 2.68 (t, *J* = 6.2 Hz, 2H), 1.93–1.75 (m, 2H). <sup>13</sup>C NMR (CDCl<sub>3</sub>) δ 156.9 (d, *J* = 241 Hz), 144.5 (d, *J* = 9.6 Hz), 130.3, 118.0 (d, *J* = 2.9 Hz), 106.7 (d, *J* = 17.8 Hz), 101.3 (d, *J* = 23.8 Hz), 41.6, 26.3, 21.6.

**7-Chloro-6-fluoro-1,2,3,4-tetrahydroquinoline (4e).** **4e** was synthesized from **7e** (1.12 g, 5.35 mmol) following *General Procedure B* and was obtained as a white powder (160 mg, 16% over two steps). <sup>1</sup>H NMR (CDCl<sub>3</sub>) δ 6.72 (d, *J* = 9.5 Hz, 1H), 6.45 (d, *J* = 6.4 Hz, 1H), 3.74 (br s, 1H), 3.33–3.18 (m, 2H), 2.70 (t, *J* = 6.4 Hz, 2H), 1.98–1.83 (m, 2H). <sup>13</sup>C NMR (CDCl<sub>3</sub>) δ 150.3 (d, *J* = 236 Hz), 141.4 (d, *J* = 2.1 Hz), 121.1 (d, *J* = 5.7 Hz), 117.9 (d, *J* = 18.5 Hz), 116.7 (d, *J* = 21.1 Hz), 114.7, 41.7, 26.6, 21.6.

**6-Bromo-1,2,3,4-tetrahydroquinoline (4g).** To a stirred solution of 1,2,3,4-tetrahydroquinoline (**4f**, 0.94 mL, 7.52 mmol) in DMF (10 mL) was dropwise added a solution of NBS (1.40 g, 7.89 mmol) in DMF (3 mL) at 0 °C. Then, the resulting mixture was slowly warmed to room temperature in 30 min and stirred for an additional 1 h. After completion of the reaction, the solution was diluted with H<sub>2</sub>O (20 mL) and then extracted with EtOAc (20 mL × 3). The combined organic extracts were washed with brine (20 mL), dried over Na<sub>2</sub>SO<sub>4</sub>, and concentrated under vacuum. The crude product was purified by flash chromatography (0–20% EtOAc/hexane) to obtain **4g** as an off-white solid (1.2 g, 76%). <sup>1</sup>H NMR (CDCl<sub>3</sub>) δ 7.12–7.00 (m, 2H), 6.33 (d, *J* = 8.3 Hz, 1H), 3.85 (br s, 1H), 3.40–3.23 (m, 2H), 2.73 (t, *J* = 6.4 Hz, 2H), 1.94–1.89 (m, 2H). <sup>13</sup>C NMR (CDCl<sub>3</sub>) δ 143.9, 132.0, 129.5, 123.5, 115.6, 108.3, 41.9, 27.0, 21.8.

**1,2,3,4-Tetrahydroquinoline-6-carbonitrile (4h).** To a solution of **4g** (500 mg, 2.38 mmol) in DMF/water (99:1, 5 mL) were added Zn(CN)<sub>2</sub> (613 mg, 5.24 mmol), S-Phos (100 mg, 0.24 mmol), and Pd<sub>2</sub>(dba)<sub>3</sub> (92 mg, 0.10 mmol) in a microwave reaction tube. Then, the resulting mixture was heated at 170 °C for 30 min in a microwave reactor. After completion of the reaction, the solution was quenched with water (10 mL) and then extracted with EtOAc (10 mL × 3). The combined organic extracts were washed with water (10 mL × 3) and brine (20 mL), dried over Na<sub>2</sub>SO<sub>4</sub>, and concentrated under vacuum. The crude product was purified by flash chromatography (0–20% EtOAc/hexane) to afford **4h** as an orange solid (200 mg, 53%). <sup>1</sup>H NMR (CDCl<sub>3</sub>) δ 7.24–7.07 (m, 2H), 6.38 (d, *J* = 8.2 Hz, 1H), 3.52–3.33 (m, 2H), 3.21 (br s, 1H), 2.73 (t, *J* = 6.3 Hz, 2H), 2.05–1.77 (m, 2H). <sup>13</sup>C NMR (CDCl<sub>3</sub>) δ 148.4, 133.3, 131.4, 121.1, 120.9, 113.4, 97.9, 41.7, 26.8, 21.1.

**3-Chloro-N-(4-chlorophenyl)propanamide (7a).** *General Procedure C.* To a round-bottom flask charged with 4-chloroaniline (**6a**, 5.00 g, 39.4 mmol) in acetone (50 mL) was added 3-chloropropanoyl chloride (1.90 mL, 19.7 mmol) at room temperature. The resulting mixture was stirred for 1 h under reflux. Then, the mixture was cooled to room temperature, 2 N HCl (30 mL) was added, and the mixture was extracted with EtOAc (25 mL × 3). The combined organic layers were washed with brine (20 mL), dried over Na<sub>2</sub>SO<sub>4</sub>, and concentrated under vacuum to afford **7a** as an off-white powder (4.6 g, 54%), which was carried on without further purification. <sup>1</sup>H NMR (CDCl<sub>3</sub>) δ 7.56 (br s, 1H), 7.46 (d, *J* = 8.7 Hz, 2H), 7.28 (d, *J* = 8.8 Hz, 2H), 3.87 (t, *J* = 6.3 Hz, 2H), 2.81 (t, *J* = 6.3 Hz, 2H). <sup>13</sup>C NMR (CDCl<sub>3</sub>) δ 167.9, 136.0, 129.8, 129.1 (2C), 121.4 (2C), 40.4, 39.8.

**3-Chloro-N-(4-fluorophenyl)propanamide (7b).** **7b** was synthesized from 4-fluoroaniline (**6b**, 1.0 g, 9.0 mmol) and 3-chloropropanoyl chloride (0.44 mL, 4.5 mmol) following *General Procedure C* and was obtained as a gray solid (1.0 g, 55%). <sup>1</sup>H NMR (CDCl<sub>3</sub>) δ 7.80 (br s, 1H), 7.51–7.35 (m, 2H), 6.99 (t, *J* = 8.6 Hz, 2H), 3.85 (t, *J* = 6.3 Hz, 2H), 2.79 (t, *J* = 6.3 Hz, 2H). <sup>13</sup>C NMR (CDCl<sub>3</sub>) δ 168.1, 159.6 (d, *J* = 243 Hz), 133.3 (d, *J* = 2.6 Hz), 122.2 (d, *J* = 7.9 Hz, 2C), 115.6 (d, *J* = 22.4 Hz, 2C), 40.2, 39.8.

**3-Chloro-N-(3,4-dichlorophenyl)propanamide (7c).** 7c was synthesized from 3,4-dichloroaniline (**6c**, 1.26 g, 7.87 mmol) and 3-chloropropanoyl chloride (0.38 mL, 3.9 mmol) following *General Procedure C* and was obtained as an off-white solid (1.08 g, 54%). <sup>1</sup>H NMR (CDCl<sub>3</sub>) δ 7.75 (d, *J* = 2.0 Hz, 1H), 7.59 (br s, 1H), 7.37 (d, *J* = 8.7 Hz, 1H), 7.33 (dd, *J* = 8.7, 2.2 Hz, 1H), 3.87 (t, *J* = 6.3 Hz, 2H), 2.82 (t, *J* = 6.3 Hz, 2H). <sup>13</sup>C NMR (CDCl<sub>3</sub>) δ 168.0, 136.8, 132.9, 130.6, 128.0, 121.9, 119.3, 40.4, 39.6.

**3-Chloro-N-(4-chloro-3-fluorophenyl)propanamide (7d).** 7d was synthesized from 4-chloro-3-fluoroaniline (**6d**, 1.45 g, 10.0 mmol) and 3-chloropropanoyl chloride (0.35 mL, 5.0 mmol) following *General Procedure C* and was obtained as an off-white solid (1.20 g, 53%). <sup>1</sup>H NMR (DMSO-*d*<sub>6</sub>) δ 10.39 (s, 1H), 7.79 (dd, *J* = 11.9, 2.2 Hz, 1H), 7.50 (t, *J* = 8.6 Hz, 1H), 7.36–7.28 (m, 1H), 3.88 (t, *J* = 6.2 Hz, 2H), 2.84 (t, *J* = 6.2 Hz, 2H). <sup>13</sup>C NMR (DMSO-*d*<sub>6</sub>) δ 168.5, 157.0 (d, *J* = 244 Hz), 139.4 (d, *J* = 8.5 Hz), 130.6, 115.9, 113.0 (d, *J* = 18.6 Hz), 107.2 (d, *J* = 25.3 Hz), 40.5, 39.3.

**3-Chloro-N-(3-chloro-4-fluorophenyl)propanamide (7e).** 7e was synthesized from 3-chloro-4-fluoroaniline (**6e**, 1.45 g, 10.0 mmol) and 3-chloropropanoyl chloride (0.35 mL, 5.0 mmol) following *General Procedure C* and was obtained as an off-white solid (1.12 g, 54%). <sup>1</sup>H NMR (CDCl<sub>3</sub>) δ 7.72 (br s, 1H), 7.67 (dd, *J* = 6.5, 2.5 Hz, 1H), 7.34–7.29 (m, 1H), 7.06 (t, *J* = 8.7 Hz, 1H), 3.86 (t, *J* = 6.3 Hz, 2H), 2.80 (t, *J* = 6.3 Hz, 2H). <sup>13</sup>C NMR (CDCl<sub>3</sub>) δ 168.1, 155.2 (d, *J* = 245 Hz), 133.9 (d, *J* = 3.3 Hz), 122.6, 121.2 (d, *J* = 18.5 Hz), 120.0 (d, *J* = 6.8 Hz), 116.6 (d, *J* = 22.0 Hz), 40.2, 39.7.

**3-Chloro-N-phenylpropanamide (7f).** 7f was synthesized from aniline (**6f**, 1.00 g, 0.98 mL, 10.8 mmol) and 3-chloropropanoyl chloride (0.54 mL, 5.4 mmol) following *General Procedure C* and was obtained as an off-white powder (1.2 g, 61%). <sup>1</sup>H NMR (CDCl<sub>3</sub>) δ 7.52 (d, *J* = 7.8 Hz, 2H), 7.35 (br s, 1H), 7.33 (t, *J* = 7.8 Hz, 2H), 7.13 (t, *J* = 7.4 Hz, 1H), 3.88 (t, *J* = 6.4 Hz, 2H), 2.81 (t, *J* = 6.4 Hz, 2H). <sup>13</sup>C NMR (CDCl<sub>3</sub>) δ 167.8, 137.5, 129.2 (2C), 124.9, 120.2 (2C), 40.7, 40.0.

**4-Chloro-N-(2-methylbut-3-yn-2-yl)aniline (8a).** To a round-bottom flask charged with 4-chloroaniline (**6a**, 635 mg, 5.0 mmol) and TEA (0.90 mL, 6.1 mmol) in Et<sub>2</sub>O/H<sub>2</sub>O (5/1 mL) were added Cu powder (3.2 mg, 0.05 mmol), CuCl (4.9 mg, 0.05 mmol), and 3-chloro-3-methyl-1-butyne (410 mg, 4.15 mmol) under an argon atmosphere at room temperature. The resulting mixture was stirred for 3 h at room temperature. The reaction was quenched with H<sub>2</sub>O (5 mL), and the mixture was extracted with EtOAc (10 mL × 3). The combined organic extracts were washed with brine (20 mL), dried over Na<sub>2</sub>SO<sub>4</sub>, and concentrated under vacuum. The crude product was purified by flash chromatography (0–30% EtOAc/hexane) to afford **8a** as a yellow oil (540 mg, 56%). <sup>1</sup>H NMR (CDCl<sub>3</sub>) δ 7.18–7.10 (m, 2H), 6.91–6.83 (m, 2H), 3.66 (br s, 1H), 2.38 (s, 1H), 1.60 (s, 6H). <sup>13</sup>C NMR (CDCl<sub>3</sub>) δ 144.1, 128.7 (2C), 123.6 (2C), 117.7, 87.4, 70.8, 48.3, 30.5 (2C).

**4-Fluoro-N-(2-methylbut-3-yn-2-yl)aniline (8b).** **8b** was synthesized from 4-fluoroaniline (**6b**, 1.11 g, 10.0 mmol) following the procedure for **8a** and was obtained as a yellow oil (1.10 g, 62%). <sup>1</sup>H NMR (CDCl<sub>3</sub>) δ 6.96–6.91 (m, 4H), 3.44 (br s, 1H), 2.37 (d, *J* = 0.7 Hz, 1H), 1.57 (s, 6H). <sup>13</sup>C NMR (CDCl<sub>3</sub>) δ 157.1 (d, *J* = 236 Hz), 141.6 (d, *J* = 2.2 Hz), 119.2 (d, *J* = 7.5 Hz, 2C), 115.2 (d, *J* = 22 Hz, 2C), 87.8, 70.6, 48.8, 30.3 (2C).

**6-Chloro-2,2-dimethyl-1,2,3,4-tetrahydroquinoline (9a).** (i) To a solution of **8a** (540 mg, 2.80 mmol) in THF (5 mL) was added CuCl (28 mg, 0.28 mmol) in a microwave reaction tube. The mixture was heated at 120 °C for 1 h in a microwave reactor. After completion of the reaction, the precipitated solid was filtered off, and the concentrated filtrate was purified by flash chromatography (0–10% EtOAc/hexane) to afford the intermediate as a yellow solid (420 mg, 78%). (ii) To a solution of the intermediate (420 mg, 2.17 mmol) in EtOAc (10 mL) was added Pd/C (10% w/w, 50 mg), and then the mixture was degassed under vacuum, and the atmosphere was replaced with H<sub>2</sub>. The resulting mixture was stirred at room temperature for 30 min. Then, the solid was filtered off, and the filtrate was concentrated under vacuum to afford **9a** as a colorless oil (360 mg, 85%). **9a** was used directly in the next step without further

purification. <sup>1</sup>H NMR (CDCl<sub>3</sub>) δ 6.96 (d, *J* = 2.4 Hz, 1H), 6.90 (dd, *J* = 8.5, 2.4 Hz, 1H), 6.37 (d, *J* = 8.5 Hz, 1H), 2.74 (t, *J* = 6.7 Hz, 2H), 1.67 (t, *J* = 6.8 Hz, 2H), 1.20 (s, 6H). <sup>13</sup>C NMR (CDCl<sub>3</sub>) δ 142.5, 128.8, 126.5, 121.6, 121.0, 115.3, 49.0, 33.9, 29.0, 24.1 (2C).

**6-Fluoro-2,2-dimethyl-1,2,3,4-tetrahydroquinoline (9b).** **9b** was synthesized from **8b** (1.1 g, 6.2 mmol) following the procedure for **9a** and was obtained as a colorless oil (650 mg, 93%). <sup>1</sup>H NMR (CDCl<sub>3</sub>) δ 6.70 (ddd, *J* = 16.9, 8.7, 2.8 Hz, 2H), 6.38 (dd, *J* = 8.6, 4.8 Hz, 1H), 3.23 (br s, 1H), 2.76 (t, *J* = 6.7 Hz, 2H), 1.68 (t, *J* = 6.8 Hz, 2H), 1.20 (s, 6H). <sup>13</sup>C NMR (CDCl<sub>3</sub>) δ 155.3 (d, *J* = 233 Hz), 140.1 (d, *J* = 1.5 Hz), 121.4 (d, *J* = 6.6 Hz), 115.3 (d, *J* = 21.6 Hz), 115.0 (d, *J* = 7.4 Hz), 113.2 (d, *J* = 22.4 Hz), 48.9, 34.0, 29.0 (2C), 24.3.

**N-(4-Chlorophenyl)-3-methylbut-2-enamide (10a).** To a round-bottom flask charged with 4-chloroaniline (**6a**, 1.27 g, 10.0 mmol) and CHCl<sub>3</sub> (20 mL) was added 3,3-dimethylacryloyl chloride (1.18 g, 10.0 mmol). The resulting mixture was heated to reflux for 2 h. Then, the mixture was cooled to room temperature, 2 N HCl (20 mL) was added, and the mixture was extracted with EtOAc (20 mL × 3). The combined organic layers were washed with brine (20 mL), dried over Na<sub>2</sub>SO<sub>4</sub>, and concentrated under vacuum. The crude product was purified by flash chromatography (0–80% EtOAc/hexane) to afford **10a** as a white powder (1.00 g, 48%). <sup>1</sup>H NMR (CDCl<sub>3</sub>) δ 7.54 (br s, 1H), 7.47 (d, *J* = 8.1 Hz, 2H), 7.22 (d, *J* = 8.8 Hz, 2H), 5.70 (s, 1H), 2.19 (s, 3H), 1.86 (s, 3H). <sup>13</sup>C NMR (CDCl<sub>3</sub>) δ 165.2, 154.0, 136.8, 128.8 (4C), 121.0, 118.4, 27.3, 20.0.

**N-(4-Fluorophenyl)-3-methylbut-2-enamide (10b).** **10b** was synthesized from 4-fluoroaniline (**6b**, 1.11 g, 10.0 mmol) and 3,3-dimethylacryloyl chloride (1.18 g, 10.0 mmol) following the procedure for **10a** and was obtained as an off-white powder (1.0 g, 52%). <sup>1</sup>H NMR (CDCl<sub>3</sub>) δ 7.67 (br s, 1H), 7.47 (dd, *J* = 7.0, 4.7 Hz, 2H), 6.94 (td, *J* = 8.8, 2.2 Hz, 2H), 5.70 (d, *J* = 1.1 Hz, 1H), 2.18 (s, 3H), 1.85 (s, 3H). <sup>13</sup>C NMR (CDCl<sub>3</sub>) δ 165.3, 159.1 (d, *J* = 242 Hz), 153.3 (d, *J* = 3.0 Hz), 134.2, 121.7 (d, *J* = 5.4 Hz, 2C), 118.5, 115.3 (d, *J* = 22 Hz, 2C), 27.2 (2C), 19.9.

**6-Chloro-4,4-dimethyl-1,2,3,4-tetrahydroquinoline (11a).** (i) To a round-bottom flask charged with **10a** (1.00 g, 4.78 mmol) in toluene (15 mL) was added AlCl<sub>3</sub> (2.50 g, 19.12 mmol) at room temperature. The resulting mixture was heated at 80 °C for 2 h. Then, the reaction was carefully quenched with 1 N HCl (10 mL) at 0 °C, and the mixture was extracted with EtOAc (15 mL × 3). The combined organic extracts were washed with brine (20 mL), dried over Na<sub>2</sub>SO<sub>4</sub>, and concentrated under vacuum. The crude product was purified by flash chromatography (0–80% EtOAc/hexane) to afford the lactam intermediate as a brown powder (640 mg, 64%). (ii) To a stirred solution of LiAlH<sub>4</sub> (250 mg, 6.60 mmol) in THF (10 mL) was dropwise added a solution of the lactam (460 mg, 2.20 mmol) in THF (20 mL) at 0 °C. The resulting mixture was stirred at the same temperature for 20 min and was then heated to reflux for an additional 1 h. The reaction was subsequently quenched with water (0.5 mL), 5 N NaOH (0.5 mL), and water (2.5 mL). The precipitate was filtered off and washed with EtOAc (20 mL × 3). The filtrate was washed with brine (20 mL), dried over Na<sub>2</sub>SO<sub>4</sub>, and concentrated under vacuum. The crude product was purified by flash chromatography (0–20% EtOAc/hexane) to afford **11a** as a colorless oil (370 mg, 86%). <sup>1</sup>H NMR (DMSO-*d*<sub>6</sub>) δ 7.05 (d, *J* = 2.5 Hz, 1H), 6.83 (dd, *J* = 8.6, 2.5 Hz, 1H), 6.44 (d, *J* = 8.6 Hz, 1H), 5.91 (br s, 1H), 3.21–3.12 (m, 2H), 1.61–1.53 (m, 2H), 1.20 (s, 6H). <sup>13</sup>C NMR (DMSO-*d*<sub>6</sub>) δ 143.1, 130.5, 125.9, 125.3, 118.3, 114.8, 37.0, 36.0, 31.5, 30.3 (2C).

**6-Fluoro-4,4-dimethyl-3,4-dihydroquinolin-2(1H)-one (11b).** **11b** was synthesized from **10b** (1.00 g, 5.24 mmol) following the procedure for **11a** and was obtained as a brown oil (310 mg, 76%). <sup>1</sup>H NMR (CDCl<sub>3</sub>) δ 6.91 (dd, *J* = 10.3, 2.9 Hz, 1H), 6.68 (ddd, *J* = 8.7, 8.2, 2.9 Hz, 1H), 6.40 (dd, *J* = 8.7, 5.0 Hz, 1H), 3.56 (br s, 1H), 3.34–3.19 (m, 2H), 1.81–1.65 (m, 2H), 1.29 (s, 6H). <sup>13</sup>C NMR (CDCl<sub>3</sub>) δ 155.6 (d, *J* = 232 Hz), 139.8 (d, *J* = 1.4 Hz), 131.7 (d, *J* = 5.7 Hz), 114.9 (d, *J* = 7.5 Hz), 113.1 (d, *J* = 22.3 Hz), 112.8 (d, *J* = 22.0 Hz), 38.7, 37.2, 32.2, 31.2 (2C).

**6-Chloro-3,4-dihydroquinolin-2(1H)-one (12a).** In a three-necked flask charged with **7a** (4.60 g, 21.1 mmol) under an argon atmosphere

was added  $\text{AlCl}_3$  (5.47 g, 42.2 mmol) at 140 °C. The resulting mixture was stirred at the same temperature for 12 h. Then, the reaction was carefully quenched with 1 N HCl (20 mL) at 0 °C, and the mixture was extracted with EtOAc (30 mL  $\times$  3). The combined organic layers were washed with brine (20 mL), dried over  $\text{Na}_2\text{SO}_4$ , and concentrated under vacuum. The crude product was purified by flash chromatography (0–80% EtOAc/hexane) to obtain **12a** as a white powder (3.10 g, 81%).  $^1\text{H}$  NMR ( $\text{CDCl}_3$ )  $\delta$  8.28 (br s, 1H), 7.19–7.11 (m, 2H), 6.71 (d,  $J$  = 8.1 Hz, 1H), 3.06–2.85 (m, 2H), 2.63 (dd,  $J$  = 8.4, 6.7 Hz, 2H).  $^{13}\text{C}$  NMR ( $\text{CDCl}_3$ )  $\delta$  171.3, 135.9, 128.1, 128.0, 127.5, 125.4, 116.4, 30.4, 25.3.

**3,4-Dihydroquinolin-2(1H)-one (12b).** **12b** was synthesized from **7f** (1.15 g, 6.56 mmol) following the procedure for **12a** and was obtained as an off-white powder (460 mg, 48%).  $^1\text{H}$  NMR ( $\text{CDCl}_3$ )  $\delta$  8.94 (br s, 1H), 7.17 (t,  $J$  = 8.1 Hz, 2H), 6.98 (t,  $J$  = 7.4 Hz, 1H), 6.83 (d,  $J$  = 7.7 Hz, 1H), 2.97 (t,  $J$  = 7.5 Hz, 2H), 2.70–2.52 (m, 2H).  $^{13}\text{C}$  NMR ( $\text{CDCl}_3$ )  $\delta$  172.2, 137.4, 128.1, 127.7, 123.8, 123.2, 115.6, 30.9, 25.5.

**6-Bromo-3,4-dihydroquinolin-2(1H)-one (12c).** To a stirred solution of **12b** (460 mg, 3.13 mmol) in DMF (5 mL) was added NBS (582 mg, 3.29 mmol) at 0 °C. Then, the resulting mixture was stirred at 0 °C for 2 h. The reaction was quenched with water (10 mL), and the mixture was extracted with EtOAc (15 mL  $\times$  3). The combined organic extracts were washed with brine (20 mL), dried over  $\text{Na}_2\text{SO}_4$ , and concentrated under vacuum to obtain **12c** as an off-white powder (650 mg, 92%), which was carried on without further purification.  $^1\text{H}$  NMR ( $\text{CDCl}_3$ )  $\delta$  8.47 (br s, 1H), 7.37–7.26 (m, 2H), 6.67 (d,  $J$  = 8.1 Hz, 1H), 2.95 (t,  $J$  = 7.5 Hz, 2H), 2.63 (dd,  $J$  = 8.4, 6.7 Hz, 2H).  $^{13}\text{C}$  NMR ( $\text{CDCl}_3$ )  $\delta$  172.4, 136.6, 130.8, 130.5, 125.7, 117.3, 115.5, 30.4, 25.2.

**Methyl 4-((6-Chloro-2-oxo-3,4-dihydroquinolin-1(2H)-yl)-methyl)benzoate (13a).** To a stirred solution of **12a** (200 mg, 1.10 mmol) in DMF (20 mL) were added NaH (80 mg, 1.65 mmol) and **3d** (300 mg, 1.33 mmol) at 0 °C. Then, the resulting mixture was stirred at room temperature for 1 h. The reaction was quenched with water (15 mL), and the mixture was extracted with EtOAc (15 mL  $\times$  3). The combined organic extracts were washed with brine (20 mL), dried over  $\text{Na}_2\text{SO}_4$ , and concentrated under vacuum. The crude product was purified by flash chromatography (0–80% EtOAc/hexane), and the title compound was obtained as a colorless oil (50 mg, 14%).  $^1\text{H}$  NMR ( $\text{CDCl}_3$ )  $\delta$  7.97 (d,  $J$  = 8.3 Hz, 2H), 7.25 (d,  $J$  = 8.3 Hz, 2H), 7.16 (d,  $J$  = 2.3 Hz, 1H), 7.04 (dd,  $J$  = 8.7, 2.4 Hz, 1H), 6.68 (d,  $J$  = 8.7 Hz, 1H), 5.19 (s, 2H), 3.89 (s, 3H), 3.01–2.90 (m, 2H), 2.79 (dd,  $J$  = 8.7, 6.0 Hz, 2H).  $^{13}\text{C}$  NMR ( $\text{CDCl}_3$ )  $\delta$  170.2, 166.8, 142.0, 138.3, 130.3 (2C), 129.4, 128.4, 128.2, 128.1, 127.4, 126.4 (2C), 116.7, 52.2, 46.1, 31.6, 25.5.

**Methyl 4-((6-Bromo-2-oxo-3,4-dihydroquinolin-1(2H)-yl)-methyl)benzoate (13b).** **13b** was synthesized from **12c** (650 mg, 2.88 mmol) following the procedure for **13a** and was obtained as an off-white powder (830 mg, 77%), which was carried on without further purification.  $^1\text{H}$  NMR ( $\text{CDCl}_3$ )  $\delta$  7.98 (d,  $J$  = 8.3 Hz, 2H), 7.31 (d,  $J$  = 2.2 Hz, 1H), 7.24 (d,  $J$  = 8.2 Hz, 2H), 7.19 (dd,  $J$  = 8.7, 2.3 Hz, 1H), 6.64 (d,  $J$  = 8.7 Hz, 1H), 5.19 (s, 2H), 3.89 (s, 3H), 3.06–2.90 (m, 2H), 2.79 (dd,  $J$  = 8.6, 6.0 Hz, 2H).  $^1\text{H}$  NMR ( $\text{CDCl}_3$ )  $\delta$  8.04–7.92 (m, 2H), 7.31 (d,  $J$  = 2.3 Hz, 1H), 7.24 (d,  $J$  = 8.5 Hz, 2H), 7.19 (dd,  $J$  = 8.7, 2.3 Hz, 1H), 6.63 (d,  $J$  = 8.7 Hz, 1H), 5.19 (s, 2H), 3.89 (s, 3H), 2.97 (dd,  $J$  = 8.5, 6.1 Hz, 2H), 2.79 (dd,  $J$  = 8.7, 6.0 Hz, 2H).  $^{13}\text{C}$  NMR ( $\text{CDCl}_3$ )  $\delta$  170.1, 167.0, 141.8, 138.7, 130.8, 130.3, 130.2 (2C), 129.3, 128.4, 126.3 (2C), 116.9, 115.9, 52.1, 46.0, 31.4, 25.3.

**Methyl 4-((6-Bromo-3,4-dihydroquinolin-1(2H)-yl)methyl)benzoate (14a).** **14a** was synthesized from **4g** (210 mg, 1.0 mmol) and **3d** (342 mg, 1.5 mmol) following *General Procedure A, Step (i)* and was obtained as a white solid (300 mg, 83%).  $^1\text{H}$  NMR ( $\text{CDCl}_3$ )  $\delta$  7.99 (d,  $J$  = 8.3 Hz, 2H), 7.32–7.24 (m, 2H), 7.08 (d,  $J$  = 2.3 Hz, 1H), 7.01 (dd,  $J$  = 8.7, 2.4 Hz, 1H), 6.26 (d,  $J$  = 8.7 Hz, 1H), 4.49 (s, 2H), 3.90 (s, 3H), 3.40–3.30 (m, 2H), 2.79 (t,  $J$  = 6.2 Hz, 2H), 2.07–1.93 (m, 2H).  $^{13}\text{C}$  NMR ( $\text{CDCl}_3$ )  $\delta$  166.5, 143.9, 143.6, 131.1, 129.6 (2C), 129.3, 128.6, 126.0 (2C), 124.1, 112.1, 107.4, 54.8, 51.7, 49.6, 27.6, 21.7.

**Methyl 4-((6-Cyano-3,4-dihydroquinolin-1(2H)-yl)methyl)benzoate (14b).** **14b** was synthesized from **4h** (200 mg, 1.27 mmol) and **3d** (433 mg, 1.90 mmol) following *General Procedure A, Step (i)* and was obtained as a white solid (200 mg, 51%).  $^1\text{H}$  NMR ( $\text{CDCl}_3$ )  $\delta$  8.01 (AA'XX' multiplet,  $J_{\text{AX}} + J_{\text{AX}'}$  = 8.3 Hz, 2H), 7.27 (AA'XX' multiplet,  $J_{\text{AX}} + J_{\text{AX}'}$  = 8.0 Hz, 2H), 7.21 (d,  $J$  = 7.7 Hz, 2H), 6.38 (d,  $J$  = 8.8 Hz, 1H), 4.59 (s, 2H), 3.91 (s, 3H), 3.48 (t,  $J$  = 5.7 Hz, 2H), 2.82 (t,  $J$  = 6.3 Hz, 2H), 2.14–1.98 (m, 2H).  $^{13}\text{C}$  NMR ( $\text{CDCl}_3$ )  $\delta$  166.8, 148.4, 142.7, 132.5, 132.0, 130.3 (2C), 129.5, 126.3 (2C), 122.6, 120.7, 110.5, 97.7, 54.8, 52.2, 50.3, 27.9, 21.6.

**Methyl 4-((6-Carbamoyl-3,4-dihydroquinolin-1(2H)-yl)methyl)benzoate (14c).** To a stirred solution of **14b** (200 mg, 0.65 mmol) and  $\text{K}_2\text{CO}_3$  (10 mg, 0.065 mmol) in DMSO (2 mL) was added an aqueous  $\text{H}_2\text{O}_2$  solution (30%, 0.8 mL) at 0 °C. The resulting mixture was slowly warmed up to room temperature and stirred for an additional 2 h. After completion of the reaction,  $\text{H}_2\text{O}$  (10 mL) was added, and the mixture was extracted with EtOAc (15 mL  $\times$  3). The combined organic extracts were washed with  $\text{H}_2\text{O}$  and brine, dried over  $\text{Na}_2\text{SO}_4$ , and concentrated under vacuum to obtain **14c** as a white solid (150 mg, 71%), which was carried on without further purification.  $^1\text{H}$  NMR ( $\text{CDCl}_3$ )  $\delta$  8.05–7.94 (m, 2H), 7.52 (d,  $J$  = 2.2 Hz, 1H), 7.39 (d,  $J$  = 8.6 Hz, 1H), 7.29 (d,  $J$  = 8.2 Hz, 2H), 6.39 (d,  $J$  = 8.6 Hz, 1H), 5.57 (br s, 2H), 4.58 (s, 2H), 3.90 (s, 3H), 3.51–3.37 (m, 2H), 2.86 (t,  $J$  = 6.3 Hz, 2H), 2.07–2.02 (m, 2H).  $^{13}\text{C}$  NMR ( $\text{CDCl}_3$ )  $\delta$  169.4, 167.0, 148.4, 143.4, 130.3 (2C), 129.3, 129.0, 127.2, 126.5 (2C), 121.9, 120.2, 110.0, 55.0, 52.2, 50.3, 28.2, 22.1.

**7-Chloro-1,3,4,5-tetrahydro-2H-benz[b]azepin-2-one (15b).** To a stirred solution of 1,3,4,5-tetrahydro-2H-benz[b]azepin-2-one (**15a**, 300 mg, 1.86 mmol) in toluene (2 mL) was added  $\text{SO}_2\text{Cl}_2$  (3.72 mL, 1 M in DCM) at 0 °C with ice cooling. The resulting mixture was stirred for an additional 40 min at 0 °C after the addition was completed and then at room temperature for an additional 3 h. The solvent and excess  $\text{SO}_2\text{Cl}_2$  were removed under vacuum. The crude product was purified via preparative HPLC (8–100%,  $\text{H}_2\text{O}/\text{CH}_3\text{CN}$ , containing 0.05% TFA) to afford **15b** as a white powder (140 mg, 39%).  $^1\text{H}$  NMR ( $\text{CDCl}_3$ )  $\delta$  9.02 (br s, 1H), 7.19 (s, 1H), 7.19–7.16 (m, 1H, overlapping with solvent signal), 6.95 (d,  $J$  = 8.0 Hz, 1H), 2.75 (t,  $J$  = 7.2 Hz, 2H), 2.34 (t,  $J$  = 7.1 Hz, 2H), 2.28–2.05 (m, 2H).  $^{13}\text{C}$  NMR ( $\text{CDCl}_3$ )  $\delta$  175.8, 136.8, 136.0, 130.7, 129.8, 127.5, 123.2, 32.9, 30.4, 28.4.

**2,3,4,5-Tetrahydro-1H-benz[b]azepine (16a).** To a stirred solution of 1,3,4,5-tetrahydro-2H-benz[b]azepin-2-one (**15a**, 483 mg, 3.0 mmol) in THF (20 mL) was added  $\text{LiAlH}_4$  (342 mg, 9.00 mmol) at 0 °C. The resulting mixture was stirred at the same temperature for 10 min and then under reflux for 2 h. After the completion of the reaction, the mixture was quenched with water (0.3 mL), 5 N NaOH (0.3 mL), and water (1.5 mL). The particulate was filtered off, and the filtrate was concentrated under vacuum. The crude product was purified by flash chromatography (0–10% EtOAc/hexane) to obtain **16a** as a colorless oil (380 mg, 86%).  $^1\text{H}$  NMR ( $\text{CDCl}_3$ )  $\delta$  7.12 (d,  $J$  = 7.3 Hz, 1H), 7.05 (t,  $J$  = 7.1 Hz, 1H), 6.84 (t,  $J$  = 7.3 Hz, 1H), 6.74 (d,  $J$  = 7.7 Hz, 1H), 3.77 (br s, 1H), 3.13–2.95 (m, 2H), 2.87–2.69 (m, 2H), 1.87–1.74 (m, 2H), 1.74–1.57 (m, 2H).  $^{13}\text{C}$  NMR ( $\text{CDCl}_3$ )  $\delta$  150.5, 133.8, 130.9, 126.7, 120.9, 119.5, 49.0, 36.2, 32.1, 27.0.

**7-Chloro-2,3,4,5-tetrahydro-1H-benz[b]azepine (16b).** **16b** was synthesized from **15b** (120 mg, 0.61 mmol) following the procedure for **16a** and obtained as a colorless oil (70 mg, 59%).  $^1\text{H}$  NMR ( $\text{CDCl}_3$ )  $\delta$  7.09 (d,  $J$  = 2.1 Hz, 1H), 6.99 (dd,  $J$  = 8.3, 2.4 Hz, 1H), 6.66 (d,  $J$  = 8.3 Hz, 1H), 3.77 (br s, 1H), 3.08–2.99 (m, 2H), 2.80–2.68 (m, 2H), 1.83–1.77 (m, 2H), 1.71–1.61 (m, 2H).  $^{13}\text{C}$  NMR ( $\text{CDCl}_3$ )  $\delta$  149.2, 135.5, 130.5, 126.3, 125.5, 120.6, 49.0, 35.9, 31.9, 26.8.

**7-Bromo-2,3,4,5-tetrahydro-1H-benz[b]azepine (16c).** To a stirred solution of **16a** (300 mg, 2.04 mmol) in DMF (7 mL) was added dropwise a solution of NBS (381 mg, 2.14 mmol) in DMF (3 mL) at 0 °C. Then, the resulting mixture was slowly warmed to room temperature in 30 min and stirred for an additional 1 h. After completion, the reaction was quenched with water (10 mL), and the mixture was extracted with EtOAc (10 mL  $\times$  3). The combined

organic extracts were washed with brine (10 mL), dried over  $\text{Na}_2\text{SO}_4$ , and concentrated under vacuum. The crude product was purified by flash chromatography (0–20% EtOAc/hexane) to afford **16c** as an off-white solid (300 mg, 65%).  $^1\text{H}$  NMR ( $\text{CDCl}_3$ )  $\delta$  7.22 (d,  $J$  = 2.2 Hz, 1H), 7.11 (dd,  $J$  = 8.3, 2.3 Hz, 1H), 6.59 (d,  $J$  = 8.3 Hz, 1H), 3.75 (br s, 1H), 3.02 (dd,  $J$  = 7.0, 3.8 Hz, 2H), 2.81–2.65 (m, 2H), 1.81–1.75 (m, 2H), 1.70–1.55 (m, 2H).  $^{13}\text{C}$  NMR ( $\text{CDCl}_3$ )  $\delta$  149.7, 135.9, 133.3, 129.3, 121.0, 112.9, 48.9, 35.9, 31.8, 26.8.

**2,3,4,5-Tetrahydro-1H-benz[b]azepine-7-carbonitrile (16d)**. To a solution of **16c** (100 mg, 0.44 mmol) in DMF/water (99:1, 2 mL) were added  $\text{Zn}(\text{CN})_2$  (112 mg, 0.48 mmol), S-Phos (18 mg, 0.04 mmol), and  $\text{Pd}_2(\text{dba})_3$  (20 mg, 0.02 mmol) in a microwave reaction tube. Then, the resulting mixture was heated at 170 °C for 30 min in a microwave reactor. After completion, the reaction was quenched with water (10 mL), and the mixture was extracted with EtOAc (10 × 3 mL). The combined organic extracts were washed with water and brine, dried over  $\text{Na}_2\text{SO}_4$ , and concentrated under a vacuum. The crude product was purified by flash chromatography (0–50% EtOAc/hexane) to afford **16d** as a colorless oil (70 mg, 93%).  $^1\text{H}$  NMR ( $\text{CDCl}_3$ )  $\delta$  7.33 (d,  $J$  = 1.6 Hz, 1H), 7.27 (dd,  $J$  = 8.2, 1.8 Hz, 1H), 6.66 (d,  $J$  = 8.2 Hz, 1H), 4.16 (br s, 1H), 3.25–3.07 (m, 2H), 2.78–2.75 (m, 2H), 1.87–1.77 (m, 2H), 1.77–1.67 (m, 2H).  $^{13}\text{C}$  NMR ( $\text{CDCl}_3$ )  $\delta$  154.5, 135.0, 132.3, 130.9, 120.2, 119.0, 102.3, 47.8, 35.3, 30.7, 26.3.

**Methyl 4-((7-Chloro-2-oxo-2,3,4,5-tetrahydro-1H-benz[b]azepin-1-yl)methyl)benzoate (17a)**. **17a** was synthesized from **15b** (140 mg, 0.72 mmol) and **3d** (196 mg, 0.86 mmol) following the procedure for **13a** and was obtained as a colorless oil (200 mg, 81%).  $^1\text{H}$  NMR ( $\text{CDCl}_3$ )  $\delta$  7.88 (d,  $J$  = 8.2 Hz, 2H), 7.25 (d,  $J$  = 8.1 Hz, 2H), 7.16 (dd,  $J$  = 8.5, 2.4 Hz, 1H), 7.08 (d,  $J$  = 2.4 Hz, 1H), 7.06 (d,  $J$  = 8.5 Hz, 1H), 4.99 (s, 2H), 3.83 (s, 3H), 2.44 (t,  $J$  = 7.1 Hz, 2H), 2.31 (t,  $J$  = 7.1 Hz, 2H), 2.16–2.06 (m, 2H).  $^{13}\text{C}$  NMR ( $\text{CDCl}_3$ )  $\delta$  172.9, 166.7, 142.6, 140.7, 137.6, 131.6, 129.8 (2C), 129.3, 129.3, 128.0 (2C), 127.5, 123.9, 52.0, 50.9, 32.9, 29.8, 28.6.

**Methyl 4-((2,3,4,5-Tetrahydro-1H-benz[b]azepin-1-yl)methyl)benzoate (17b)**. **17b** was synthesized from **16a** (70 mg, 0.48 mmol) and **3d** (163 mg, 0.71 mmol) following General Procedure A, Step (i) and was obtained as a colorless oil (120 mg, 85%).  $^1\text{H}$  NMR ( $\text{CDCl}_3$ )  $\delta$  8.02 (d,  $J$  = 8.3 Hz, 2H), 7.51 (d,  $J$  = 8.3 Hz, 2H), 7.15–7.12 (m, 2H), 6.96 (d,  $J$  = 7.8 Hz, 1H), 6.90 (td,  $J$  = 7.4, 0.9 Hz, 1H), 4.38 (s, 2H), 3.92 (s, 3H), 2.90 (s, 4H), 1.64 (s, 4H).  $^{13}\text{C}$  NMR ( $\text{CDCl}_3$ )  $\delta$  167.2, 152.3, 145.5, 136.4, 130.2, 129.8 (2C), 129.1, 128.4(2C), 126.8, 121.7, 117.8, 58.5, 54.0, 52.1, 35.1, 30.1, 25.9.

**Methyl 4-((7-Chloro-2,3,4,5-tetrahydro-1H-benz[b]azepin-1-yl)methyl)benzoate (17c)**. **17c** was synthesized from **16b** (70 mg, 0.36 mmol) and **3d** (125 mg, 0.55 mmol) following General Procedure A, Step (i) and was obtained as a colorless oil (70 mg, 85%).  $^1\text{H}$  NMR ( $\text{CDCl}_3$ )  $\delta$  8.01 (d,  $J$  = 8.2 Hz, 2H), 7.47 (d,  $J$  = 8.1 Hz, 2H), 7.11 (d,  $J$  = 2.4 Hz, 1H), 7.06 (dd,  $J$  = 8.5, 2.5 Hz, 1H), 6.83 (d,  $J$  = 8.5 Hz, 1H), 4.33 (s, 2H), 3.91 (s, 3H), 2.96–2.79 (m, 4H), 1.62 (s, 4H).  $^{13}\text{C}$  NMR ( $\text{CDCl}_3$ )  $\delta$  167.1, 150.7, 144.9, 138.0, 129.84 (2 C), 129.82, 129.2, 128.2 (2 C), 126.4, 126.3, 119.0, 58.5, 54.1, 52.2, 34.8, 29.8, 25.5.

**Methyl 4-((7-Bromo-2,3,4,5-tetrahydro-1H-benz[b]azepin-1-yl)methyl)benzoate (17d)**. **17d** was synthesized from **16c** (190 mg, 0.84 mmol) and **3d** (287 mg, 1.26 mmol) following General Procedure A, Step (i) and was obtained as an off-white solid (100 mg, 31%).  $^1\text{H}$  NMR ( $\text{CDCl}_3$ )  $\delta$  8.02 (d,  $J$  = 8.2 Hz, 2H), 7.48 (d,  $J$  = 8.2 Hz, 2H), 7.27 (d,  $J$  = 2.4 Hz, 1H), 7.21 (dd,  $J$  = 8.5, 2.4 Hz, 1H), 6.79 (d,  $J$  = 8.5 Hz, 1H), 4.34 (s, 2H), 3.93 (s, 3H), 2.87 (d,  $J$  = 14.3 Hz, 4H), 1.63 (s, 4H).  $^{13}\text{C}$  NMR ( $\text{CDCl}_3$ )  $\delta$  167.1, 151.2, 144.9, 138.4, 132.7, 129.9 (2C), 129.4, 129.2, 128.2 (2C), 119.4, 113.9, 58.43, 54.0, 52.2, 34.8, 29.8, 25.5.

**Methyl 4-((7-Cyano-2,3,4,5-tetrahydro-1H-benz[b]azepin-1-yl)methyl)benzoate (17e)**. **17e** was synthesized from **16d** (70 mg, 0.41 mmol) and **3d** (139 mg, 0.61 mmol) following General Procedure A, Step (i) and was obtained as a colorless oil (60 mg, 46%).  $^1\text{H}$  NMR ( $\text{CDCl}_3$ )  $\delta$  8.01 (d,  $J$  = 8.3 Hz, 2H), 7.38 (d,  $J$  = 8.2 Hz, 2H), 7.35–7.29 (m, 2H), 6.78 (d,  $J$  = 8.3 Hz, 1H), 4.45 (s, 2H), 3.90 (s, 3H), 3.14 (d,  $J$  = 4.9 Hz, 2H), 2.87 (d,  $J$  = 5.4 Hz, 2H), 1.81–1.67 (m,

4H).  $^{13}\text{C}$  NMR ( $\text{CDCl}_3$ )  $\delta$  166.9, 155.3, 143.7, 134.2, 134.0, 131.3, 130.0 (2C), 129.4, 127.7 (2C), 120.0, 117.2, 102.6, 57.7, 53.1, 52.2, 34.1, 28.2, 24.9.

**4-((7-Chloro-2-oxo-2,3,4,5-tetrahydro-1H-benz[b]azepin-1-yl)methyl)-N-hydroxybenzamide (18a)**. **18a** was synthesized from **17a** (200 mg, 0.58 mmol) following General Procedure A, Step (ii) and was obtained as a white powder (140 mg, 70%).  $^1\text{H}$  NMR ( $\text{DMSO}-d_6$ )  $\delta$  11.12 (br s, 1H), 8.98 (br s, 1H), 7.63 (d,  $J$  = 8.3 Hz, 2H), 7.34 (dd,  $J$  = 8.3, 2.5 Hz, 1H; d,  $J$  = 2.5 Hz, 1H, overlapping), 7.26 (d,  $J$  = 8.2 Hz, 2H), 5.02 (s, 2H), 2.52–2.50 (m, 2H, overlapping with solvent peak), 2.23 (t,  $J$  = 7.1 Hz, 2H), 2.09–2.07 (m, 2H).  $^{13}\text{C}$  NMR ( $\text{DMSO}-d_6$ )  $\delta$  171.9, 163.9, 141.0, 140.7, 137.5, 131.7, 129.8, 129.0, 127.7 (2C), 127.3, 127.0 (2C), 124.3, 49.4, 32.7, 29.1, 28.1. ESI HRMS calcd for  $\text{C}_{18}\text{H}_{17}\text{ClN}_2\text{O}_3$ :  $[\text{M} + \text{H}]^+$ ,  $m/z$  344.1000; found: 344.0098.

**N-Hydroxy-4-((2,3,4,5-tetrahydro-1H-benz[b]azepin-1-yl)methyl)benzamide (18b)**. **18b** was synthesized from **17b** (120 mg, 0.41 mmol) following General Procedure A, Step (ii) and was obtained as a white powder (110 mg, 90%).  $^1\text{H}$  NMR ( $\text{DMSO}-d_6$ )  $\delta$  11.14 (br s, 1H), 7.70 (d,  $J$  = 8.2 Hz, 2H), 7.47 (d,  $J$  = 8.0 Hz, 2H), 7.11 (d,  $J$  = 7.4 Hz, 1H), 7.09–7.02 (m, 1H), 6.94 (d,  $J$  = 8.0 Hz, 1H), 6.82 (t,  $J$  = 7.1 Hz, 1H), 4.36 (s, 2H), 2.95–2.77 (m, 4H), 1.60–1.56 (m, 4H).  $^{13}\text{C}$  NMR (126 MHz,  $\text{DMSO}-d_6$ )  $\delta$  164.1, 151.6, 142.9, 135.5, 131.5, 129.9, 128.0, 126.9 (2C), 126.6 (2C), 121.12, 117.70, 57.3, 54.1, 34.3, 25.4. ESI HRMS calcd for  $\text{C}_{18}\text{H}_{19}\text{N}_2\text{O}_2$ :  $[\text{M} - \text{H}]^-$ ,  $m/z$  295.1452; found: 295.1446.

**4-((7-Chloro-2,3,4,5-tetrahydro-1H-benz[b]azepin-1-yl)methyl)-N-hydroxybenzamide (18c)**. **18c** was synthesized from **17c** (70 mg, 0.21 mmol) following General Procedure A, Step (ii) and was obtained as a white powder (55 mg, 79%).  $^1\text{H}$  NMR (500 MHz,  $\text{DMSO}-d_6$ )  $\delta$  11.14 (s, 1H), 8.98 (br s, 1H), 7.69 (d,  $J$  = 7.9 Hz, 2H), 7.44 (d,  $J$  = 7.9 Hz, 2H), 7.17 (d,  $J$  = 2.6 Hz, 1H), 7.08 (dd,  $J$  = 8.5, 2.6 Hz, 1H), 6.92 (d,  $J$  = 8.6 Hz, 1H), 4.35 (s, 2H), 2.87 (t,  $J$  = 5.0 Hz, 2H), 2.83–2.76 (m, 2H), 1.60–1.55 (m, 4H).  $^{13}\text{C}$  NMR (126 MHz,  $\text{DMSO}-d_6$ )  $\delta$  164.1, 150.4, 142.6, 137.5, 131.5, 129.2, 127.8 (2C), 126.9 (2C), 126.0, 124.5, 119.2, 57.3, 53.9, 33.8, 29.3, 25.0. ESI HRMS calcd for  $\text{C}_{18}\text{H}_{18}\text{ClNO}_2$ :  $[\text{M} - \text{H}]^-$ ,  $m/z$  329.1062; found: 329.1068.

**4-((7-Bromo-2,3,4,5-tetrahydro-1H-benz[b]azepin-1-yl)methyl)-N-hydroxybenzamide (18d)**. **18d** was synthesized from **17d** (50 mg, 0.13 mmol) following General Procedure A, Step (ii) and was obtained as an off-white powder (45 mg, 92%).  $^1\text{H}$  NMR (500 MHz,  $\text{DMSO}-d_6$ )  $\delta$  11.14 (s, 1H), 7.69 (d,  $J$  = 8.0 Hz, 2H), 7.44 (d,  $J$  = 8.0 Hz, 2H), 7.29 (d,  $J$  = 2.4 Hz, 1H), 7.20 (dd,  $J$  = 8.5, 2.5 Hz, 1H), 6.86 (d,  $J$  = 8.6 Hz, 1H), 4.35 (s, 2H), 2.88 (t,  $J$  = 5.1 Hz, 2H), 2.83–2.76 (m, 2H), 1.61–1.53(m, 4H).  $^{13}\text{C}$  NMR (126 MHz,  $\text{DMSO}-d_6$ )  $\delta$  164.1, 150.8, 142.6, 137.9, 132.0, 131.5, 128.9, 127.8 (2C), 126.9 (2C), 119.7, 112.5, 57.2, 53.8, 33.8, 29.2, 25.0. ESI HRMS calcd for  $\text{C}_{18}\text{H}_{18}\text{BrN}_2\text{O}_2$ :  $[\text{M} - \text{H}]^-$ ,  $m/z$  373.0557; found: 373.0547.

**4-((7-(1H-Pyrazol-4-yl)-2,3,4,5-tetrahydro-1H-benz[b]azepin-1-yl)methyl)-N-hydroxybenzamide (18e)**. **18e** was synthesized from **17d** (50 mg, 0.13 mmol) following the procedure for **1q** and was obtained as a gray powder (5.2 mg, 11% over two steps).  $^1\text{H}$  NMR ( $\text{DMSO}-d_6$ )  $\delta$  11.14 (s, 1H), 7.92 (s, 2H), 7.69 (d,  $J$  = 8.1 Hz, 2H), 7.47 (d,  $J$  = 8.1 Hz, 2H), 7.36 (s, 1H), 7.27 (dd,  $J$  = 8.2, 1.9 Hz, 1H), 6.91 (d,  $J$  = 8.3 Hz, 1H), 4.38 (s, 2H), 2.86 (br s, 4H), 1.60 (br s, 4H). ESI HRMS calcd for  $\text{C}_{21}\text{H}_{21}\text{N}_4\text{O}_2$ :  $[\text{M} - \text{H}]^-$ ,  $m/z$  361.1670; found: 361.1666.

**4-((7-Cyano-2,3,4,5-tetrahydro-1H-benz[b]azepin-1-yl)methyl)-N-hydroxybenzamide (18f)**. **18f** was synthesized from **17e** (30 mg, 0.094 mmol) following General Procedure A, Step (ii) and was obtained as a white powder (28 mg, 93%).  $^1\text{H}$  NMR ( $\text{DMSO}-d_6$ )  $\delta$  11.16 (s, 1H), 9.01 (br s, 1H), 7.71 (d,  $J$  = 8.1 Hz, 2H), 7.47 (d,  $J$  = 1.8 Hz, 1H), 7.43–7.40 (m, 1H), 7.38 (d,  $J$  = 8.0 Hz, 2H), 6.82 (d,  $J$  = 8.4 Hz, 1H), 4.51 (s, 2H), 3.20 (s, 2H), 2.86 (s, 2H), 1.69 (s, 4H). ESI HRMS calcd for  $\text{C}_{19}\text{H}_{18}\text{N}_3\text{O}_2$ :  $[\text{M} - \text{H}]^-$ ,  $m/z$  320.1392.

**1-(4-(Hydroxycarbonyl)benzyl)-2,3,4,5-tetrahydro-1H-benz[b]azepine-7-carboxamide (18g)**. (i) To a stirred solution of **17e** (30 mg, 0.094 mmol) and  $\text{K}_2\text{CO}_3$  (1.3 mg, 0.0094 mmol) in DMSO (1 mL) was added aqueous  $\text{H}_2\text{O}_2$  solution (30%, 0.5 mL) at 0 °C. The resulting mixture was slowly warmed to room temperature and stirred

overnight. After completion, the reaction was quenched with H<sub>2</sub>O (5 mL), and the mixture was extracted with EtOAc (10 mL × 3). The combined organic layers were washed with H<sub>2</sub>O and brine, dried over Na<sub>2</sub>SO<sub>4</sub>, and concentrated under vacuum to afford the intermediate. (ii) Compound **18g** was synthesized from the intermediate following *General Procedure A, Step (ii)* and was obtained as a white powder (14 mg, 44% for two steps). <sup>1</sup>H NMR (DMSO-*d*<sub>6</sub>) δ 11.15 (s, 1H), 7.70 (d, *J* = 8.1 Hz, 3H, overlapping with 1H of CONH<sub>2</sub>), 7.62 (d, *J* = 1.8 Hz, 1H), 7.55 (dd, *J* = 8.6, 1.9 Hz, 1H), 7.43 (d, *J* = 8.1 Hz, 2H), 7.04 (br s, 1H, CONH<sub>2</sub>), 6.86 (d, *J* = 8.4 Hz, 1H), 4.44 (s, 2H), 3.01 (s, 2H), 2.84 (s, 2H), 1.64 (s, 4H). <sup>13</sup>C NMR (126 MHz, DMSO-*d*<sub>6</sub>) δ 167.8, 164.1, 153.8, 142.6, 133.2, 131.5, 129.6, 127.7 (2C), 127.0 (2C), 126.2, 125.9, 116.4, 57.0, 53.5, 34., 28.8, 25.0. ESI HRMS calcd for C<sub>19</sub>H<sub>20</sub>N<sub>3</sub>O<sub>3</sub>: [M-H]<sup>-</sup>, *m/z* 338.1510; found: 338.1502.

**Molecular Docking Studies.** Docking models of the ligand bound to HDAC6 and HDAC1 were developed using the Molecular Operating Environment (MOE) computational suite's Builder utility. The energy minimization of ligands was conducted in the gas phase using the force field MMFF94X followed by the conformational search protocol to generate structural conformation databases. The zHDAC6 (PDB entry 6THV; resolution: 1.1 Å)<sup>24</sup> and hHDAC1 (PDB entry 5ICN; resolution: 3.3 Å)<sup>37</sup> crystal structures used as templates were obtained from the Protein Data Bank. The receptor preparation step was initiated with the removal of solvent. Hydrogens were then placed, while ionization states were assigned throughout the system. Finally, ligands and binding sites were isolated in 3D, and then a molecular surface was drawn around the binding site to visualize the space available for docked ligands. Ligand placement employed the  $\alpha$  triangle method with Affinity dG scoring generating 300 data points that were further refined using the induced fit method with GBVI/WSA dG scoring to obtain the top 50 docking results. The docking result of each ligand was analyzed for selection of the best docking pose, based on the score and reported X-ray structures. All renderings presented in **Figures 2** and **S5** were then performed in PyMOL.

**HDAC1 and 6 Enzymatic Assay Procedure.** HDAC inhibition assays in **Table 1** were performed by the Reaction Biology Corporation (Malvern, PA) using human full-length recombinant HDAC1 and 6, isolated from a baculovirus expression system in Sf9 cells. An acetylated, fluorogenic peptide derived from residues 379–382 of p53 (RHKKAc) was used as the substrate in the assays. The reaction buffer contained 50 mM Tris·HCl (pH 8.0), 137 mM NaCl, 2.7 mM KCl, 1 mM MgCl<sub>2</sub>, 1 mg/mL BSA, and a final concentration of 1% DMSO. The enzyme was added into wells of the reaction plate, and stock solutions of compounds were distributed into the enzyme mixture by Acoustic technology (Echo550 instrument; nanoliter range). The plates were spun down and preincubated for 5–10 min. The substrate was then delivered to all reaction wells to initiate the reaction, which was incubated for 2 h at 30 °C. After incubation, developer and trichostatin A (TSA) were added to quench the reaction and generate fluorescence. Kinetic measurements were then taken for 1.5 h at 15 min intervals to ensure that development was complete. Endpoint readings were taken for analysis after the development reached a plateau. Dose–response curves were generated, and the IC<sub>50</sub> value for each compound was extrapolated from the generated plots (ten-dose IC<sub>50</sub> curves were generated using a threefold serial dilution pattern starting at 30  $\mu$ M).

**Expression and Purification of Human HDACs 1–9 and 11.** Large-scale expression of human HDACs was carried out in HEK293/T17 cells essentially as described previously.<sup>45,46</sup> Briefly, transiently transfected cells were harvested three days post-transfection and the cell pellets were resuspended in a lysis buffer (50 mM Tris, 150 mM NaCl, 10 mM KCl, 2 mM MgCl<sub>2</sub>, 10% glycerol, 0.2% NP-40, and 2 U/mL benzonase, pH 8) supplemented with a cocktail of protease inhibitors (Roche, Basel, Switzerland). Cells were lysed by sonication (30 W; 3 × 20 s) on ice, and the cell lysate was cleared by centrifugation at 40 000g for 30 min at 4 °C. Recombinant fusion HDAC proteins were purified via Strep-Tactin affinity chromatography (IBA, Göttingen, Germany) with the elution buffer comprising 50 mM HEPES, 100 mM NaCl, 50 mM KCl, 10% glycerol, and 3 mM

desthiobiotin, pH 7.5. Purified proteins were concentrated to 1 mg/mL, aliquoted, flash-frozen in liquid nitrogen, and stored at –80 °C until further use.

**Determination of Inhibition Constants.** IC<sub>50</sub> values in **Tables 3** and **6** were determined using a fluorescence-based assay with 10  $\mu$ M Ac-GAK(Ac)-AMC (HDAC1, 2, 3, 6) and 10  $\mu$ M Boc-Lys(TFA)-AMC (HDAC 4, 5, 7, 8, 9, 11) as a substrate.<sup>47</sup> Briefly, individual HDACs were preincubated with dilution series of tested inhibitors in a 384-well plate in the total volume of 30  $\mu$ L for 10 min at 37 °C in a reaction buffer comprising 50 mM HEPES, 140 mM NaCl, 10 mM KCl, 1 mM TCEP, and 0.1% BSA at pH 7.4. Deacetylation reactions were started by the addition of 10  $\mu$ L of a 40  $\mu$ M substrate into the HDAC/inhibitor mixture. Following 30 min incubation at 37 °C, the reaction was terminated by the addition of 25  $\mu$ L of trypsin solution (4 mg/mL). Trypsin treatment was carried out at 37 °C for 15 and 60 min for the Ac-GAK(Ac)-AMC and Boc-Lys(TFA)-AMC substrates, respectively. Released aminomethyl coumarin was quantified using a CLARIOstar fluorimeter with  $\lambda_{EX}/\lambda_{EM}$  = 365/440 nm. Nonlinear regression analysis was employed to calculate IC<sub>50</sub> values using GraphPad Prism software. Fourteen-point IC<sub>50</sub> values were generated using a 3-fold inhibitor dilution series; inhibitor concentration ranges used: 100  $\mu$ M to 63 pM for HDACs 1–5, 7–9, 11; and 3  $\mu$ M to 1.88 pM for HDAC6. Reactions without the enzyme or the inhibitor were used to define 0 and 100% of the HDAC activity, respectively.

**$\alpha$ -Tubulin Acetylation and Histone Acetylation in N2a Cells.** Mouse neuroblastoma (N2a) cells were grown in a 1:1 mixture of DMEM (Dulbecco's modified Eagle's medium) and F12 medium supplemented with glutamax (ThermoFisher Scientific Inc., Pittsburgh, PA), 100  $\mu$ g/mL streptomycin, 100 U/mL penicillin (ThermoFisher Scientific), 10% fetal calf serum (Greiner Bio-One, Alphen aan den Rijn, NL), 1% nonessential amino acids (ThermoFisher Scientific), and 1.6% NaHCO<sub>3</sub> (ThermoFisher Scientific) at 37 °C and 7.5% CO<sub>2</sub>. To split the cells, cells were washed with Versene (ThermoFisher Scientific) and dissociated with 0.05% trypsin-EDTA (ThermoFisher Scientific). The N2a cells were treated overnight at 37 °C with 0.01 or 1.0  $\mu$ M of the tested compounds or an equivalent dose of DMSO (Sigma-Aldrich, Diegem, Belgium).

The treated cells were then washed with phosphate-buffered saline (PBS) and collected using the EpiQuik Total Histone Extraction Kit (EpiGenetek, Farmingdale, NY) according to the manufacturer's instructions. Protein concentrations were determined using the microBCA kit (ThermoFisher Scientific) according to the manufacturer's instructions. Before resolving the samples in a 12% sodium dodecyl sulfate-polyacrylamide gel electrophoresis (SDS-PAGE) gel, samples containing equal amounts of protein were supplemented with reducing sample buffer (Thermo Scientific) and heated at 95 °C for 5 min. After electrophoresis, the proteins were transferred to a poly(vinylidene difluoride) (PVDF) membrane (Merck Millipore Corp.). The nonspecific binding was blocked by incubation of the membrane in 5% bovine serum albumin (BSA), diluted in tris buffered saline Tween (TBS-T, 50 mM TRIS, 150 mM NaCl, 0.1% Tween-20 (Applichem, Darmstadt, Germany)) for 1 h at room temperature followed by incubation with primary antibodies overnight. The antibodies, diluted in TBS-T, were directed against  $\alpha$ -tubulin (1/5000, T6199, Sigma-Aldrich), acetylated  $\alpha$ -tubulin (1/5000, T6793 monoclonal, Sigma-Aldrich), histone H3 acetyl k9+k14 (1/1000, 9677L, Cell Signaling), and histone H4 (1/1000, ab10158, Abcam). The secondary antibodies, coupled to alkaline phosphatase (antimouse or antirabbit, 1/5000, Sigma-Aldrich), were used to detect the signal of the primary antibodies. Blots were visualized by adding the ECF substrate (Enhanced Chemical Fluorescence, GE Healthcare, Uppsala, Sweden) and imaged with the ImageQuant LAS 4000. A mild reblotting buffer (Merck Millipore Corp.) was applied to strip the blots. ImageQuant TL version 7.0 software was used to quantify the blots. GraphPad Prism version 8.0 software was used to prepare the figures in **Figures S1–S4**.

**Metabolic Stability Assessment in Mouse and Human Microsomes.** Pooled male mouse liver microsomes (CD1) (20 mg/mL, Cat. 452701), pooled human liver microsomes (20 mg/mL, Cat. 452161), potassium phosphate buffer (0.5 M, pH 7.4, Cat. 451201),

and NADPH regenerating system solution A (5 mL, Cat. 451220, 26 mM NADP<sup>+</sup>, 66 mM glucose-6-phosphate, and 66 mM MgCl<sub>2</sub> in H<sub>2</sub>O) and solution B (1.0 mL, Cat. 451200, 40 U/mL glucose-phosphate dehydrogenase in 5 mM sodium citrate) were purchased from Corning (NY). Microsomes and NADPH solution were stored at -80 and -20 °C prior to use, respectively. Then, 10 μL of 20 mg/mL liver microsomes and NADPH regenerating system solution A (20 μL) and solution B (4 μL) were added to the incubation tubes. The final concentrations of microsomes, NADPH, glucose-6-phosphate, glucose-phosphate dehydrogenase, and MgCl<sub>2</sub> were 0.5 mg/mL, 1.3 mM, 3.3 mM, 0.4 U/mL, and 3.3 mM, respectively. The reaction was started with the addition of 4 μL of 200 μM test compound solutions or positive control solution (verapamil) at the final concentration of 2 μM followed by incubation at 37 °C. Aliquots of 50 μL were taken from the reaction solution at 0, 15, 30, 45, and 60 min. The reaction solutions were stopped by the addition of 4 volumes of cold acetonitrile with an internal standard (0.5 μM). Samples were centrifuged at 3220g for 10 min. Aliquot of 200 μL of the supernatant was filtered and used for quantitative analysis performed by LC-MS/MS. All experiments were performed in duplicate. Liquid chromatography separation was performed using the Agilent1290 infinity system. The mass spectrometric analysis was performed using an API 6500 instrument from AB Inc (Canada) with an ESI interface. The data acquisition was performed using Analyst 1.5.2 software from ABI Inc. All calculations were carried out using Microsoft Excel. Peak areas were determined from extracted ion chromatograms. The slope value, *k*, was determined by linear regression of the natural logarithm of the remaining percentage of the parent drug vs incubation time curve. The half-life (*t*<sub>1/2</sub>) value was determined from the slope value following the equation: *t*<sub>1/2</sub> = -0.693/*k*. Liver microsomal stability results of the tested compounds are shown as the remaining percentages at 60 min and half-lives in Table 5.

**Cell Transfection, Treatments, and BRET Measurements.** NanoBRET target engagement was performed against HDAC6 (CD2) and HDAC1 according to the manufacturer's protocol (Promega) in HEK293 cells (ATCC). Plasmid constructs encoding NanoLuc-HDAC6 (CD2) and HDAC1-NanoLuc encoded HDAC open reading frames matching a previous work.<sup>39</sup> HDAC6 (CD2) encoded a GSSGAlA linker between NanoLuc and HDAC6 (CD2), and HDAC1-NanoLuc encoded a SWTWEGNKWTWK linker between HDAC1 and NanoLuc. For target engagement analysis for HDAC6, a HEK293 cell line stably expressing full-length NanoLuc-HDAC6 was used (Promega). NanoBRET HDAC Tracer (Promega) was added to a final concentration of 250, 1000, or 100 nM for HDAC6 (CD2), HDAC1, and HDAC6, respectively, immediately prior to test compound addition. Tracer concentrations were selected for each HDAC such that tracer occupancy did not impart a shift in the observed compound IC<sub>50</sub> value. Serially diluted test compounds were then added to the cells and allowed to equilibrate for 2 h prior to BRET measurements. To measure BRET, NanoBRET NanoGlo Substrate-(Promega) and Extracellular NanoLuc inhibitor was added as per the manufacturer's protocol, and filtered luminescence was measured on a GloMax Discover luminometer equipped with a 450 nm BP filter (donor) and a 610 nm LP filter (acceptor), using 0.5 s integration time. Milli-BRET units (mBU) are the BRET values × 1000. Competitive displacement data were then graphed with GraphPad Prism software using a 3-parameter curve fit with the following equation:  $Y = \text{bottom} + (\text{top} - \text{bottom}) / (1 + 10^{((X - \text{Log IC}_{50}))})$ .

**Cell-Based Determination of Inhibitor Potency.** Cellular EC<sub>50</sub> values of inhibitors against HDAC6 were determined using quantification of tubulin acetylation levels by Western blotting as a functional readout. To this end, RPMI8226 lymphoblasts were cultured in an RPMI-1640 medium supplemented with 10% FBS in a 5% CO<sub>2</sub> atmosphere at 37 °C. Cells were transferred into Eppendorf tubes at a concentration of 2 × 10<sup>5</sup> cells/tube, and dilution series of inhibitor solutions in PBS were added to the final volume of 200 μL. Cells were incubated with inhibitors for 6 h and harvested by centrifugation at 500g at room temperature for 5 min. The cell pellet

was resuspended in 75 μL of the lysis buffer (20 mM Tris, 4 M urea, 5 mM MgCl<sub>2</sub>, 0.5% Triton X-100, pH 8.2) supplemented with protease inhibitors and benzonase (5 μL/mL). Following a 5 min incubation, Laemmli SDS-PAGE buffer (4×) was added, and samples were boiled for 5 min. Samples were separated by SDS-PAGE (1 × 10<sup>4</sup> cells per lane) and electrotransferred onto a PVDF membrane. Total α-tubulin (α-tub) and acetylated α-tubulin (Ac-α-tub) were labeled using α-Tub (rabbit, #Ab18251; Abcam; 1:4000) and Ac-α-Tub (mouse, #T451; Sigma; 1:2500) antibodies, respectively. The α-GAPDH (mouse, #ACR001PS; Acris; 1:2500) was used as a loading control. Alexa Fluor 568 DAR (#A10042; Invitrogen; 1:5000) and Alexa Fluor 488 GAM (#A11029; Invitrogen; 1:5000) secondary antibodies were used, and fluorescence intensity was quantified using a Typhoon FLA 9500 imager together with Quantity One 4.6.6 software. Finally, nonlinear regression analysis was employed to calculate EC<sub>50</sub> values using GraphPad Prism software.

**zHDAC6 Expression and Purification.** The CD2 catalytic domain of *Danio rerio* HDAC6 (amino acids 440–798, zHDAC6-CD2) was expressed and purified as described previously.<sup>40</sup> Briefly, the N-terminally tagged (TEV-cleavable His-MBP) fusion construct was expressed in *E. coli* BL21-Codon Plus (DE3)-RIPL at 16 °C overnight. Following the affinity purification on a HisTrap HP column, the tag was removed using TEV protease (20:1) at 4 °C overnight. zHDAC6-CD2 was further purified by amylose affinity and HiTrap Q Sepharose ion-exchange chromatography. Size-exclusion chromatography on Superdex 75 pg with 50 mM HEPES, 100 mM KCl, 5% glycerol, and 1 mM TCEP, pH 7.5, as the mobile phase was used as the final purification step. The protein preparation was concentrated by ultrafiltration to 10 mg/mL, aliquoted, flash-frozen in liquid nitrogen, and stored at -80 °C until further use.

**Crystallization and Data Collection.** The zHDAC6-CD2 stock solution (10 mg/mL) was mixed with 1/20 volume of the SW-101 solution (80 mM in DMSO), and the crystallization droplets were prepared by combining 0.1 μL of the complex solution with 0.2 μL of a reservoir solution containing 21% PEG 3350 (Sigma-Aldrich), 0.2 M KSCN (Hampton research), and 0.1 M Bis-Tris (Sigma-Aldrich) at pH 6.5. To boost the nucleation step, the droplets were streak-seeded using the seed stock prepared from crystals of the HDAC6-CD2/SAHA complex using a Crystal Crusher (Hampton Research). Crystals were grown by the sitting drop vapor diffusion method at 283 K. Diffraction quality crystals were vitrified in liquid nitrogen from the mother liquor supplemented with 15% (v/v) glycerol. The diffraction data were collected from a single crystal at 90 K using synchrotron radiation at a Bessy II beamline MX14.2 (Berlin, Germany) equipped with a Pilatus 2M detector at an X-ray wavelength of 0.92 Å. Data processing was performed with the XDSAPP software package.<sup>48</sup>

**Structure Determination and Refinement.** The difference Fourier method was used to determine the structure of the zHDAC6-CD2/SW-101 complex using the zHDAC6-CD2/SS-208 complex (PDB code: 6R0K)<sup>36</sup> without the inhibitor and water molecules as a starting model.<sup>36</sup> Iterative refinement and model building cycles were performed using Refmac 5.8 and Coot, respectively.<sup>49,50</sup> Ligand topologies and coordinates were generated with AceDRG,<sup>51</sup> and the inhibitor was fitted into the  $|F_o| - |F_c|$  electron density map in the final stages of the refinement. Approximately 2500 randomly selected reflections were kept aside for cross-validation (*R*<sub>free</sub>) during the refinement process. The final model was validated using the MolProbity server.<sup>52</sup> The data collection and structure refinement statistics are summarized in Table S1.

**Animals.** All mice in these experiments were housed and bred in the Small Animal Facility at AgResearch, Hamilton, New Zealand, under the Animal Ethics Protocol 14154. CMT2A mice were engineered by Cartoni et al.<sup>43</sup> using mutant human MFN2 (mhMfn2; R94Q amino acid substitution), whose expression is controlled by a neuron-specific enolase promoter. Expression of mhMfn2 in these mice occurs in neurons of the peripheral and central nervous system, including motoneurons and dorsal root sensory ganglia, from embryonic day 13.<sup>43</sup>

**SW-101 Treatment.** SW-101 was dissolved in PBS/PEG400/Tween80/EtOH (50/35/10/5 wt %), which was also used as the vehicle in control mice. Transgenic and WT mice were treated daily with an IP injection of 20 mg per kg body weight or an equivalent amount of vehicle. This dose was based on drug-dosing experiments using WT mice.

**Assessment of Motor Performance and Neuropathic Pain. Rotarod.** General motor performance was assessed on an accelerating RotaRod (Ugo Basile). Mice were placed on the rotating rod spinning from 4 to 40 rpm on a 300 s ramp duration. Each animal was tested three times with a 1 min resting interval between trials. The motor performance was measured as the average time spent on the rotating rod.

**Mechanical Allodynia (Von Frey Test).** Following habituation to the wired mesh grid and 10 × 10 cm acrylic chambers of the testing apparatus for 40 min, mice were tested for mechanical allodynia using calibrated von Frey hair monofilaments (Aesthesio, set of 20 monofilaments, Ugo Basile). Monofilaments were applied to the plantar surface of the hind paw to deliver target forces from 0.004 to 4 g, increasing in an approximately logarithmic scale. A single von Frey hair was applied for 2 s unless the mouse withdrew its paw. The up-and-down method described by Chaplan<sup>53</sup> was adapted as follows: testing began with a 0.4 g filament applied three times. A positive response was recorded if paw withdrawal was seen at all three stimuli, and the next smallest filament was applied (turning point). A negative response was followed by testing with the next largest filament (turning point). Paw withdrawal thresholds (PWTs) were calculated as the median of 23–30 determined turning points.

**Thermal Hyperalgesia (Hargreaves Test).** Following habituation to the glass plate surface and 10 cm × 10 cm acrylic chambers of the testing apparatus for 40 minutes, mice were tested for thermal hyperalgesia. A focused infrared light source (Hargreaves Apparatus, Ugo Basile) was used to create a radiant-heat spot of 4 mm × 6 mm on the hind paw, and the paw withdrawal latency (PWL) was measured. A heat cutoff of 20 s was used as a safety precaution to prevent tissue damage. Heat stimuli presentations were repeated five times with a stimulus interval of 1 min.

**Western Blot.** Animal sciatic nerves were collected postmortem, and total proteins were extracted with RIPA lysis and extraction buffer (Life Technologies, cat. 89900) according to the manufacturer's instructions. Protein concentrations were determined using the Pierce BCA protein assay kit (Life Technologies, cat. 23227) according to the manufacturer's instructions. Lysates containing equal amounts of protein were added to 4 × Bolt LDS sample buffer (Life Technologies cat. B0007), heated to 95 °C for 5 min, and loaded on a 4–12% Bis-Tris polyacrylamide electrophoresis gel. Separated proteins were transferred to a PVDF membrane (Merck Millipore). Membranes were blocked for nonspecific binding with the Odyssey blocking buffer or BSA at room temperature for 1 h before incubation with primary antibodies. Antibodies and dilutions used in this study include total  $\alpha$ -tubulin (Sigma-Aldrich, cat. T8203, 1:2000), acetyl- $\alpha$ -tubulin (Sigma-Aldrich, cat. T7451, 1:2000), and glyceraldehyde 3-phosphate dehydrogenase (Sigma-Aldrich, cat. G9545, 1:2000). The secondary antibodies and dilutions include goat antimouse IgG HRP (ThermoFisher Scientific, cat. A16066, 1:5000) and goat antirabbit IgG HRP (Life technologies, cat. 656120, 1:2000). Pierce enhanced chemiluminescent Western blotting substrate (ThermoFisher Scientific, cat. 32209) was used for secondary antibody HRP detection, and Image J was used for densitometric analysis of the blots.

**Immunostaining and Confocal Microscopy.** Sciatic nerves were sectioned (14  $\mu$ m thick) using a cryostat and mounted on polylysine-coated slides. Mounted tissue sections were permeabilized with 0.2% Triton X-100 in PBS for 15 min, followed by incubation with 10% normal goat serum (NGS) for 30 min at room temperature. Sections were then incubated with the following primary antibodies and dilutions: Ac- $\alpha$ -tub (Lys40) (Cell Signaling, cat. CTE5335S, 1:500), neurofilament H (EMD Millipore, cat. AB5539, 1:200), and total  $\alpha$ -tubulin (Sigma-Aldrich, cat. T8203, 1:200). Antibodies were incubated overnight at 4 °C before washing with 0.2% Triton X-100 in PBS, and the addition of the secondary antibodies—Alexa

Fluor 488 (Invitrogen, cat. A32731), Alexa Fluor 555 (Invitrogen, cat. A32727), and Alexa Fluor 633 (Invitrogen, cat. A21103) conjugated secondary antibodies (all 1:1000)—was carried out for 60 min at room temperature. All antibodies were diluted in PBS-T with 10% NGS. Sections were imaged with confocal microscopy, and collapsed Z-stacks were quantified using Image J with FIJI plug-in analysis software. Neurofilament staining was used to identify axons within the sciatic nerves and create a mask for Ac- $\alpha$ -tub and total  $\alpha$ -tubulin quantification.

**Statistics.** All statistical analyses were performed using GraphPad Prism software version 7 (GraphPad Software Inc).

## ■ ASSOCIATED CONTENT

### Supporting Information

The Supporting Information is available free of charge at <https://pubs.acs.org/doi/10.1021/acs.jmedchem.0c02210>.

Results for  $\alpha$ -tubulin/histone acetylation evaluation of HDAC6is **1b**, **1e**, **1f**, **1g**, and **1h** in N2a cells (Figure S1); results for  $\alpha$ -tubulin/histone acetylation evaluation of HDAC6is **1m**, **1q**, **1s**, **18a–c**, and **18e–g** in N2a cells (Figures S2–S4); molecular docking studies on hHDAC1 (Figure S5); omit  $F_o - F_c$  difference map (green mesh) for the zHDAC6-bound SW-101 (Figure S6); inhibition of hERG potassium channel activity by SW-101 (Figure S7); table for crystallization data collection and refinement statistics (Table S1); Mini-Ames genotoxicity assay results for SW-101 (Table S2); and <sup>1</sup>H NMR spectra, <sup>13</sup>C NMR spectra, and HPLC purity reports for SW-100 (**1a**) and SW-101 (**1s**) (PDF)

Molecular formula strings of compounds **1a–s** and **18a–g** including screening data (CSV)

### Accession Codes

Atomic coordinates and corresponding structure factors for the zHDAC6-CD2/SW-101 complex have been deposited at the Protein Data Bank (PDB) as the 6ZW1 entry. Authors will release the atomic coordinates upon article publication.

## ■ AUTHOR INFORMATION

### Corresponding Authors

Cyril Bařinka – Institute of Biotechnology of the Czech Academy of Sciences, 252 50 Vestec, Czech Republic; [orcid.org/0000-0003-2751-3060](https://orcid.org/0000-0003-2751-3060); Phone: +420-325-873-777; Email: [Cyril.Barinka@ibt.cas.cz](mailto:Cyril.Barinka@ibt.cas.cz)

Brett Langley – School of Health, The University of Waikato, Hamilton 3240, New Zealand; Phone: +64-7-838-4060; Email: [blangley@waikato.ac.nz](mailto:blangley@waikato.ac.nz)

Alan P. Kozikowski – Bright Minds Biosciences, Toronto, ON M5H 3V9, Canada; Phone: +1-773-793-5866; Email: [alan@brightmindsbio.com](mailto:alan@brightmindsbio.com)

### Authors

Sida Shen – Department of Medicinal Chemistry and Pharmacognosy, College of Pharmacy, University of Illinois at Chicago, Chicago, Illinois 60612, United States;

[orcid.org/0000-0002-0295-2545](https://orcid.org/0000-0002-0295-2545)

Cristina Picci – School of Health, The University of Waikato, Hamilton 3240, New Zealand

Kseniya Ustinova – Institute of Biotechnology of the Czech Academy of Sciences, 252 50 Vestec, Czech Republic

Veronick Benoy – Laboratory of Neurobiology, Center for Brain & Disease (VIB) and Leuven Brain Institute (LBI), KU Leuven, B-3000 Leuven, Belgium

Zsófia Kutil – Institute of Biotechnology of the Czech Academy of Sciences, 252 50 Vestec, Czech Republic

Guiping Zhang – Department of Medicinal Chemistry and Pharmacognosy, College of Pharmacy, University of Illinois at Chicago, Chicago, Illinois 60612, United States;

[orcid.org/0000-0001-9818-4773](https://orcid.org/0000-0001-9818-4773)

Maurício T. Tavares – Department of Medicinal Chemistry and Pharmacognosy, College of Pharmacy, University of Illinois at Chicago, Chicago, Illinois 60612, United States;

[orcid.org/0000-0002-4400-7787](https://orcid.org/0000-0002-4400-7787)

Jiří Pavlíček – Institute of Biotechnology of the Czech Academy of Sciences, 252 50 Vestec, Czech Republic

Chad A. Zimprich – Promega Corporation, Madison, Wisconsin 53711, United States

Matthew B. Robers – Promega Corporation, Madison, Wisconsin 53711, United States

Ludo Van Den Bosch – Laboratory of Neurobiology, Center for Brain & Disease (VIB) and Leuven Brain Institute (LBI), KU Leuven, B-3000 Leuven, Belgium

Complete contact information is available at:

<https://pubs.acs.org/10.1021/acs.jmedchem.0c02210>

### Author Contributions

<sup>†</sup>S.S. and C.P. contributed equally to this paper. A.P.K., B.L., and C.B. conceived the original idea, initiated the project, oversaw all of the chemical, biological, crystallographic, ADMET as well as animal experimental designs/data analysis, and revised the manuscript. S.S. designed and synthesized compounds, performed liver microsomal stability assays, oversaw all of the experimental design, analyzed the data, and wrote the manuscript with assistance from the other authors. C.P. designed and performed all cellular and animal experimental designs, analyzed data, and contributed to the manuscript writing. J.P. crystallized the zHDAC6/SW-101 complex. K.U. solved, refined the zHDAC6/SW-101 complex, and contributed to cell-based assays in RPMI8226 cells. V.B. and L.V.D.B. contributed to  $\alpha$ -tubulin/histone acetylation studies in N2a cells. Z.K. determined the enzymatic IC<sub>50</sub> values of HDAC isoforms. G.Z. and M.T.T. contributed to intermediate preparation and the scale-up work of SW-101. C.A.Z. and M.B.R. contributed to the cellular HDAC target engagement assays in HEK293 cells.

### Notes

The authors declare no competing financial interest.

### ACKNOWLEDGMENTS

We thank Dr. Werner Tueckmantel for proofreading the article and providing comments and Barbora Havlinova, Jana Mikesova, and Lucia Motlova for their excellent technical assistance. This work was funded by NIH R01NS079183, R43HD093464, R41AG058283 (A.P.K.) and Hereditary Neuropathy Foundation (B.L.). Additionally, this work was in part supported by the CAS (RVO: 86652036) and the Czech Science Foundation (21-31806S to C.B.). We acknowledge the Helmholtz-Zentrum Berlin for the allocation of synchrotron radiation beamtime at the MX14.2 beamline and the support by the project CALIPSOplus (grant agreement 730872) from the EU Framework Programme for Research and Innovation HORIZON 2020 and CMS-Biocev (“Crystallization/Diffraction”) supported by MEYS CR (LM2018127). V.B. was supported by the “Agency for Innovation by Science and Technology in Flanders” (IWT-Vlaanderen).

### ABBREVIATIONS

ADMET, absorption, distribution, metabolism, excretion, and toxicity; rt, room temperature; DMF, *N,N*-dimethylformamide; NBS, *N*-bromosuccinimide; AIBN, azobisisobutyronitrile; DCM, dichloromethane; TEA, triethylamine; THF, tetrahydrofuran; Pd<sub>2</sub>(dba)<sub>3</sub>, tris(dibenzylideneacetone)dipalladium(0); S-Phos, 2-dicyclohexylphosphino-2',6'-dimethoxybiphenyl; DMSO, dimethyl sulfoxide; SD, standard deviation; SEM, standard errors; TLC, thin-layer chromatography; HPLC, high-performance liquid chromatography; TFA, trifluoroacetic acid; NADPH, nicotinamide adenine dinucleotide phosphate; TCEP, tris(2-carboxyethyl)phosphine; hERG, human ether-a-go-go related gene; CRISPR, clustered regularly interspaced short palindromic repeats

### REFERENCES

- (1) Shen, S.; Kozikowski, A. P. Why hydroxamates may not be the best histone deacetylase inhibitors—what some may have forgotten or would rather forget? *ChemMedChem* **2016**, *11*, 15–21.
- (2) Glozak, M. A.; Sengupta, N.; Zhang, X.; Seto, E. Acetylation and deacetylation of non-histone proteins. *Gene* **2005**, *363*, 15–23.
- (3) Ganai, S. A. Histone deacetylase inhibitors modulating non-epigenetic players: the novel mechanism for small molecule based therapeutic intervention. *Curr. Drug Targets* **2018**, *19*, 593–601.
- (4) de Ruijter, A. J. M.; van Gennip, A. H.; Caron, H. N.; Kemp, S.; van Kuilenburg, A. B. Histone deacetylases (HDACs): characterization of the classical HDAC family. *Biochem. J.* **2003**, *370*, 737–749.
- (5) Ustinova, K.; Novakova, Z.; Saito, M.; Meleshin, M.; Mikesova, J.; Kutil, Z.; Baranova, P.; Havlinova, B.; Schutkowski, M.; Matthias, P.; Barinka, C. The disordered N-terminus of HDAC6 is a microtubule-binding domain critical for efficient tubulin deacetylation. *J. Biol. Chem.* **2020**, *295*, 2614–2628.
- (6) Kutil, Z.; Skultetyova, L.; Rauh, D.; Meleshin, M.; Snajdr, I.; Novakova, Z.; Mikesova, J.; Pavlicek, J.; Hadzima, M.; Baranova, P.; Havlinova, B.; Majer, P.; Schutkowski, M.; Barinka, C. The unraveling of substrate specificity of histone deacetylase 6 domains using acetylome peptide microarrays and peptide libraries. *FASEB J.* **2019**, *33*, 4035–4045.
- (7) Osko, J. D.; Christianson, D. W. Structural basis of catalysis and inhibition of HDAC6 CD1, the enigmatic catalytic domain of histone deacetylase 6. *Biochemistry* **2019**, *58*, 4912–4924.
- (8) Miyake, Y.; Keusch, J. J.; Wang, L.; Saito, M.; Hess, D.; Wang, X.; Melancon, B. J.; Helquist, P.; Gut, H.; Matthias, P. Structural insights into HDAC6 tubulin deacetylation and its selective inhibition. *Nat. Chem. Biol.* **2016**, *12*, 748–754.
- (9) Seigneurin-Berny, D.; Verdel, A.; Curtet, S.; Lemerrier, C.; Garin, J.; Rousseaux, S.; Khochbin, S. Identification of components of the murine histone deacetylase 6 complex: link between acetylation and ubiquitination signaling pathways. *Mol. Cell Biol.* **2001**, *21*, 8035–8044.
- (10) Hammond, J. W.; Huang, C. F.; Kaech, S.; Jacobson, C.; Banker, G.; Verhey, K. J. Posttranslational modifications of tubulin and the polarized transport of kinesin-1 in neurons. *Mol. Biol. Cell* **2010**, *21*, 572–583.
- (11) Zhang, L.; Liu, C.; Wu, J.; Tao, J. J.; Sui, X. L.; Yao, Z. G.; Xu, Y. F.; Huang, L.; Zhu, H.; Sheng, S. L.; Qin, C. Tubastatin A/ACY-1215 improves cognition in Alzheimer's disease transgenic mice. *J. Alzheimer's Dis.* **2014**, *41*, 1193–1205.
- (12) Majid, T.; Griffin, D.; Criss, Z., 2nd; Jarpe, M.; Pautler, R. G. Pharmacologic treatment with histone deacetylase 6 inhibitor (ACY-738) recovers Alzheimer's disease phenotype in amyloid precursor protein/presenilin 1 (APP/PS1) mice. *Alzheimers Dementia* **2015**, *1*, 170–181.
- (13) d'Ydewalle, C.; Krishnan, J.; Chiheb, D. M.; Van Damme, P.; Irobi, J.; Kozikowski, A. P.; Vanden Berghe, P.; Timmerman, V.; Robberecht, W.; Van Den Bosch, L. HDAC6 inhibitors reverse axonal

loss in a mouse model of mutant HSPB1-induced Charcot-Marie-Tooth disease. *Nat. Med.* **2011**, *17*, 968–974.

(14) Benoy, V.; Van Helleputte, L.; Prior, R.; d'Ydewalle, C.; Haeck, W.; Geens, N.; Scheveneels, W.; Scheveneels, B.; Cader, M. Z.; Talbot, K.; Kozikowski, A. P.; Vanden Berghe, P.; Van Damme, P.; Robberecht, W.; Van Den Bosch, L. HDAC6 is a therapeutic target in mutant GARS-induced Charcot-Marie-Tooth disease. *Brain* **2018**, *141*, 673–687.

(15) Mo, Z.; Zhao, X.; Liu, H.; Hu, Q.; Chen, X. Q.; Pham, J.; Wei, N.; Liu, Z.; Zhou, J.; Burgess, R. W.; Pfaff, S. L.; Caskey, C. T.; Wu, C.; Bai, G.; Yang, X. L. Aberrant GlyRS-HDAC6 interaction linked to axonal transport deficits in Charcot-Marie-Tooth neuropathy. *Nat. Commun.* **2018**, *9*, No. 1007.

(16) Guo, W.; Naujock, M.; Fumagalli, L.; Vandoorne, T.; Baatsen, P.; Boon, R.; Ordovas, L.; Patel, A.; Welters, M.; Vanwelden, T.; Geens, N.; Tricot, T.; Benoy, V.; Steyaert, J.; Lefebvre-Omar, C.; Boesmans, W.; Jarpe, M.; Sternecker, J.; Wegner, F.; Petri, S.; Bohl, D.; Vanden Berghe, P.; Robberecht, W.; Van Damme, P.; Verfaillie, C.; Van Den Bosch, L. HDAC6 inhibition reverses axonal transport defects in motor neurons derived from FUS-ALS patients. *Nat. Commun.* **2017**, *8*, No. 861.

(17) Gold, W. A.; Lacina, T. A.; Cantrill, L. C.; Christodoulou, J. MeCP2 deficiency is associated with reduced levels of tubulin acetylation and can be restored using HDAC6 inhibitors. *J. Mol. Med.* **2015**, *93*, 63–72.

(18) Kozikowski, A. P.; Shen, S.; Pardo, M.; Tavares, M. T.; Szarics, D.; Benoy, V.; Zimprich, C. A.; Kutil, Z.; Zhang, G.; Barinka, C.; Robers, M. B.; Van Den Bosch, L.; Eubanks, J. H.; Jope, R. S. Brain penetrable histone deacetylase 6 inhibitor SW-100 ameliorates memory and learning impairments in a mouse model of Fragile X Syndrome. *ACS Chem. Neurosci.* **2019**, *10*, 1679–1695.

(19) Shen, S.; Kozikowski, A. P. A patent review of histone deacetylase 6 inhibitors in neurodegenerative diseases (2014–2019). *Expert Opin. Ther. Pat.* **2020**, *30*, 121–136.

(20) Züchner, S.; Vance, J. M. Mechanisms of disease: a molecular genetic update on hereditary axonal neuropathies. *Nat. Clin. Pract. Neurol.* **2006**, *2*, 45–53.

(21) Barisic, N.; Claeys, K. G.; Sirotkovic-Skerlev, M.; Lofgren, A.; Nelis, E.; De Jonghe, P.; Timmerman, V. Charcot-Marie-Tooth disease: a clinico-genetic confrontation. *Ann. Hum. Genet.* **2008**, *72*, 416–441.

(22) Prior, R.; Van Helleputte, L.; Klingl, Y. E.; Van Den Bosch, L. HDAC6 as a potential therapeutic target for peripheral nerve disorders. *Expert Opin. Ther. Targets* **2018**, *22*, 993–1007.

(23) Butler, K. V.; Kalin, J.; Brochier, C.; Vistoli, G.; Langley, B.; Kozikowski, A. P. Rational design and simple chemistry yield a superior, neuroprotective HDAC6 inhibitor, tubastatin A. *J. Am. Chem. Soc.* **2010**, *132*, 10842–10846.

(24) Shen, S.; Svoboda, M.; Zhang, G.; Cavin, M. A.; Motlova, L.; McKinsey, T. A.; Eubanks, J. H.; Bařinka, C.; Kozikowski, A. P. Structural and in vivo characterization of Tubastatin A, a widely used histone deacetylase 6 inhibitor. *ACS Med. Chem. Lett.* **2020**, *11*, 706–712.

(25) Ha, N.; Choi, Y. I.; Jung, N.; Song, J. Y.; Bae, D. K.; Kim, M. C.; Lee, Y. J.; Song, H.; Kwak, G.; Jeong, S.; Park, S.; Nam, S. H.; Jung, S.-C.; Choi, B.-O. A novel histone deacetylase 6 inhibitor improves myelination of Schwann cells in a model of Charcot-Marie-Tooth disease type 1A. *Br. J. Pharmacol.* **2020**, *177*, 5096–5113.

(26) Züchner, S.; De Jonghe, P.; Jordanova, A.; Claeys, K. G.; Guergueltcheva, V.; Cherninkova, S.; Hamilton, S. R.; Van Stavern, G.; Krajewski, K. M.; Stajich, J.; Tournev, I.; Verhoeven, K.; Langerhorst, C. T.; de Visser, M.; Baas, F.; Bird, T.; Timmerman, V.; Shy, M.; Vance, J. M. Axonal neuropathy with optic atrophy is caused by mutations in mitofusin 2. *Ann. Neurol.* **2006**, *59*, 276–281.

(27) Picci, C.; Wong, V. S. C.; Costa, C. J.; McKinnon, M. C.; Goldberg, D. C.; Swift, M.; Alam, N. M.; Prusky, G. T.; Shen, S.; Kozikowski, A. P.; Willis, D. E.; Langley, B. HDAC6 inhibition

promotes alpha-tubulin acetylation and ameliorates CMT2A peripheral neuropathy in mice. *Exp. Neurol.* **2020**, *328*, No. 113281.

(28) Penagarikano, O.; Mulle, J. G.; Warren, S. T. The pathophysiology of fragile x syndrome. *Annu. Rev. Genomics Hum. Genet.* **2007**, *8*, 109–129.

(29) Shen, S.; Benoy, V.; Bergman, J. A.; Kalin, J. H.; Frojuello, M.; Vistoli, G.; Haeck, W.; Van Den Bosch, L.; Kozikowski, A. P. Bicyclic-capped histone deacetylase 6 inhibitors with improved activity in a model of axonal Charcot-Marie-Tooth disease. *ACS Chem. Neurosci.* **2016**, *7*, 240–258.

(30) Gu, C.; Collins, R.; Holsworth, D. D.; Walker, G. S.; Voorman, R. L. Metabolic aromatization of N-alkyl-1,2,3,4-tetrahydroquinoline substructures to quinolinium by human liver microsomes and horseradish peroxidase. *Drug Metab. Dispos.* **2006**, *34*, 2044–2055.

(31) Tago, T.; Toyohara, J.; Ishii, K. Preclinical evaluation of an (18)F-labeled SW-100 derivative for PET imaging of histone deacetylase 6 in the brain. *ACS Chem. Neurosci.* **2021**, *12*, 746–755.

(32) Flipo, M.; Charton, J.; Hocine, A.; Dassonneville, S.; Deprez, B.; Deprez-Poulain, R. Hydroxamates: relationships between structure and plasma stability. *J. Med. Chem.* **2009**, *52*, 6790–6802.

(33) Porter, N. J.; Osko, J. D.; Diedrich, D.; Kurz, T.; Hooker, J. M.; Hansen, F. K.; Christianson, D. W. Histone deacetylase 6-selective inhibitors and the influence of capping groups on hydroxamate-zinc denticity. *J. Med. Chem.* **2018**, *61*, 8054–8060.

(34) Osko, J. D.; Porter, N. J.; Narayana Reddy, P. A.; Xiao, Y. C.; Rokka, J.; Jung, M.; Hooker, J. M.; Salvino, J. M.; Christianson, D. W. Exploring structural determinants of inhibitor affinity and selectivity in complexes with histone deacetylase 6. *J. Med. Chem.* **2020**, *63*, 295–308.

(35) Noonepalle, S.; Shen, S.; Ptacek, J.; Tavares, M. T.; Zhang, G.; Stransky, J.; Pavlicek, J.; Ferreira, G. M.; Hadley, M.; Pelaez, G.; Barinka, C.; Kozikowski, A. P.; Villagra, A. Rational design of Suprastat: a novel selective histone deacetylase 6 inhibitor with the ability to potentiate immunotherapy in melanoma models. *J. Med. Chem.* **2020**, *63*, 10246–10262.

(36) Shen, S.; Hadley, M.; Ustinova, K.; Pavlicek, J.; Knox, T.; Noonepalle, S.; Tavares, M. T.; Zimprich, C. A.; Zhang, G.; Robers, M. B.; Barinka, C.; Kozikowski, A. P.; Villagra, A. Discovery of a new isoxazole-3-hydroxamate-based histone deacetylase 6 inhibitor SS-208 with antitumor activity in syngeneic melanoma mouse models. *J. Med. Chem.* **2019**, *62*, 8557–8577.

(37) Watson, P. J.; Millard, C. J.; Riley, A. M.; Robertson, N. S.; Wright, L. C.; Godage, H. Y.; Cowley, S. M.; Jamieson, A. G.; Potter, B. V.; Schwabe, J. W. Insights into the activation mechanism of class I HDAC complexes by inositol phosphates. *Nat. Commun.* **2016**, *7*, No. 11262.

(38) Vögerl, K.; Ong, N.; Senger, J.; Herp, D.; Schmidtkunz, K.; Marek, M.; Müller, M.; Bartel, K.; Shaik, T. B.; Porter, N. J.; Robaa, D.; Christianson, D. W.; Romier, C.; Sippl, W.; Jung, M.; Bracher, F. Synthesis and biological investigation of phenothiazine-based benzhydroxamic acids as selective histone deacetylase 6 inhibitors. *J. Med. Chem.* **2019**, *62*, 1138–1166.

(39) Robers, M. B.; Dart, M. L.; Woodroffe, C. C.; Zimprich, C. A.; Kirkland, T. A.; Machleidt, T.; Kupcho, K. R.; Levin, S.; Hartnett, J. R.; Zimmerman, K.; Niles, A. L.; Ohana, R. F.; Daniels, D. L.; Slater, M.; Wood, M. G.; Cong, M.; Cheng, Y. Q.; Wood, K. V. Target engagement and drug residence time can be observed in living cells with BRET. *Nat. Commun.* **2015**, *6*, No. 10091.

(40) Hai, Y.; Christianson, D. W. Histone deacetylase 6 structure and molecular basis of catalysis and inhibition. *Nat. Chem. Biol.* **2016**, *12*, 741–747.

(41) Osko, J. D.; Christianson, D. W. Structural determinants of affinity and selectivity in the binding of inhibitors to histone deacetylase 6. *Bioorg. Med. Chem. Lett.* **2020**, *30*, No. 127023.

(42) Daina, A.; Michielin, O.; Zoete, V. SwissADME: a free web tool to evaluate pharmacokinetics, drug-likeness and medicinal chemistry friendliness of small molecules. *Sci. Rep.* **2017**, *7*, No. 42717.

(43) Cartoni, R.; Arnaud, E.; Medard, J. J.; Poirrot, O.; Courvoisier, D. S.; Chrast, R.; Martinou, J. C. Expression of mitofusin 2(R94Q) in

a transgenic mouse leads to Charcot-Marie-Tooth neuropathy type 2A. *Brain* **2010**, *133*, 1460–1469.

(44) Benoy, V.; Vanden Berghe, P.; Jarpe, M.; Van Damme, P.; Robberecht, W.; Van Den Bosch, L. Development of improved HDAC6 inhibitors as pharmacological therapy for axonal Charcot-Marie-Tooth disease. *Neurotherapeutics* **2017**, *14*, 417–428.

(45) Skultetyova, L.; Ustinova, K.; Kutil, Z.; Novakova, Z.; Pavlicek, J.; Mikesova, J.; Trapl, D.; Baranova, P.; Havlinova, B.; Hubalek, M.; Lansky, Z.; Barinka, C. Human histone deacetylase 6 shows strong preference for tubulin dimers over assembled microtubules. *Sci. Rep.* **2017**, *7*, No. 11547.

(46) Kutil, Z.; Novakova, Z.; Meleshin, M.; Mikesova, J.; Schutkowski, M.; Barinka, C. Histone deacetylase 11 is a fatty-acid deacylase. *ACS Chem. Biol.* **2018**, *13*, 685–693.

(47) Wu, H.; Yang, K.; Zhang, Z.; Leisten, E.; Li, Z.; Xie, H.; Liu, J.; Smith, K. A.; Novakova, Z.; Barinka, C.; Tang, W. Development of multi-functional histone deacetylase 6 degraders with potent anti-myeloma activity. *J. Med. Chem.* **2019**, *62*, 7042–7057.

(48) Sparta, K. M.; Krug, M.; Heinemann, U.; Mueller, U.; Weiss, M. S. XDSAPP2.0. *J. Appl. Crystallogr.* **2016**, *49*, 1085–1092.

(49) Vagin, A. A.; Steiner, R. A.; Lebedev, A. A.; Potterton, L.; McNicholas, S.; Long, F.; Murshudov, G. N. REFMACS dictionary: organization of prior chemical knowledge and guidelines for its use. *Acta Crystallogr., Sect. D: Biol. Crystallogr.* **2004**, *60*, 2184–2195.

(50) Emsley, P.; Lohkamp, B.; Scott, W. G.; Cowtan, K. Features and development of Coot. *Acta Crystallogr., Sect. D: Biol. Crystallogr.* **2010**, *66*, 486–501.

(51) Long, F.; Nicholls, R. A.; Emsley, P.; Graeulis, S.; Merkys, A.; Vaitkus, A.; Murshudov, G. N. AceDRG: a stereochemical description generator for ligands. *Acta Crystallogr. D Struct. Biol.* **2017**, *73*, 112–122.

(52) Chen, V. B.; Arendall, W. B., 3rd; Headd, J. J.; Keedy, D. A.; Immormino, R. M.; Kapral, G. J.; Murray, L. W.; Richardson, J. S.; Richardson, D. C. MolProbity: all-atom structure validation for macromolecular crystallography. *Acta Crystallogr., Sect. D: Biol. Crystallogr.* **2010**, *66*, 12–21.

(53) Chaplan, S. R.; Bach, F. W.; Pogrel, J. W.; Chung, J. M.; Yaksh, T. L. Quantitative assessment of tactile allodynia in the rat paw. *J. Neurosci. Methods* **1994**, *53*, 55–63.